June 2017

# The effects of simulated inflammatory conditions on the corrosion and fretting corrosion of CoCrMo alloy

Yangping Liu
*Syracuse University*

## Recommended Citation

## Abstract

In vivo corrosion of CoCrMo alloy and its potential adverse effects on the body have been recognized as major concerns in recent years. While the underlying concepts of general and mechanically-assisted corrosion have been well documented, recent report of inflammatory cell-induced corrosion (ICIC) of CoCrMo alloy challenged traditional understanding of the relationship between biology and corrosion of hip implants. To better understand the role biology may play in the corrosion of CoCrMo-based implants, this study explored the mechanism of ICIC on CoCrMo alloy and investigated how simulated inflammatory (SI) conditions affected the electrochemistry, oxide film and fretting corrosion behavior of CoCrMo alloy.

A range of SI solutions, based on phosphate buffered saline with $H_2O_2$, HCl, HClO and $Fe^{3+}$ additions, were investigated. Results of electrochemistry tests (open circuit potential, polarization and electrochemistry impedance spectroscopy) indicated the corrosion susceptibility of CoCrMo alloy can be significantly increased by SI solutions, increasing the oxidizing power and decreasing the passivity of the oxide film. Physiologically possible potential of CoCrMo alloy has been found to be as positive as 0.9 V, a much higher level than previously thought. Inflammatory cell-based chemicals such as $H_2O_2$, HClO, acid and Fenton reaction ($H_2O_2$ and $Fe^{3+}$) were able to facilitate the corrosion of CoCrMo alloy and demonstrated part of the mechanism of inflammatory cell induced corrosion. The effect of inflammatory species hydrogen peroxide and voltage on the passive oxide film of CoCrMo alloy was studied by Electrochemical Atomic Force Microscopy (ECAFM). The results showed

that simulated inflammatory condition ($H_2O_2$) and potential significantly altered oxide film behavior (surface roughness, topography, corrosion resistance). Variation of surface roughness, corrosion resistance were related with potential and time-dependent oxide film topography.

Fretting corrosion behavior of CoCrMo/CoCrMo alloy combinations was significantly affected by SI conditions and potential. Presence of Fenton reaction resulted in less stable oxide film and increased oxidizing ability of solution, altering the fretting corrosion behavior of CoCrMo alloy. Additionally, a fundamental study was conducted to investigate the effect of electrode area on the cathodic voltage excursion of metallic biomaterials due to fretting corrosion. This work linked the area-dependent impedance characteristics to the time dependent voltage changes observed during fretting corrosion. Results showed that voltage shifts decreased as the exposed area increased and that this behavior was described well using the impedance-based theory model.

# THE EFFECTS OF SIMULATED INFLAMMATORY CONDITIONS ON THE CORROSION AND FRETTING CORROSION OF CoCrMo ALLOY

By

YANGPING LIU

B.S Materials Science & Engineering, Central South University, 2010

DISSERTATION

Submitted in partial fulfillment of the requirements for the degree of

Doctor of Philosophy in Bioengineering

Syracuse University

May 2017

# Acknowledgement

First and foremost, I would like to thank my advisor Dr. Jeremy Gilbert. It has been a great honor and pleasure to be his Ph.D student and work with him in the past 7 years. I appreciate all his time, patience, ideas and support contributed to my Ph.D study. He has been a great mentor for me and has been offering valuable advices, encouragement and wisdom when I was confused and anxious about my study and future. He guided me the direction in my study and provided me mentorship in how to become an excellent researcher. He patiently offered me help in every detail of experiment, presentation and writing. He opened the door of biomaterials to me and led me to feel the beauty of science and the pleasure of exploration, creation and discovery in research through every part of his work. His passion for research, rich knowledge and rigorous scholarship has been motivational for me and driving me move forward in my Ph.D pursuit. I am thankful of all he has offered to me and feel lucky to have the chance to be his student.

I would also like to thank the members of the Gilbert group, who have offered me tremendous help in my work. I am especially grateful for Shiril Sivan and Viswanathan Swaminathan, who trained me in a variety of research skills and offered me valuable advices in my study.

For this dissertation, I would like to thank my committee members: Dr. Scott Erdman, Dr. Dacheng Ren, Dr. Julie Hasenwinkel, Dr. Pranav Soman and Dr. James Henderson for their time, interest, and helpful comments.

Lastly, I would like to thank my parents, my family and all my friends for their love, support, encouragement and accompany in my life and work.

<div align="right">

Yangping Liu

Syracuse University

May 2017

</div>

# TABLE OF CONTENTS

# List of Figures and Tables

# Chapter 1 Introduction

## 1.1 Background and Significance

The application of implanted devices in orthopedic surgery has been continuously increasing in recent years, and the total industry is estimated to grow to more than 41 billion dollars by 2016 [1]. The number of total joint replacements is expected to grow to 572,000 by 2030 [2-3]. Total joint replacement implants are designed to help patients, who suffer from joint injury or osteoarthritis, relieve pain and regain normal movement of a healthy joint. Metallic orthopedic implants mainly consists of cobalt-chromium-molybdenum (CoCrMo alloy), titanium, and stainless steel alloys have been widely used to replace the bone or articular surface due to their excellent mechanical, corrosion and biocompatibility properties.

CoCrMo alloys were introduced by Smith-Peterson in 1923 and were first used as dental alloys and later for orthopedic, spinal and cardiovascular implant applications [4, 5]. CoCrMo alloys have been approved for use in hip replacements since the early 1970s and their bulk mechanical properties have been improved by various materials processing and heat treatment techniques [6]. Because of their past success, these alloys continue to be used in many current medical devices, such as total hip replacement and total knee replacement. The use of metal-on-metal (MOM) implants had been gaining favor in the recent past due to superior wear performance compared to hip systems with polyethylene as bearing surface [7]. While the overall performance of CoCr alloys has been satisfactory, the degradation of metals

caused by mechanical motion and corrosion remains a potential concern [8-13].

**Current understanding---MAC (Mechanically Assisted Corrosion) affects biological response**

Recently, there have been serious concerns raised about the effect of metal ions and particles released from CoCrMo alloy on the body's responses [14-18]. The in vivo corrosion and its associated adverse biological responses in MOM hip replacement have become a global health concern [14, 17, 18]. Regulatory agencies of the US and UK have issued alerts for the use of MOM hip implants and recalls from major medical device manufactures have further brought the use of MOM devices into question [19, 20]. Wear and corrosion damage of the implant have been associated with a series of biological responses including: inflammation [21, 22], cytotoxicity [23-25], hypersensitivity [26, 27], and genotoxicity [28-30] to human cells. Adverse local tissue reaction (ALTR), associated with mechanically assisted corrosion has been a significant concern and an important contributor to hip implant failure. ALTR refers to inflammatory soft tissue lesions or adverse histological reactions associated with corrosion debris or ions from degradation of metal implants [31, 32]. Aseptic lymphocyte-dominated vasculitis-associated lesions (ALVaL), Pseudotumors and osteolysis are three major ALTRs related to metallic hip system reported by clinicians and researchers [31].

MAC, including fretting corrosion, corrosion fatigue, wear-assisted corrosion, stress-assisted corrosion and stress-corrosion cracking, is corrosion caused by the combination of mechanical and electrochemical factors [33]. It occurs in a variety of hip implants with modular designs, including the modular-head design, acetabular component design and head-neck/neck-stem taper design [34]. Modularity in hip implants has gained popularity since their

development in the mid-1980s due to its significant advantages such as intraoperative flexibility in implant geometry, more simple revision surgery and reduced cost and inventories. All modular junctions are potential sites for mechanically-assisted corrosion or crevice corrosion, which significantly increase the degradation of the implant and has been thought to be the major source of ions and particles coming from the surface and may cause failures of MOM devices [35-38]. A series of phenomenon occur following the abrasion of oxide film and dramatic acceleration of corrosion in MAC, including changes in oxide film structure and properties (mechanics, electrochemistry), local depletion of oxygen, cathodic shifting in open circuit potential as well as decrease of pH [4]. These MAC-affected factors, in turn, significantly affect MAC and may further increase corrosion susceptibility and corrosion damage of metallic biomaterials [33]. Increase in corrosion rate of metallic biomaterials even after ceasing of MAC has been reported [34]. Meanwhile, byproducts of metallic alloys coming from MAC are known to induce various untoward biological responses [31]. High levels of metal in blood or serum are related with ALTRs, which have only been found in modular conjunctions involving at least one CoCr component [39]. For CoCrMo alloy, the presence of wear debris and metal ions not only lead to increased local tissue inflammation [35], but also may cause metal allergies [40], tissue and DNA damage [41] as well as death of inflammatory cells [42]. Implantation of MOM arthroplasty has been associated with hypersensitivity reactions to metal ions [43]. Co and Cr ions may be toxic at high concentrations and are able to react with endogenous target molecules such as DNA, receptors, protein and reactive oxygen species (ROS), dramatically altering the biological environment and resulting in structural and functional damage of target molecules [44]. The concentration of both cobalt and chromium

ions significantly increase in patients after both short-term (<2 years) and long-term (20 years) hip implant surgery [45]. Hexavalent chromium ($Cr^{6+}$), classified as group 1 carcinogen, has been reported to be formed and released from CoCr implants [46]. Co ions are known to significantly inhibit osteoblast proliferation and function, causing decreased lymphocyte proliferation and abnormal chemokine secretion [47], and have been associated with neurological and cardiac manifestations in patients with MoM implants [48]. When MAC occurs, cathodic shifts of voltage on implant surface may significantly alter not only electrochemistry reaction, but also cell metabolism and behavior. Recent studies show that, at sufficiently negative voltage (below -400 mV (vs Ag/AgCl)), cell death on CoCrMo alloy by apoptosis is not driven by metal ions and particles, but by reduction reactions [49, 50].

**New perspective---Biological response affects corrosion of CoCrMo alloy**

One important process in the implant-body interaction system is the immune response of the local cells near the implant. It is known that the implantation of medical device as well as the debris and metal ions from MAC will induce inflammatory responses of the body. Inflammatory cells use acid and ROS to attack invading bacteria and foreign bodies [51-53]. It has been known that a series of ROS, including superoxide, hydrogen peroxide, hydroxyl radical, hypochlorous acid, can be induced by a variety of soluble and particulate stimuli in inflammatory cells such as macrophages osteoclasts and neutrophils (Figure 1.1) [54, 55]. The adhesion and activation of inflammatory cells or phagocytic cells produces a microenvironment between the cell membrane and the surface of metal [52]. The biomaterial surface in this region is susceptible to locally high concentrations of degradative and oxidative

agents [55, 56]. Thus, the local biological process of inflammatory cells are likely to affect the biodegradation and corrosion of the implant.

There have been several studies on inflammatory cells and how their released chemical species affect metallic biomaterials. Cadosh, et al. [57, 58] reported in vitro biocorrosion of stainless steel and titanium alloy by inflammatory cells (human mature osteoclasts). Lin, et al. showed that macrophage cells altered the surface oxide compositions of CoCrMo alloy after 3 days in cell culture medium and the results supported their hypothesis that macrophage released reactive chemical species (RCS) such as NO and ROS reacted with the surface and changed the oxide layer [59]. Pan, et al. investigated the effect of $H_2O_2$ on titanium surface and found that $H_2O_2$ addition into PBS increases the growth rate of oxide film and facilitates the phosphate ions into the oxide film [60]. Bearinger et al. applied electrochemical atomic force microscopy( ECAFM) to study the influence of $H_2O_2$ modified PBS solution on CP Ti alloy oxide and showed less oxide dome coarsening and significant change of oxide resistance and capacitance due to the presence of $H_2O_2$ [61]. Mabilleau et al. studied the effect of macrophage and bacteria on the corrosion behavior of pure titanium using AFM and reported that activated inflammatory cells and bacteria can release various oxidants which led to Ti corrosion at nanometric scale [62]. Royhman investigated the influence of pH in simulated artificial joint fluid on Ti6Al4V and CoCrMo alloy and showed that increased acidity resulted in decreased corrosion resistance [63]. Brooks et al. evaluated the effect simulated inflammatory solutions on titanium electrochemistry and found that inflammatory conditions with $H_2O_2$ led to the formation of a thin and defective film on Cp Ti and Ti6Al4V and increased

the corrosion susceptibility of titanium alloy [64]. Garcia et al. studied the effect of simulated inflammatory condition on cp Ti and Stainless steel and found that simulated inflammation conditions led to significant modifications on surface composition, surface roughness and surface energy on both alloys while $H_2O_2$ induced stronger changes on cp Ti compared to stainless steel surface [65].

Recently, new evidence of direct in vivo inflammatory cell-induced corrosion (ICIC) of CoCrMo alloy in retrieved MOM and MOP hip and knee implants has been first reported by Gilbert et al. [66]. Their study found evidences that cellular attack may leave patterns of corrosion damage on retrieved CoCrMo implant surfaces with or without MAC. This study indicates that inflammatory cells may be able to attach to implant surface and release acid and ROS (e.g. $H_2O_2$) driving the corrosion of CoCrMo alloy even without wear or fretting. Metallic iron, which is known to further aggravate inflammation in the presence of reactive oxygen species [67, 68], has been found consistently on CoCrMo components in regions undergoing extensive corrosive attack by the phagocytic cells [66]. Thus, Fenton reaction (the reaction between iron ions and $H_2O_2$), which is known to produce a series of highly oxidative agents, may play an important role in facilitating the in vivo ICIC of CoCrMo alloy. This study raises significant new questions about the mechanism of corrosion of CoCrMo alloy in vivo and the clinical consequences of such corrosion interactions. Recent study by Laura et al. investigated the clinical relevance of ICIC in 100 CoCr alloy hips and found 59% of the implants showed evidence of surface damage associated with ICIC and there was a significant association between the ICIC patterns and aseptic loosening for the ASR and Duron modular

systems [69]. Munoz et al. studied the corrosion behavior of CoCrMo alloy in human synovial fluids in patients with different degree of inflammation and found that CoCrMo electrochemistry is significantly altered by synovial fluid and is affected by patient inflammation [70]. Reactive oxygen species are thought to play a significant role in determining the cathodic and anodic electrochemical response of CoCrMo alloy.

The observation of ICIC on CoCrMo alloy alters current one-way perspective of implant-biology interaction. Local biology (e.g. inflammatory cells) may induce implant corrosion and it is likely that metal ions and corrosion debris released from ICIC further stimulate local biological system and form a positive feedback process which is self-sustaining. However, the ICIC mechanism is not well understood. Which cell types are involved in the process is unknown and what chemical species the inflammatory cells or phagocytic cells use to induce CoCrMo corrosion have not been studied. The clinically observed corrosion phenomena hasn't yet been fully reproduced in laboratory by research community. The inflammatory cell-based solution chemistry appears to be one important element based on current knowledge. Thus, it is of great significance to understand how the simulated inflammatory conditions affect the electrochemistry of CoCrMo alloy.

Inflammatory cells like macrophages and neutrophils are able to secret more than 100 substances, which influence almost every aspect of the immune and inflammatory responses [71]. Among them, ROS and HCl, which possess high oxidizing ability compared to metal alloys or have the power to increase oxidative power of the solution, are most likely to induce ICIC of CoCrMo alloy. Reactive oxygen species released by mononuclear phagocytes includes: $H_2O_2$,

HClO, superoxide and hydroxyl radicals [52, 55, 71, 72]. Highly oxidative free radicals (hydroxyl radicals) can be produced from Fenton reaction ($Fe^{3+}$, $Fe^{2+}$, $H_2O_2$), which is widely used as oxidative agent in industry [73] and may be another important contributor to ICIC of CoCrMo alloy. Meanwhile, metal ions released from CoCrMo alloy, such as Co, Cr, Mo ions, can react with $H_2O_2$ and induce a series of Fenton-like reactions [68, 74], which may further increase the oxidizing power of the solution and damage CoCrMo oxide. Thus, there is need to investigate if these inflammatory species ($H_2O_2$, HCl, HClO and Fenton reaction) are able to influence the corrosion susceptibility of CoCrMo alloy.

CoCrMo alloys receive a high degree corrosion resistance due to the spontaneously formed 1-10 nm oxide film on the surface [75, 76]. Under normal biological conditions, these oxide films are stable and protect the bulk material from reacting with body fluid. However, these oxide film are actually dynamic, being able to react with specific in vivo solution elements, and highly surface voltage dependent [77]. Any factor affecting the surface potential might influence the microstructure and chemistry of the oxide film, leading to significant changes in its mechanical and corrosion properties [4, 5]. Inflammatory cell based chemical species such as ROS are highly reactive and potentially able to alter the oxide film and the corrosion behavior of CoCrMo alloy. Thus, it is important to better understand them under simulated inflammatory conditions, which can be used to develop better heat treatment and processing techniques of CoCrMo alloy and control corrosion of implant devices.

Fretting corrosion is one corrosion mechanism under the category of MAC and is the

corrosion caused by cyclic micro-motion (<100 um) on metal surface [34]. Fretting corrosion

and its associated reactions are thought to be a major concern for MOM modular implants [8,

78, 79]. Its mechanism has been widely studied and well documented [33, 34, 37, 80]. A

common characteristic of fretting corrosion is the cathodic voltage excursion. The voltage drop

can be -800 mV (vs Ag/AgCl) for CoCrMo alloy [81], which is sufficiently negative to induce cell

death on CoCrMo surface within 2h [49]. It is known that solution factors (solution species,

pH) significantly affect fretting corrosion response of CoCrMo alloy couples [10, 82]. Surface

potential, which influences both cell functions and oxide resistance of metallic biomaterials

[49, 50, 83, 84] may be altered by the combination effect of fretting motion and simulated

inflammatory solution. Thus, understanding the effect of simulated inflammatory conditions

on fretting corrosion behavior of CoCrMo couples will help in explaining observed ICIC and

fretting corrosion damage on CoCrMo bearing surfaces and their related biological processes.

Fretting corrosion on metallic biomaterials causes disruption and repassivation of oxide

film and burst release of electrons on implant surface, which lead to time-dependent transient

or sustained cathodic voltage excursion [34, 85]. These voltage shifts change the resistance

and capacitance of the oxide film of metallic biomaterials and might affect the behavior of

cells surrounding the implant [49, 50, 86, 87]. The extent of voltage drop depends on factors

such as the extent of fretting motion and the impedance of the surface [34]. The total exposed

area of the implant alters the extrinsic impedance of the alloy and therefore can potentially

affect the voltage shifts during fretting corrosion. However, to date no research has been done

to assess how the impedance of the exposed area affects voltage excursions during fretting

corrosion. Understanding the impedance based-area effect on voltage shifts will provide meaningful information for designing hip implants and measuring the exposed area of implants.

## 1.2 Objectives

The objective of this research is to explore the mechanism of inflammatory cell induced corrosion and better understand the role biological responses may play in implant corrosion. This research aims to understand how SI conditions (ROS, pH, Fenton reaction) affect the electrochemistry, oxide film and fretting corrosion behavior of CoCrMo alloy. Electrochemical corrosion experiments including OCP test, anodic polarization and electrochemical impedance spectroscopy (EIS) will be applied for assessing electrochemistry performance of CoCrMo alloy in simulated inflammatory solution. A customized pin-on-disk fretting corrosion system [34] will be used to evaluate the fretting corrosion performance, which includes fretting currents, coefficient of friction, normal load, tangential forces, displacement, etc., at different potentials and SI solutions. The fretting corrosion system will be applied in investigating the area-dependent impedance-based voltage shifts during fretting corrosion of Ti-6Al-4V biomaterials. Scanning electron microscopy (SEM) and digital optical microscopy will be applied to characterize CoCrMo surface. In-situ electrochemical AFM will be used to image the oxide behavior of CoCrMo alloy at SI solutions and electrochemical information will be simultaneously recorded or controlled.

## 1.3 Specific aims and Hypothesis

### 1.3.1 Specific aim 1

To evaluate the effect of SI conditions (hydrogen peroxide, pH, iron ions) on corrosion behavior of CoCrMo alloy in PBS solution using electrochemical tests.

**Hypothesis:**

a. Corrosion behavior of CoCrMo alloy is solution dependent. Reactive oxygen species ($H_2O_2$, $OH^.$) and Fenton reactions may induce corrosion of CoCrMo alloy in a concentration-dependent way.

b. Different concentrations of $H_2O_2$, pH and Fenton reactions ($Fe^{2+}/Fe^{3+}$, $H_2O_2$) will alter Open circuit potential (OCP), polarization behavior and impedance of CoCrMo alloy in PBS

### 1.3.2 Specific aim 2

To investigate the effect of pH (HCl) and inflammatory species hypoclorous acid on the electrochemical behavior of CoCrMo alloy

**Hypothesis:**

a. The presence of inflammatory cells-based acids (HClO, HCl) may increase corrosion susceptibility of CoCrMo alloy

b. OCP, polarization behavior and oxide impedance behavior will be affected by simulated inflammatory acid (HClO, HCl)

### 1.3.3 Specific aim 3

To image how surface oxide of CoCrMo alloy responds to voltage and simulated inflammatory

species ($H_2O_2$) using in-situ Electrochemical AFM. To investigate if any changes of oxide surface morphology observed can be related to the electrochemical behavior of the alloy.

**Hypothesis:**

a. Surface oxide of CoCrMo in simulated physiological solutions (PBS and inflammatory condtion) changes with time.

b. ROS ($H_2O_2$) influences surface oxide (topography, surface roughness, chemistry) and corrosion of CoCrMo alloy

c. Combination voltage and $H_2O_2$ affects surface oxide and electrochemistry of CoCrMo alloy

### 1.3.4 Specific aim 4

To study the effect of simulated inflammatory conditions ($H_2O_2$, pH, Fenton reaction) on fretting corrosion behavior of CoCrMo couples.

**Hypothesis:**

a. Fretting corrosion response of CoCrMo alloy is potential dependent and solution chemistry dependent.

b. Simulated inflammatory conditions (pH, $H_2O_2$, Fenton reaction) will influence static corrosion currents, fretting corrosion current, coefficient of friction (COF) and work done per fretting cycle.

### 1.3.5 Specific aim 5

To use an impedance-based fretting corrosion model to investigate how surface impedance and electrode area affects the time-dependent voltage excursion during fretting corrosion of

Ti-6Al-4V/Ti-6A-l4V couples in PBS solution.

**Hypothesis:**

Under fretting conditions, voltage drops of metallic biomaterials are electrode area and materials dependent and governed by the surface impedance.

## 1.4 Structure of Dissertation

This dissertation is based on a number of manuscripts that are either published or intended to be published in peer-reviewed journals.

Chapter 1 primarily introduces the background and significance of this study and includes the research objective, specific aims and hypotheses of this work.

Chapter 2 investigates the effects of simulated inflammatory species including $H_2O_2$, pH and Fenton reaction on the corrosion behavior of CoCrMo alloy using electrochemical corrosion tests.

Chapter 3 explores how inflammatory cell-based acid (HClO and HCl) affect the electrochemistry of CoCrMo alloy. OCP measurement, polarization tests and EIS analysis are conducted.

Chapter 4 presents the results of the in-situ electrochemical atomic force microscopy with electrochemical tests on CoCrMo alloy in simulated inflammatory species ($H_2O_2$) modified PBS solution. The effects of both voltage and inflammation-based solution chemistry on CoCrMo oxide (surface morphology and roughness) and corrosion behavior are investigated at nanoscale.

Chapter 5 presents the effect of simulated inflammatory conditions (pH, $H_2O_2$ and Fenton

reaction) on fretting corrosion performance of CoCrMo/CoCrMo interfaces utilizing a customized fretting corrosion system.

Chapter 6 investigates how the area of electrode and surface impedance characteristics affect the cathodic voltage excursion during fretting corrosion of Ti-6Al-4V biomaterials using an impedance-based fretting corrosion model.

Chapter 7 includes the synthesis of the results from this work.

Chapter 8 presents the conclusion of the dissertation

Chapter 9 provides suggestions to future work based on findings on this dissertation.
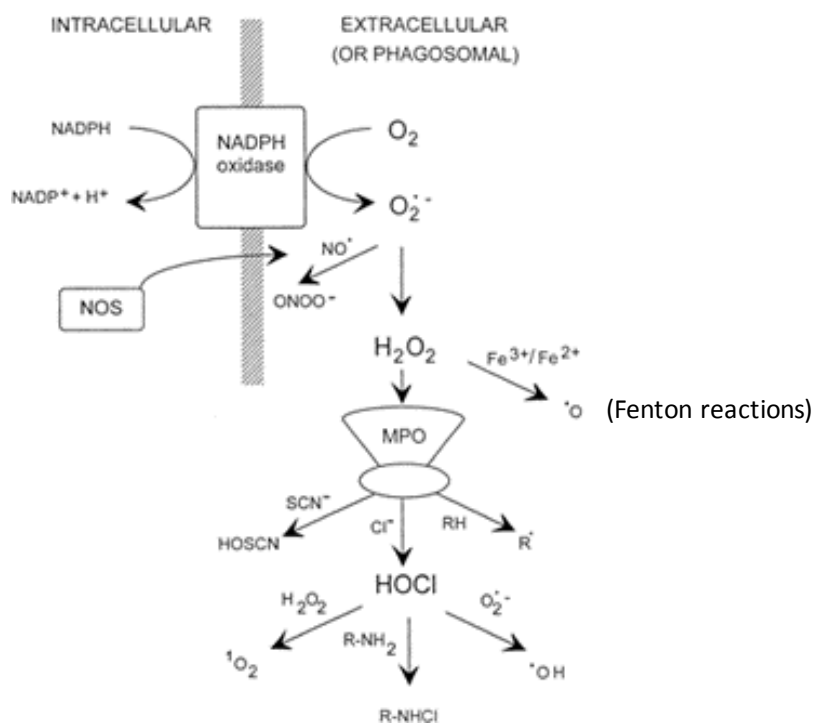


Figure 1.1 Possible oxidant generating reactions with stimulated neutrophils. NOS, nitric oxide synthase; MPO, myeloperoxidase [55].

# Chapter 2 The effect of simulated inflammatory conditions and Fenton chemistry on the electrochemistry of CoCrMo alloy

## 2.1 Introduction

Cobalt-chromium-molybdenum (Co-Cr-Mo) alloys (ASTM F-75 and F-1537) have been widely used in biomedical implants since their development in the early 1920's. They have been widely used as dental alloy and biomaterials for orthopedic, spinal and cardiovascular implant applications due to their outstanding mechanical properties and excellent biocompatibility [4, 5]. However, the degradation of metals caused by mechanical surface disruption combined with corrosion remains as a significant concern [8-13].

Recently, there have been serious concerns raised about the effects of ions and particles released from CoCrMo based alloys on the body's responses. Wear and corrosion damage of the implant are thought to be associated with adverse effects on the body which have been described as pseudotumors [14], adverse reactions to metal debris [15, 16] and adverse local tissue reactions [35, 88].

MAC or tribocorrosion has been thought to be the major source of ions and particles coming from the surface and may be associated with some revisions of Metal-On-Metal devices [14, 15]. Adverse body reactions in patients after hip arthroplasty due to MAC have been reported [32, 89]. The implantation of medical devices and the debris caused by MAC may induce inflammatory responses of the body. It has been known that superoxide, hydrogen peroxide and hydroxyl radical production can be induced by a variety of soluble and

particulate stimuli in neutrophils and other phagocytic cells. Inflammatory cells are known to use acid and reactive oxygen species (ROS) to attack invading foreign bodies [51, 53, 54, 56]. The adhesion and activation of macrophages produces unique and aggressive microenvironments between the cell membrane and the materials surface. The metallic biomaterials surface may be susceptible to potentially high concentrations of degradative and oxidative agents (Figure 2.1) [72, 90]. Currently, there are several studies on cells and how their released biochemical species affect metallic biomaterials [52, 55, 57, 58]. Cadosh et al. [57, 58] have reported in vitro biocorrosion of stainless steel and titanium by osteoclasts. Lin et al. [59] have reported that macrophage cells and their released reactive chemical species (RCS) alter the surface oxide compositions of CoCrMo alloy. Munoz et al. [70] studied the CoCrMo electrochemistry in human synovial fluids and found that inflammatory degree of the patient significantly affects the corrosion behavior of CoCrMo alloy and cell reaction related ROS are probably the main contributors.

Recently, evidences of direct inflammatory cell induced corrosion of CoCrMo alloy in retrieved hip and knee implants have been reported [66]. They reported evidence of apparent cell-based patterns of corrosion damage in retrieved implant surfaces with or without MAC. This raises significant new questions about the mechanism of in vivo corrosion of CoCrMo alloy and the clinical consequences of such corrosion interactions [69]. Iron ions are known be present in vivo in ferritins (proteins that sequester iron) and may further aggravate inflammation in the presence of ROS [67] and Fenton reactions. These ions can be released and interact with inflammatory ROS to adversely affect corrosion behavior of CoCrMo. The

Fenton reaction or Fenton-like reactions are known to produce highly oxidizing agents such as hydroxyl radical and superoxide anions [68]. Therefore, cell-released chemical species as well as Fenton reactions are thought to be involved in inflammatory-cell-induced (ICI) corrosion processes and may accelerate the corrosion of CoCrMo alloy in vivo.

However, the ICI corrosion phenomenon is poorly understood and there have been few systematic studies on how inflammatory cell-released species and Fenton reactions influence the corrosion behavior of CoCrMo [63]. The purpose of this study was to evaluate how simulated inflammatory conditions ($H_2O_2$, pH and iron ions) affects the electrochemistry of CoCrMo alloy. Electrochemical measurements were conducted in SI solutions with varied pH, hydrogen peroxide concentrations and iron ions. Physiologically-possible concentrations of ROS species and Fenton reaction species were covered in these experiments. The underlying hypothesis is that the presence of ROS in joint fluids will alter the oxide film corrosion resistance and increase the oxidizing power of the solution to increase corrosion of CoCrMo.

## 2.2 Materials & Methods

**Sample, corrosion cell and electrolyte:** CoCrMo (ASTM F-1537 high carbon) disks were prepared by polishing through a series of grits to 600 grit with wet emery paper. A three electrode electrochemical cell was used where the CoCrMo alloy was the working electrode, the counter electrode was a carbon rod and a saturated silver-silver chloride (Ag/AgCl) reference electrode (0.22V vs NHE) was used. A potentiostat (Solartron 1280C Potentiostat/Frequency Response Analyzer, Solartron Analytical Inc.,) was used for all electrochemical testing with software for control and acquisition of electrochemical signals

(Corrware 2.0 for polarization test and Zplot 2.0 for impedance study).

SI Solutions were comprised phosphate buffered saline (PBS, Sigma) made with distilled water with additions of ROS-specific chemical species. Different pH (1, 3, 5, 7.4) and simulated inflammatory solutions were created by adding hydrochloric acid (HCl) to adjust the pH and hydrogen peroxide which ranged from 0.1 mM to 30 mM to cover physiologically possible levels [33, 91]. For Fenton-like reaction tests, 10 mM $H_2O_2$ was added into PBS solutions first and then ferric chloride ($FeCl_3$) powders were added to reach a concentration of 0.1 mM. This composition was termed Fenton chemistry or Fenton reagent.

**Electrochemical measurements**

**Open circuit potential vs time**: OCP of CoCrMo disks was monitored for at least 0.5 h for each solution. $H_2O_2$ was added after the start of the test in PBS solution to identify the change in OCP due to the additions.

**Polarization tests**: After the electrolyte was added and the OCP reached a stable level, polarization tests were performed from -1 V to +1 V with a scan rate of 1 mV/s. The polarization curves in different simulated inflammatory conditions were compared and were used to identify the corrosion current density ($I_{corr}$), the corrosion potential ($E_{corr}$). The polarization test in Fenton reagent solution was started at the voltage 30 mV below OCP.

**Electrochemical Impedance Spectroscopy analysis**: EIS test were performed by immersing samples in solution for 15 minutes, then potentiostatically holding at OCP, and then applying 10 mV sinusoidal voltage superimposed on the OCP. The frequency of the sinusoidal

voltage ranged from 20 kHz to 0.01 Hz. Impedance magnitude and phase angle were obtained and used for analysis of the surface impedance. The data were analyzed using the Randles circuit model to determine electrochemical characteristics of the interface. The standard Randles circuit contains $R_s$, solution resistor, in series with a parallel combination of an oxide resistor ($R_{ox}$) and capacitance ($C_{ox}$) of the electrochemical double layer. The capacitance element was modified in this study to a constant phase element (CPE) due to the non-ideal behavior of the interface.

In all results, tests were repeated at least 3 times. Only representative plots are presented, however, the behavior observed is consistent across repeated testing.

**Statistical analyses**

Statistical analyses were performed using analysis of variance (ANOVA) methods followed by Tukey's post hoc analysis to assess the significance of inflammatory condition ($H_2O_2$, acid) and Fenton reaction on OCP, Randles circuit parameters ($R_{ox}$, C, $R_s$, alpha) and anodic polarization results ($E_{corr}$, $I_{corr}$). One-way ANOVA was used and a p-level of 0.05 was considered significant in all statistical tests.

**2.3 Results**

**2.3.1 Open circuit potential behavior**

As an example of OCP tests with $H_2O_2$ additions, Figure 2.2 A illustrates how the OCP evolution with time of CoCrMo alloy in PBS solutions was affected by the addition of 30 mM $H_2O_2$ in different pH solutions. OCP becomes significantly more positive due to the addition of

$H_2O_2$, showing at least 0.5 V positive increase at all pHs. The OCP also increases with decreasing pH in PBS solutions with 30 mM $H_2O_2$. At pH 7.4, the OCP is about 0.35 V in PBS with $H_2O_2$ and shifts positively to above 0.6 V in pH 1 condition.

Figure 2.2B presents the summary of OCP at all tested pHs and $H_2O_2$ concentrations in PBS. Only small decreases (less than 0.2) of pH were observed even with the addition of 30 mM $H_2O_2$ at pH 7.45. Among all the conditions, pH 1 solution with 30 mM $H_2O_2$ shows the highest OCP (0.62 V) while OCP in PBS-only solution (pH 7.4) is the lowest (-0.2 V). Even with the addition of only 0.1 mM $H_2O_2$, OCP jumps to above 0.1V region at all tested pHs. The OCP evolution with time of CoCrMo in PBS solution at pH 7.4 with the addition of Fenton's reagent is shown in Figure 2.2C. The OCP shifts from -0.3 V to 0.35 V with the addition of 10 mM $H_2O_2$ and further jumped to 0.6 V after 0.1 mM $FeCl_3$ was added. The dashed line in Figure 2.2C represents a typical CoCrMo OCP in PBS.

### 2.3.2 Polarization behavior

**$H_2O_2$ concentration effect at pH 7.4**

Figure 2.3A presents the polarization curves of CoCrMo in PBS solution with different $H_2O_2$ concentrations at pH 7.4 [66]. Large increases in corrosion current densities are observed with the increase of $H_2O_2$ concentration. Note, this result is from our previous study and is cited here for comparison purposes.

**pH effect in solution with 30 mM $H_2O_2$**

Figure 2.3B shows representative plots of the polarization behavior of CoCrMo in

different SI solutions with varying pH and 30 mM $H_2O_2$. Leftward shifts of the polarization curves in Figure 2.3B were observed with decreases in pH indicating a reduced corrosion current density with lower pH. In both the cathodic and anodic branches, the largest current density was observed in pH 7.4 solution. The current density became 20 times larger as pH increases from 1 (0.7 uA/cm$^2$) to 7.4 (14 uA/cm$^2$). Corrosion potential stays at the same level (around 0.25V) as pH decreases from 7.4 to 3 while it decreases to around 0 V at pH 1. Among the investigated pHs, pH 1 condition exhibits the widest passivation region and shows the lowest current density at all voltages. These results show that for 30 mM $H_2O_2$ in PBS, the most severe corrosion occurs at physiologic pH (7.4).

**Fenton reaction**

Representative potentiodynamic polarization plots for CoCrMo in PBS solution and PBS solution with Fenton reagent are shown in Figure 2.3C. The corrosion potential is significantly more electropositive in Fenton reagent (0.58 V) than in the PBS only case (-0.7 V). In addition, the corrosion current is about 5 times larger in the Fenton reagent condition (13.2 uA/cm$^2$) than that in PBS solution (2.2 uA/cm$^2$), showing an increase susceptibility to corrosion of CoCrMo alloy due to the presence of Fenton reagent.

Results of corrosion potential ($E_{corr}$) and corrosion current ($I_{corr}$) measured from the polarization tests with 30 mM $H_2O_2$ at different pHs are shown in Figure 2.4 A and 2.4 B. The values for $I_{corr}$ and $E_{corr}$ for all investigated SI conditions are presented in Table 2.1. Besides the results shown above, it is interesting to note that the corrosion currents in pH 1 and pH 3 PBS solution with 30 mM $H_2O_2$ are smaller than that in PBS only solution. $E_{corr}$ in the polarization

curves doesn't line up with OCP and this is because the polarization test was started at -1V.

### 2.3.3 Electrochemical impedance spectroscopy behavior

Representative Bode plots obtained from EIS tests for CoCrMo alloy under different pH and $H_2O_2$ concentrations are shown in Figure 2.5 A-E. The EIS circuit parameters, polarization resistance, capacitance and CPE exponent, alpha are presented in Figure 2.6. All the values for Rs, $R_{ox}$, $CPE_{ox}$, α are presented in Table 2.2.

**$H_2O_2$ concentration effect at pH 7.4 (cited from previous study for comparison) [66]**

The variation in impedance of CoCrMo alloy in PBS solution (pH 7.4), with varying $H_2O_2$ concentrations are shown in Figure 2.5A and 2.5B. The presence of as small as 0.1 mM $H_2O_2$ statistically decreased the oxide resistance (P < 0.05) about 10 times and 30 mM $H_2O_2$ further decreased it over 100 times compared to PBS only.

**pH effect in solutions with 30mM $H_2O_2$**

Figure 2.5C and 2.5D shows the Bode plots in different pH solutions with the addition of 30mM $H_2O_2$ and are compared with the PBS only case. Under all pH conditions (with 30 mM $H_2O_2$), the low-frequency impedance magnitude (Figure 2.5C, which reflects the oxide resistance) decreased with the narrowing of the phase angle (Figure 2.5D). The drop of oxide resistance compared to PBS alone was the largest (over two orders of magnitude) in pH 7.4 $H_2O_2$ containing solution. As pH decreases from 7.4 to 1, the oxide resistance increases significantly from $5*10^3$ Ω $cm^2$ to $1.62*10^5$ Ω $cm^2$ while the capacitance exhibits the opposite trend, showing the largest value (55 μF/$cm^2$) in pH 7.4 solution and smallest (31 μF/$cm^2$) under

pH 1 condition.

**Fenton reaction on EIS**

Reprehensive Bode plots obtained from EIS tests for CoCrMo under Fenton reagent conditions (10 mM $H_2O_2$, 0.1 mM $FeCl_3$) in PBS solution and PBS only solution case are shown in Figure 2.5E and 2.5F. A drop in low-frequency impedance and narrowing of the frequency range of the phase angle is shown in PBS solution with the addition of the Fenton Reagent. Compared with the PBS only case ($R_{ox}$:4.8*$10^5$ Ω cm$^2$, $CPE_{ox}$:30 uF/cm$^2$), the presence of Fenton reagent decreased the oxide resistance about 15 times to 3.2*$10^4$ Ω cm$^2$, and increased the capacitance about 1.5 times to 45 uF/cm$^2$).

**Summary of impedance results**

The effects of 30 mM $H_2O_2$ and pH (1 to 7.4) on the Randles parameters are summarized in Figure 2.6. Figure 2.6A shows that solution resistance increases (P<0.05) as pH gets higher. Oxide resistance (Figure 2.6B) in 30 mM $H_2O_2$ solutions are significantly lower (P<0.05) than that in PBS only condition regardless of the solution pH and show an increase at lower pH. Figure 2.6C shows an inverse' correlation to $R_{ox}$ where C decreased with lower pH and C was larger in $H_2O_2$-pH 7.4 solution than PBS only solution. The CPE exponent (Figure 2.6D) at pH 7.4 conditions are significantly lower (P<0.05) than that in pH 1 and pH 3 solutions with 30 mM $H_2O_2$.

**2.3.4 Statistical analyses**

OCP is significantly affected by $H_2O_2$ concentration at any specific pH (p<0.05). OCP is

significantly affected by pH at any specific $H_2O_2$ concentration (p<0.05). Acid significantly affects $E_{corr}$ (p=0.0002) and $I_{corr}$ (p=4.1* $10^{-7}$) in 30 mM $H_2O_2$ modified PBS solutions. For $I_{corr}$, only pH 1 and 3 solutions were not significantly different. For $E_{corr}$, only pH 1 solution has significantly different (lower) value than that of other conditions (p<0.05). PBS solution has significantly lower $E_{corr}$ and different $I_{corr}$ than those of any specific pH solution with 30 mM $H_2O_2$ (p<0.05). pH significantly affects $R_s$ (p=0.0096), $R_{ox}$ (p=0.0001), C (p=1.2*$10^{-5}$) and alpha (p=0.012) in PBS solutions with 30 mM $H_2O_2$. For $R_s$, pH 1 and 5, and pH 1 and 7 solutions were significantly different. $R_s$ in PBS solution is significantly higher than that in pH 1 PBS solution with 30 mM $H_2O_2$ (p=0.01). No significant differences were found between PBS and 30 mM $H_2O_2$ modified PBS solutions at other pH's (p>0.05). For $R_{ox}$ and C, pH 1 and 5, pH 1 and 7, pH 3 and 5, and pH 3 and 7 solutions were significantly different. $R_{ox}$ in PBS solution is significantly higher than that in any specific pH solution with 30 mM $H_2O_2$ (p<0.05). C in PBS solution is significant lower than that in pH 5 (p=0.0025) and pH 7 (p=6.1*$10^{-5}$) solutions with 30 mM $H_2O_2$. While no significant difference was found between PBS and lower pH (pH 1 and pH 3) solutions with 30 mM $H_2O_2$ (p>0.05). For alpha, only pH 1 and 7, pH 3 and 7 are significantly different. No significant difference were found between PBS and 30 mM $H_2O_2$ modified PBS solution at any specific pH.

**2.4 Discussion**

This study has shown that the corrosion susceptibility of CoCrMo alloys in PBS solutions is highly sensitive to both $H_2O_2$ and $H^+$ ion concentration. Simulated inflammatory solutions affect both the resistive and capacitive character of the oxide, but also introduces a highly

oxidizing solution condition. This combined effect results in a significant increase in corrosion currents.

**The influence of $H_2O_2$ on CoCrMo electrochemistry**

The addition of $H_2O_2$ largely raises the OCP of CoCrMo alloy, indicating that the solution becomes more oxidizing due to the presence of $H_2O_2$ and results in increasing the defected nature of the oxide film. In comparison to neutral PBS condition, $H_2O_2$ containing solutions exhibit significantly lower oxide resistance at all tested pHs and higher capacitance at pH 5 and pH 7 (Figure 2.6). Therefore, the susceptibility to corrosion of CoCrMo alloy increases the most as a result of addition of $H_2O_2$ near normal physiological pH (near pH 7) and that as pH drops, a more passivating surface develops, increasing corrosion resistance. Previous studies by Brooks et al. [64] has shown that under simulated inflammation condition where $H_2O_2$ is present, the corrosion susceptibility of titanium alloy is significantly increased.

**pH effect on CoCrMo electrochemistry in $H_2O_2$ contained solution**

In $H_2O_2$ containing solutions, the increase of acidity increases oxide resistance and decreases capacitance. Interestingly, corrosion susceptibility decreases in more acidic solutions. This is further supported by the polarization test results where the corrosion current becomes significantly smaller in lower pH conditions. This finding is counterintuitive in that increases in acidity are normally associated with accelerate corrosion. Importantly, this result indicates that when $H_2O_2$ is released by inflammatory cells in vivo, neutral pH may be the most aggressive condition that facilitates the corrosion of CoCrMo alloy. In addition, development of more acidic environments, in the presence of $H_2O_2$ may actually cause the surface oxide

film to become more resistant to corrosion attack.

**Fenton reactions on CoCrMo electrochemistry**

Significant increases of OCP (Figure 2.2C), corrosion potential, corrosion current (Figure 2.4) and large decreases of oxide impedance (Figure 2.6) indicate that the presence of Fenton's reagent increases the corrosion susceptibility of CoCrMo alloy, resulting in a more defective and less stable oxide film on the surface. This implies that when transition metal cations, which includes $Co^{2+}$, $Cr^{3+}$. etc, are present in solution, inflammatory species are further enhanced in their oxidizing power and result in greater corrosion susceptibility.

**Possible involved reactions**

The corrosion behavior of CoCrMo alloy under simulated inflammatory conditions is determined by the interaction among solution chemistry (PBS, acid, $H_2O_2$, Fenton reaction) and the surface oxide film. Several possible reactions will be discussed: Anodic reactions at voltages near the OCP are the passivation reactions of metals which produce a protective oxide film on the surface. In normal simulated physiological solutions without reactive oxygen species, $Cr_2O_3$ predominates in the outer layer of oxide when the voltage is below 0.4 V (vs Ag/AgCl) with a small portion of CoO and $MoO_3$. Possible oxide formation reactions are:

$$2Cr + 3H_2O \text{----} Cr_2O_3 + 6H^+ + 6e^-$$

$$Co + H_2O \text{----} CoO + 2H^+ + 2e^-$$

$$Mo + 3H_2O \text{----} MoO_3 + 6H^+ + 6e^-$$
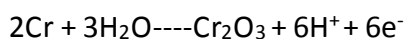
More Co and Mo enter into the passive layer at potentials higher than 0.5 V. CoO is oxidized into $Co_2O_3$ and $Co_3O_4$ while there are Cr (III) oxidized into Cr (VI) in the oxide film [75]. Possible

reactions near and above the transpassive voltage are:

$$Cr_2O_3 + 3H_2O \text{----} 2CrO_3 + 6H^+ + 6e^-$$

$$2CoO + H_2O \text{----} Co_2O_3 + 2H^+ + 2e^-$$

$$3CoO + H_2O \text{----} Co_3O_4 + 2H^+ + 2e^-$$
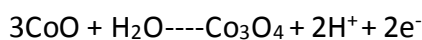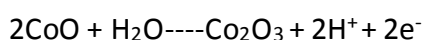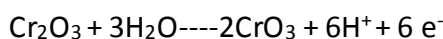
Based on the Pourbaix diagram [92], Cr (VI) species normally presents in solution as $CrO_4^{2-}$ or $HCrO_4^-$ depending on pH while Co dissolves into solution as $Co^{3+}$. At higher voltages, elements will be oxidized into higher valance state species:

$$Cr_2O_3 + 5H_2O \text{----} 2CrO_4^{2-} + 10H^+ + 6e^- \qquad (pH > 6.5) \qquad A$$

$$Cr_2O_3 + 5H_2O \text{----} 2HCrO_4^- + 8H^+ + 6e^- \qquad (pH < 6.5) \qquad B$$

$$CoO + 2H^+ \text{---} Co^{3+} + H_2O + e^- \qquad (pH < 8) \qquad C$$
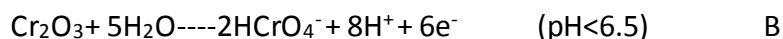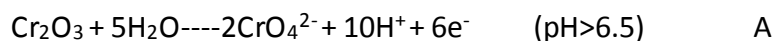
Without species like HCl and $H_2O_2$, CoCrMo alloy is at the normal OCP range from -0.3 V to -0.1 V vs Ag/AgCl. The dominant cathodic half reaction is the dissolved oxygen reduction reaction:

$$O_2 + 4H^+ + 4e^- \text{---} 2H_2O.$$
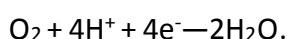
This half-cell reaction has a higher redox potential than that of $Cr_2O_3$ and CoO (reaction A, B, C). Therefore, the oxidation reactions of Cr (III) and Co (II) into Cr (VI) and Co (III) respectively are thermodynamically possible.

Hydrogen evolution reaction occurs when the voltage becomes more negative than OCP and pH drops: $2H^+ + 2e^- \text{---} H_2$. When $H_2O_2$ is present, additional reduction reactions are possible:

$$H_2O_2 + 2H^+ + 2e^- \text{---} 2H_2O$$
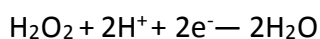
Besides, reactions involving both oxygen and $H_2O_2$ are possible:

$$O_2 + 2H^+ + 2e^- ---H_2O_2 \qquad\qquad H_2O_2 ---O_2 + 2H_2O$$
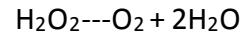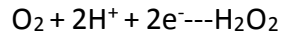
Furthermore, a series of more complex reactions might happen with the presence of $H_2O_2$ and Fe ions based on Fenton chemistry:

$$Fe^{2+} + H_2O_2 ---- Fe^{3+} + OH^{\cdot} + OH^-$$

$$Fe^{3+} + H_2O_2 ---- Fe^{2+} + HO_2^{\cdot} + H^+$$

$$OH^{\cdot} + H_2O_2 ----- H_2O + HO_2^{\cdot}$$

$$HO_2^{\cdot} ---- H^+ + O_2^{\cdot-}$$

$$OH^{\cdot} + H_2O_2 --- O_2^{\cdot-} + H_3O^+$$
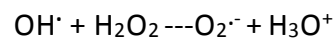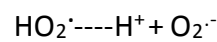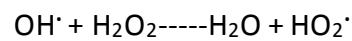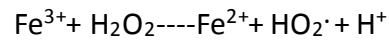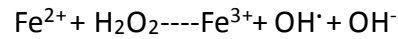
During inflammatory activation, cells release ROS species and iron in ferritins are released [30, 93], resulting in the generation of reactive oxygen intermediate species which will further accelerate corrosion, stimulate the cells and change the redox status of the cells. Moreover, Cr and Co ions are also able to react with $H_2O_2$ to become catalysts in these reactions (the Haber-Weiss Cycle) [94]:

$$M^{n+} + H_2O_2 --- M^{(n+1)+} + OH^{\cdot} + OH^-$$

$$M^{(n+1)+} + O_2^{\cdot-} --- O_2 + M^{n+}$$
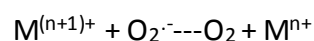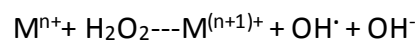
All these reactions are affected by pH and some reactions change the pH dramatically. It is possible these ROS-involved reactions are able to accelerate the corrosion of CoCrMo alloy as well as produce highly toxic metal ions such as Cr (VI) in vivo. These reactions produce highly reactive free radicals like OH• which acts as both signaling molecules and toxic species in vivo [68] and therefore may have significant effects on the degradation of the implant and health of the patient.

**Evan's diagram**

Based on the mixed potential theory [95], the OCP of an electrode stabilizes at the potential where the total anodic current due to the oxidation reactions equals to the total cathodic current produced by cathodic reactions of the hydrogen ion, oxygen or hydrogen peroxide. The Evan's diagram can be applied to explain the variation of OCP and corrosion current at different simulated inflammatory conditions.

**Effect of $H_2O_2$ and $Fe^{3+}$ ions at pH 7.4 in PBS:**

Among all the simulated inflammatory conditions investigated, the corrosion current is the largest at pH 7.4 with 30 mM additions of $H_2O_2$. The cathodic reaction controlled by $H_2O_2$ is:

$$H_2O_2 + 2H^+ + 2e^- — H_2O$$
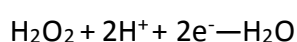
Significant increases of OCP and corrosion current are partly due to the shift of reduction reaction to more positive values when $H_2O_2$ or Fenton reactions are present based on the Evan's diagram (Figure 2.7A). In addition, $H_2O_2$ and Fenton reagent interacts with the oxide film to result in more defective oxide film at pH 7.4 PBS solution. These lead to accelerated anodic reaction and contributes to significant increases in the corrosion current.

**Effect of $H_2O_2$ in acidic solution**

In solutions with both acid and 30 mM $H_2O_2$, the OCP still increases with the lower of pH. The Cathodic reaction shifts upwards to more positive potentials in the lower pH cases, but the anodic reaction shifts to left due to the passivation effect $H_2O_2$ has on CoCrMo oxide in highly acidic conditions (pH 1 and pH 3), resulting in lower corrosion current in low pH

29

solutions compared with the PBS only case (Figure 2.7B). The oxide appears to become less defective as pH decreases from 7.4 to 1 in PBS solutions with 30 mM $H_2O_2$.

**Inflammatory species on cathodic reaction**

Dramatic change of cathodic reaction in the negative voltage range in inflammatory human synovial fluids was also reported by Munoz et al. [70], which are consistent with what was found in this study. They found the variation of cathodic behavior of CoCrMo alloy is both patient and inflammatory degree dependent. The change of redox status of the cells as well as the ROS species such as $H_2O_2$ significantly influences the cathodic reactivity of synovial fluid. Brooks et al. [64] found inflammatory conditions decreased cathodic cathodic slope of Cp Ti when compared to normal conditions.

**Other reactive chemical species**

The in vivo environment is more complex than simulated in vitro experiments. Other powerful reactive chemical species such as nitric oxide (NO), hypochlorous acid (HOCl), superoxide ($O_2^-$) may be present and involved in the cell induced corrosion process [55]. For example, estimation of the $O^{2-}$ production is in the range of 10-50 uM/s and the generation rate of HOCl, a major oxidative species of the neutrophil, is thought to be as high as 134 mM/min in the neutrophil phagosome [72]. Which specie is the prime factor in the corrosion process and the actual concentration of these reactive oxygen species are still not clear. However, their concentrations could be instantaneously very high and create a locally highly corrosive environment between the inflammatory cell membrane and implant surface.

**Clinical relevance**

The findings of this study provide insights into some of the clinical issues associated with total joint replacements. Recent implant retrieval studies have reported evidence of inflammatory cell induced corrosion on titanium alloy [96] and in in vitro tests have shown cathodic inflammatory environment significantly increases the corrosion susceptibility of Ti6Al4V alloy [64]. Furthermore, in vitro biocorrosion induced by activated inflammatory cells on titanium and stainless steel has been reported [57, 58]. These findings further support that activated inflammatory cells and their released ROS have significant influence on increasing the corrosion susceptibility of metallic implants. The current study shows that highly oxidizing conditions are created by ROS resulting in increased open circuit potential of CoCrMo alloy up to the transpassive corrosion region, which may lead to larger amounts of metal ions released into the joint space in vivo. Increased blood cobalt and chromium ions after total hip implant [97] and total knee implant have been reported [98]. Higher cobalt and chromium levels were associated with patients with asymptomatic pseudotumors after metal-on-metal hip resurfacing arthroplasty [14].

Based on our study, the range of physiologically-possible OCP for CoCrMo alloy has been found to be -1 V to 0.65 V, a much wider positive range than what had been thought before. The OCP for CoCrMo alloy in physiologically non-fretting condition is usually thought to be in the range of -0.3 V-0.05 V. A recent study by Munoz et al. [70] reported that the OCP in human synovial fluids of high inflammatory level can reach 0.15 V (vs Ag/AgCl) while -0.1 V is the OCP level in non-inflamed synovial fluid. Their study showed the OCP is more positive in higher inflammatory synovial fluid. Our study reports consistent results that OCP shifts to more

positive values in the presence of inflammatory species such as $H_2O_2$, acid and Fenton reagents.

The in vivo local condition under inflammatory cells might be more aggressive than that in general synovial fluid condition. Thus, it is possible that the OCP could be higher than that (0.15 V) in general synovial fluid due to the presence of ROS, Fenton reagent and higher temperature.

The oxide film on CoCrMo also becomes more defective under severe in vivo local inflammatory conditions. The positive shifts of voltage may have significant effect on cell viability and adjoining tissue. Previous in vitro studies have shown cells cultured on CoCrMo alloy surface treated at +500 mV for 24 h show morphological features of necrosis with near 0% viability [49]. The presence of ROS and Fenton reaction drive OCP to more positive ranges and might be involved in clinically observed tissue reactions. Cr, Co, Fe ions react as catalysts in Fenton-like reactions (e.g., Harber-Weiss reaction). This means, once activated, these reactions are self-sustaining and continually produce highly oxidative radicals like (OH•) to accelerate the corrosion process as long as there is metal ion present. Actually, cells are able to maintain iron homeostasis using ferritin and result in accumulation of iron in the joint [99]. Iron is involved in inflammation of joints and is able to accelerate inflammation when ROS are present [100]. Thus, it is not surprising to see that Fenton-like reactions are widely present in inflammatory processes in vivo and facilitate cell induced corrosion of CoCrMo alloy. Finally, the production and release of significant amounts of inflammatory species (e.g., ROS) may also have adverse effects of the cells and tissues adjacent to the implant as well, potentially

inducing some of the necrosis observed in severe cases of pseudotumor. These effects are an as-yet untested hypothesis in the clinical research community.

2.5 Conclusions

In summary, this study has explored the mechanism of inflammatory cell induced corrosion. The corrosion susceptibility of CoCrMo alloy can be significantly increased by inflammatory cell released reactive oxygen species ($H_2O_2$ & acid) and Fenton reactions. These cell-released chemicals create a highly aggressive environment, raising the oxidizing potential of the solution and decreasing the passivity of the oxide film, facilitate the corrosion on CoCrMo surfaces and demonstrates at least part of the mechanism of inflammatory cell induced corrosion. The addition of $H_2O_2$ and Fenton reagent into PBS solution has two main effects on CoCrMo electrochemistry. On the one hand, it increases the oxidizing power of the solution, significantly altering cathodic behavior of CoCrMo alloy. In addition, it decreases the impedance of surface on CoCrMo, making the oxide more defective and less stable. This combined affect led to significantly increased corrosion currents and significantly more positive OCP. Physiologically possible potential of CoCrMo alloy has been found to be as positive as 0.65 V, a much higher level than previously thought. Increases of OCP to the 0.65 V range raises the oxidizing potential of the solution bringing Cr ion near to +6 state. In $H_2O_2$ inflammatory conditions, decreases of acidity significantly increases the corrosion resistance of CoCrMo alloy and increases the impedance (i.e. resistive) character of the oxide film. Alternatively, pH 7.4 physiological solutions with $H_2O_2$ were the most aggressive in their damage to the CoCrMo surface.
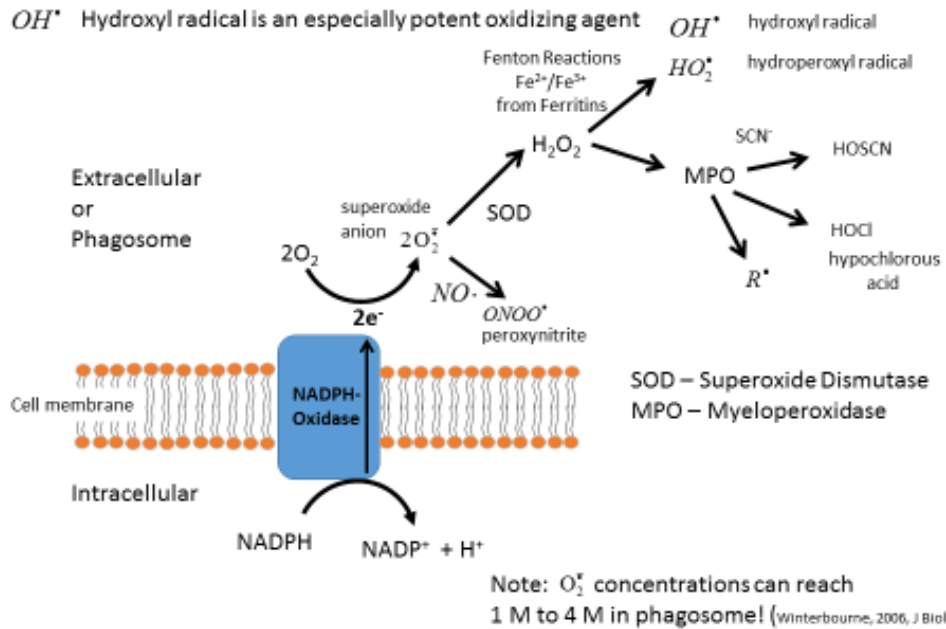
Figure 2.1 ROS generating reactions due to phagocytic cells (e.g., neutrophils [55]). Adapted with permission [90].
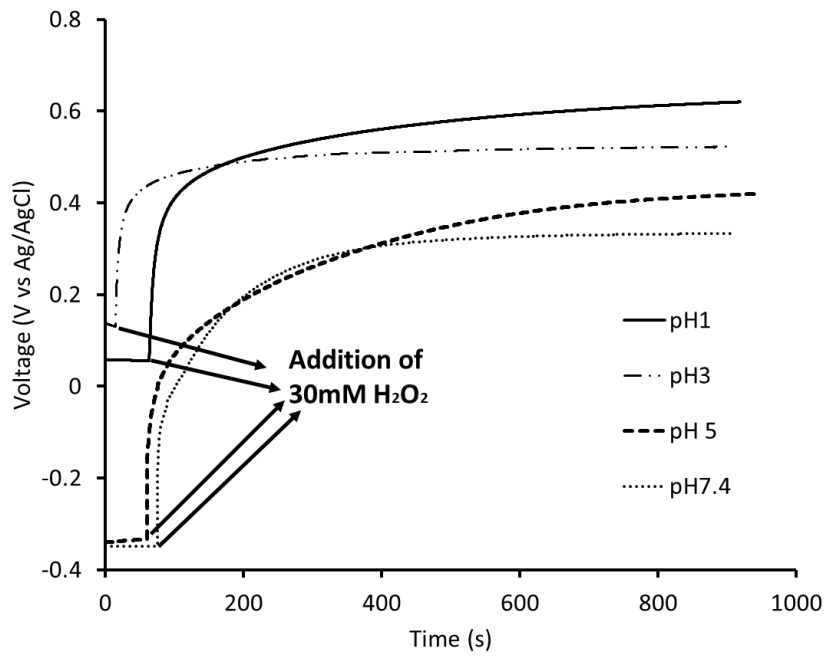
A
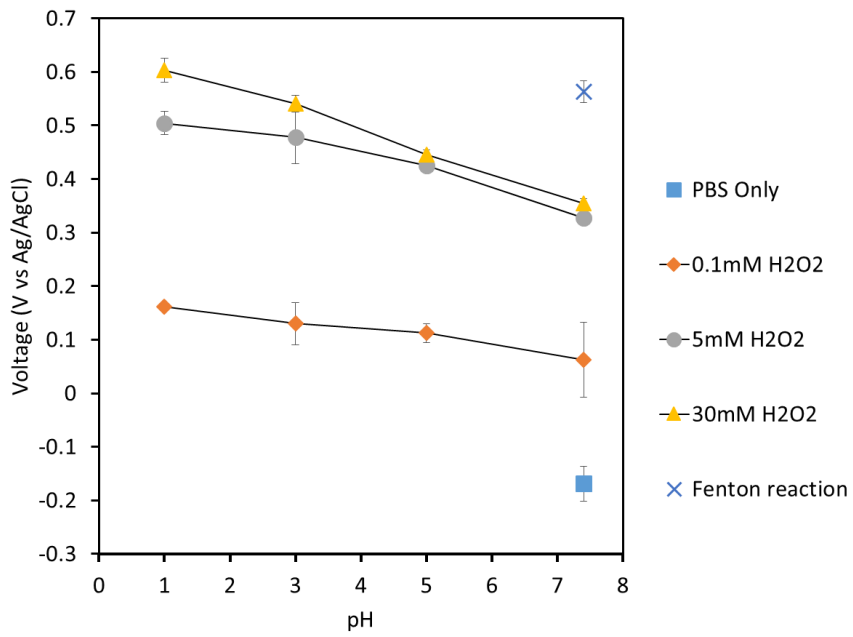


B
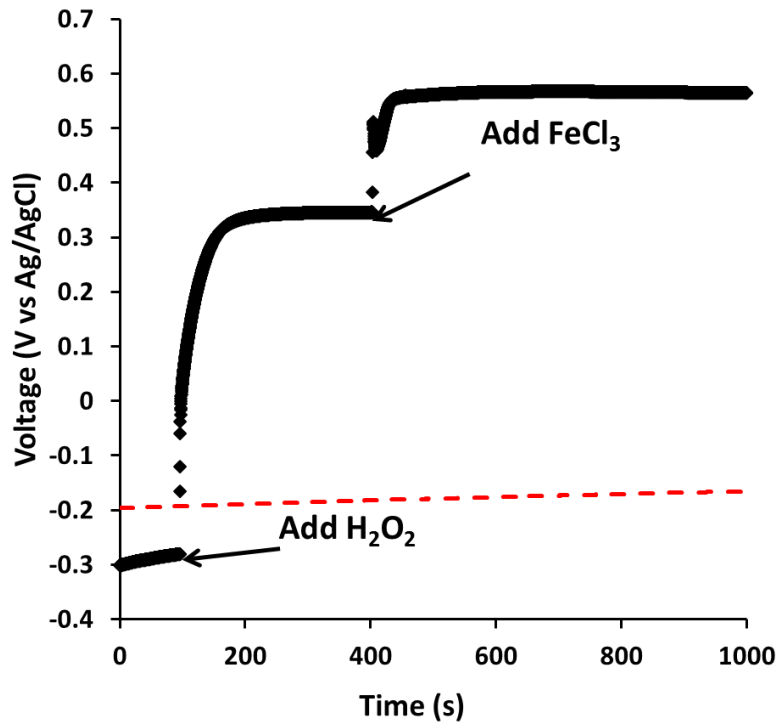
C

Figure 2.2 Open circuit cotential plots of CoCrMo alloy in PBS solution, in SI PBS solutions modified with HCl (pH 1,3,5,7) and different concentrations of $H_2O_2$ (0.1, 5 and 30 mM) and in solutions with Fenton reagent. A) OCP rises due to the addition of 30 mM $H_2O_2$ at different pH in PBS solutions. As pH decreases, OCP becomes more positive. B) Summary of OCP in all investigated pH solutions with different concentrations of $H_2O_2$. OCP in PBS-only solution is the lowest and increases with the increases of $H_2O_2$ concentration. When both acid and $H_2O_2$ are added to PBS, the OCP rises to above 0.6 V vs Ag/AgCl which is a highly oxidizing condition for CoCrMo. C) OCP variation over time due to the present of Fenton reagent. 10 mM $H_2O_2$ increases OCP to 0.35V vs Ag/AgCl while further addition of 0.1 mM $FeCl_3$ rises OCP to 0.6V vs Ag/AgCl.
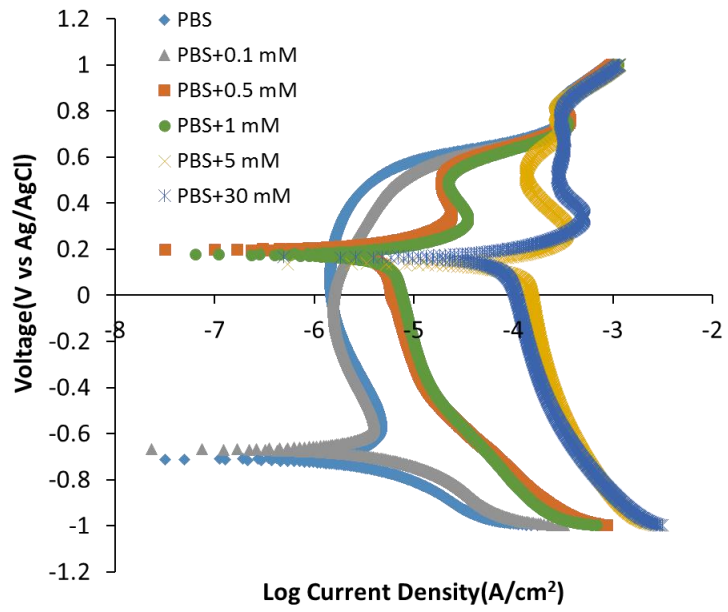
A
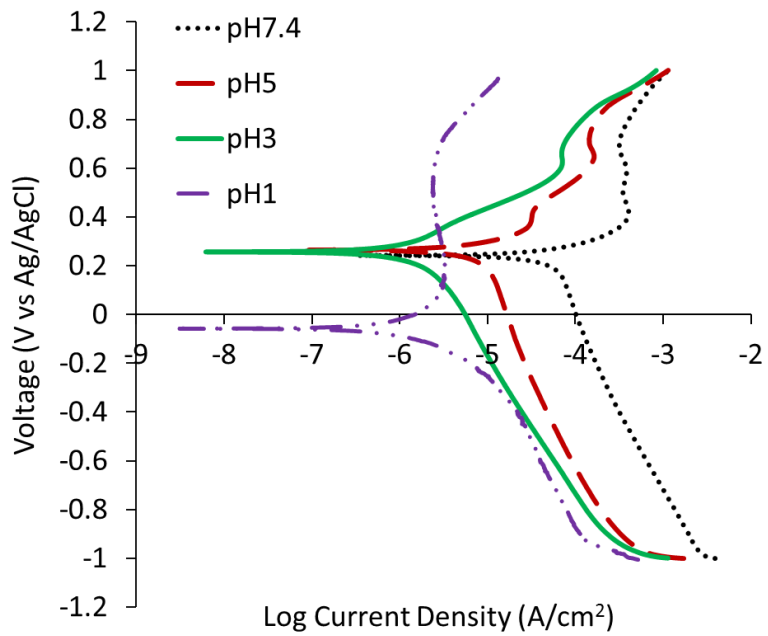


B
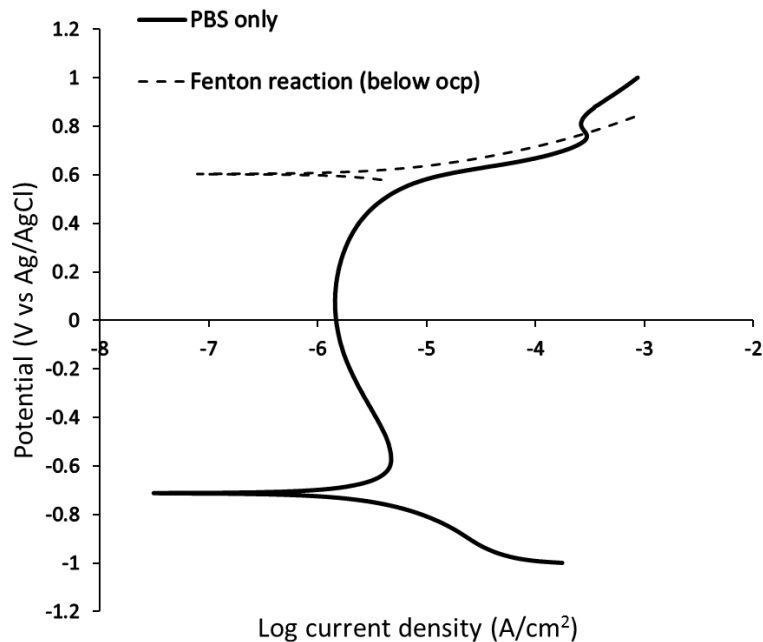
C

Figure 2.3 A) Polarization plots of CoCrMo in PBS solution with differing amount of $H_2O_2$ [66]. As $H_2O_2$ concentration increases from 0.1 mM to up to 30 mM, the corrosion currents rise significantly above the PBS alone case and the corrosion potential shifts positively from -0.7 V to 0.2 V. Corrosion potential rises from -0.7 V to -0.4 V due to the presence of Fenton reagent. B) Potentiodynamic curves of CoCrMo alloy at different pH in PBS solutions with 30 mM $H_2O_2$. Corrosion current increases as pH gets higher. It rises from $10^{-7}$ A/cm$^2$ level at pH 1 to $10^{-5}$ A/cm$^2$ level at pH 7.4. C) Polarization plots of CoCrMo in PBS (pH 7.4) and in solutions with 30 mM $H_2O_2$ and 0.1 mM FeCl$_3$. Corrosion current increases about 5 times in Fenton reagent modified PBS solution compared to PBS-only solution.

A



B
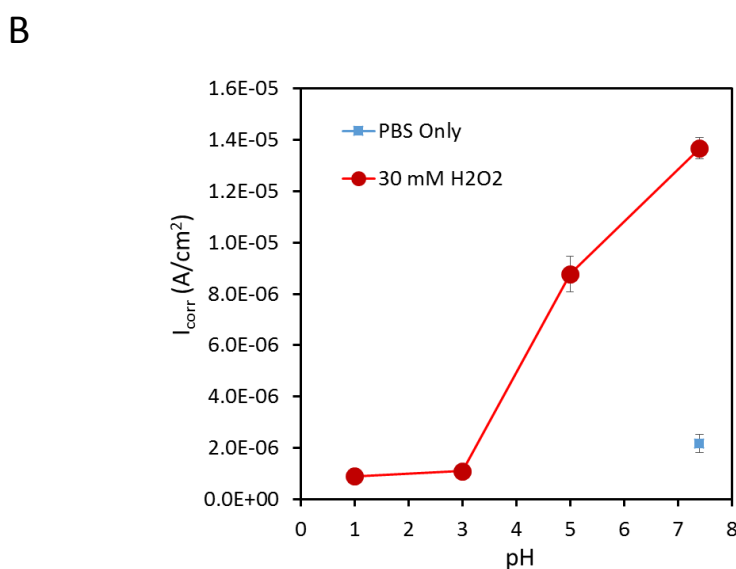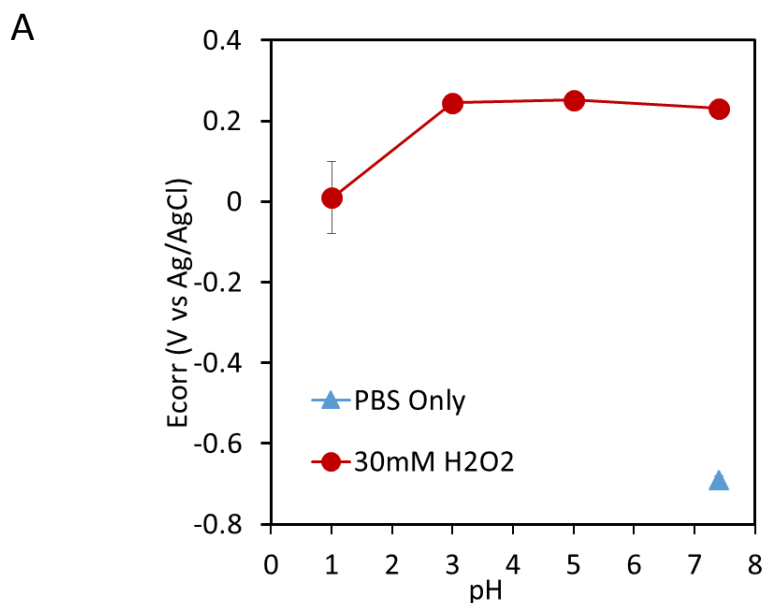


Figure 2.4 Corrosion potential and corrosion current density in PBS solutions and PBS solution with 30 mM $H_2O_2$ at all tests pHs. A) Corrosion potential in $H_2O_2$ modified solution is at least 0.7 V higher than that in PBS only case. B) Corrosion current increases as pH increases in PBS solution with 30 mM $H_2O_2$. Corrosion current in pH 5 and 7.4 condition are significantly higher than that in PBS only condition, while those in pH 1 and 3 condition are significantly lower than that in PBS solution. （Values are shown in Table 2.1）
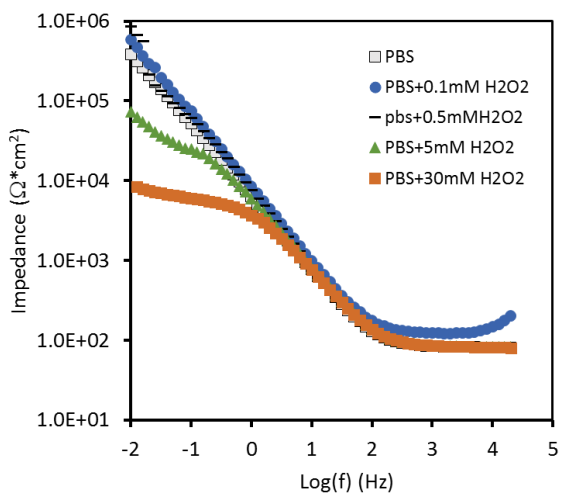
A
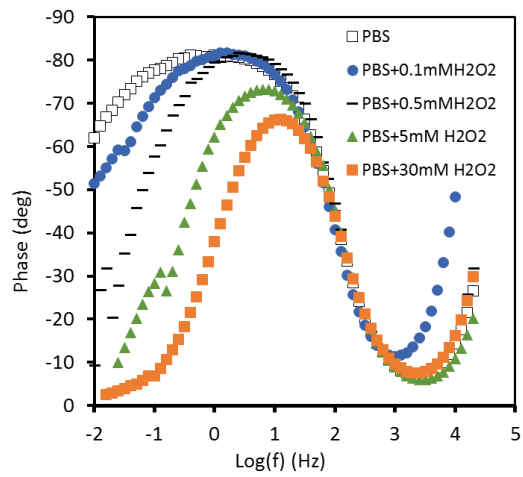


B
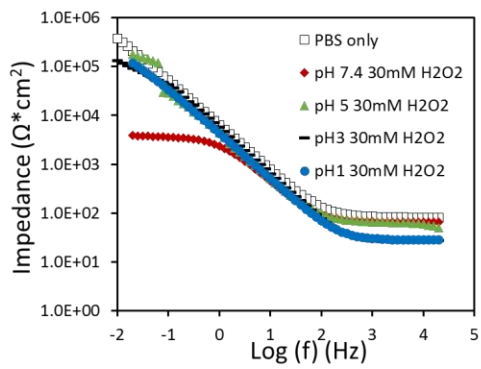


C
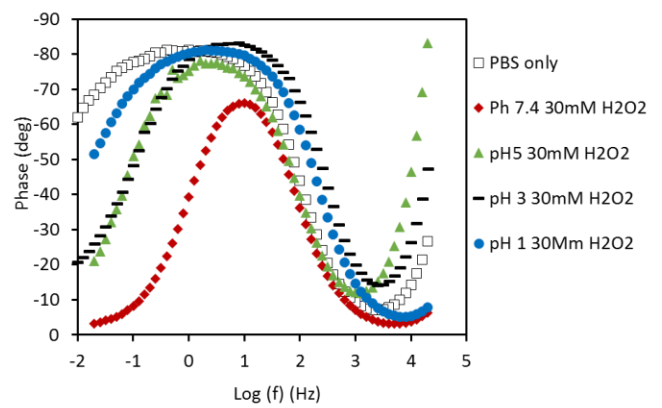


D
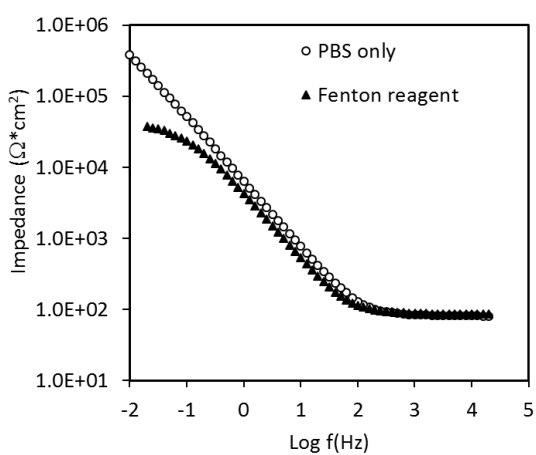


E
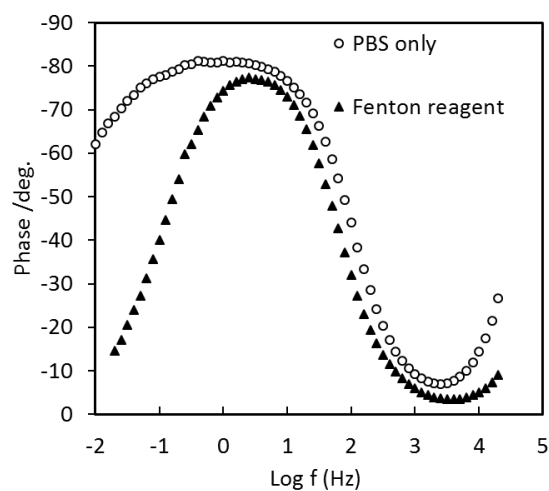


F

Figure 2.5 (A & B) Impedance analysis results for CoCrMo in PBS containing differing

40

concentrations of $H_2O_2$ [66], Representative Bode impedance (C) and phase angle (D) plots of CoCrMo alloy at different pHs in PBS solutions with 30 mM $H_2O_2$ and PBS alone solution . Decrease of pH result in large (two orders of magnitude) increase in the low frequency impedance, reflective of the oxide resistance of the surface. Representative Bode impedance (E) and phase angle (F) plots of CoCrMo alloy in PBS solution and PBS solution (pH 7.4) with Fenton reagent. Low frequency impedance decreases about 10 times due to the addition of Fenton reagent, indicating a more defective surface oxide film was formed in Fenton reagent containing PBS solution compared to PBS alone case.
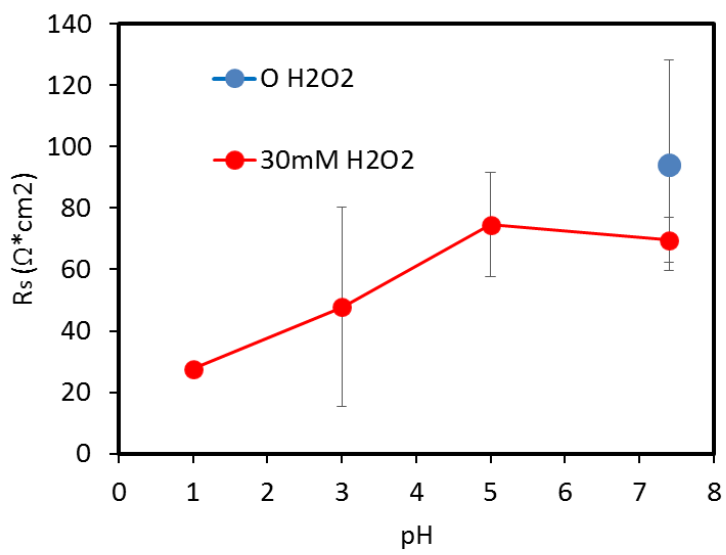
A
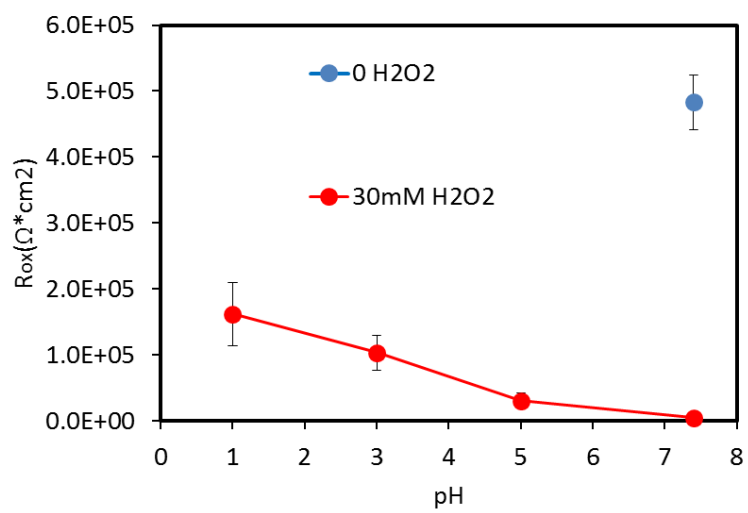


B
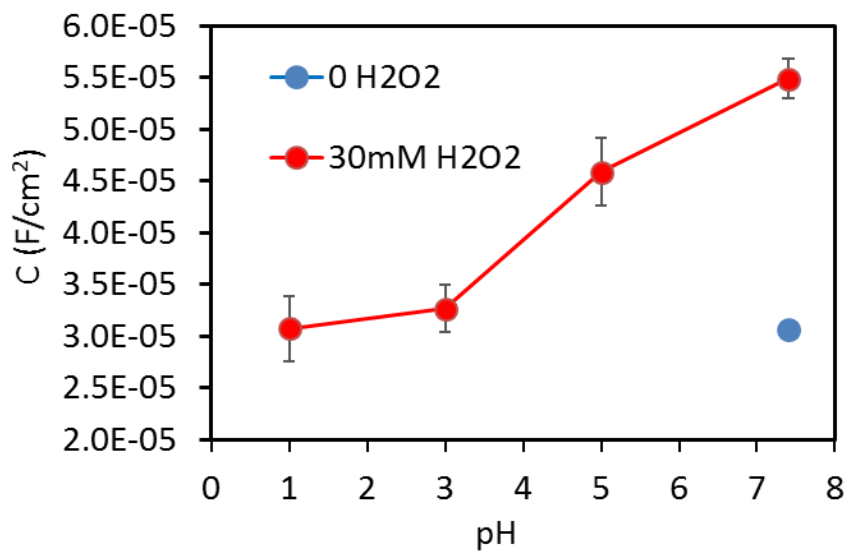
C
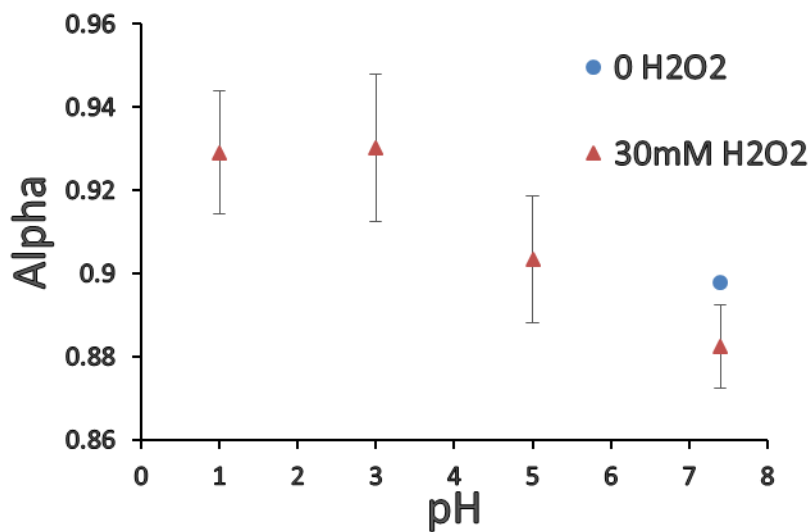


D

Figure 2.6 Plots of solution resistance, oxide resistance, capacitance and CPE exponent from EIS of CoCrMo alloy in different pH and $H_2O_2$ conditions. A) solution resistance shows the lowest value in pH 1 conditions, B ) Oxide resistance of CoCrMo surface decreases due to the presence of 30 mM $H_2O_2$ at all pHs compared to PBS only condition. In solutions with 30 mM

$H_2O_2$, $R_{ox}$ increases as pH decreases, C) Capacitance in 30 mM $H_2O_2$ modified PBS solution at pH 5 & 7.4 are significantly higher than that in PBS only condition, while that in 30 mM $H_2O_2$ modified PBS solution at pH 1 & 3 is at the same level compared to PBS only case. D) CPE exponent value show smaller values (lower than 0.9) at pH 7.4 conditions compared to pH 1 & 3 solutions with 30 mM $H_2O_2$.

A
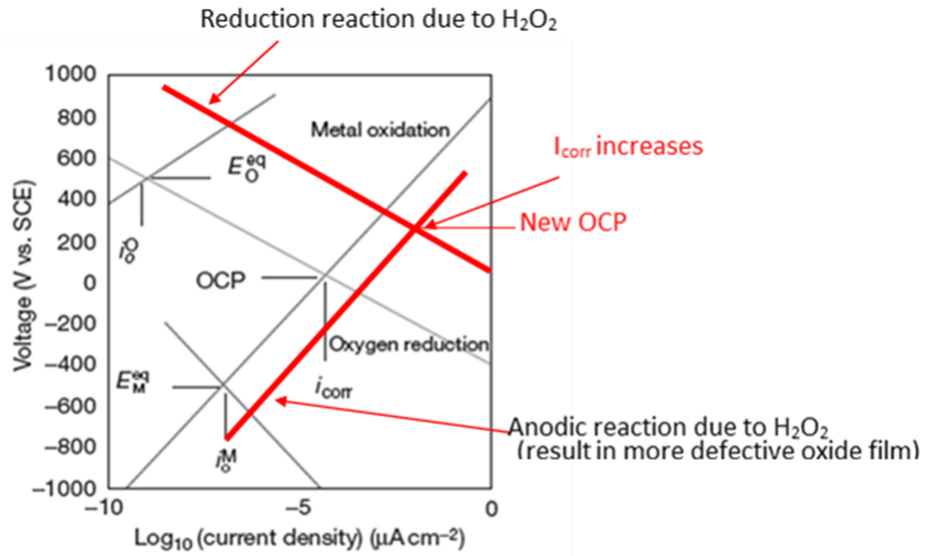
Evan's diagram of possible reaction



B
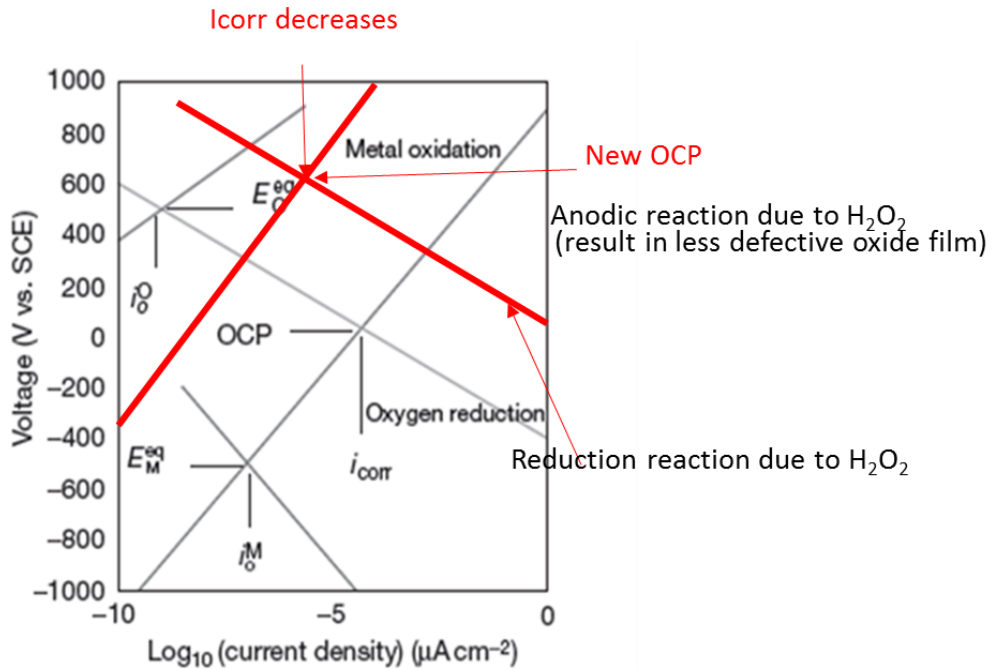
Evan's diagram of possible reaction

Figure 2.7 A) Significant increase of OCP and corrosion current due to presence of $H_2O_2$ at pH 7.4 based on Evan's diagram. B) Significant increase of OCP and decrease of corrosion current at acidic solutions due to addition of 30 mM $H_2O_2$ based on Evan's diagram.

Table 2.1 Electrochemical test results: Corrosion potential ($E_{corr}$: the potential where the current density changes from cathodic to anodic) and corrosion current density ($I_{corr}$: current density at corrosion potential derived from cathodic extrapolation of the polarization curves). Means and standard deviations are presented.

| electrochemistry parameters | Different pHs (30 mM $H_2O_2$ modified solution) | | | | PBS only solution |
|---|---|---|---|---|---|
| | pH 1 | pH 3 | pH 5 | pH 7.4 | |
| $E_{corr}$ (V) | 0.01±0.09 | 0.25±0.02 | 0.25±0.02 | 0.23±0.02 | -0.69±0.01 |
| $I_{corr}$ (uA/cm2) | 0.70±0.28 | 1.09±0.03 | 8.78±0.69 | 13.7±0.41 | 2.17±0.35 |

Table 2.2 Simulated impedance parameters found by nonlinear square fitting of the modified Randles circuit model to the Impedance data. Means and standard deviations are presented.

| Circuit parameters | Different pHs (30 mM $H_2O_2$ modified solution) | | | | PBS only solution |
|---|---|---|---|---|---|
| | pH 1 | pH 3 | pH 5 | pH 7.4 | |
| $R_s$ ($\Omega$ cm$^2$) | 27.5±1.1 | 47.8±32.5 | 74.6±16.9 | 69.6±7.4 | 94.0±0.0 |
| $R_{ox}$ (M$\Omega$ cm$^2$) | 0.162±0.05 | 0.103 ±0.03 | 0.031±0.12 | 0.005±0.00 | 0.483±0.41 |
| $CPE_{ox}$ ($\mu$F/cm$^2$) | 30.7±3.2 | 32.7±2.3 | 45.8±3.3 | 54.9±1.9 | 30.7±1.6 |
| $\alpha$ (%) | 92.9±1.5 | 93.0±1.8 | 90.3±1.5 | 88.2±1.0 | 89.8±1.7 |

# Chapter 3 The effect of the inflammatory species hypochlorous acid and pH on the electrochemical behavior of Co-Cr-Mo Alloys

## 3.1 Introduction

Metallic orthopedic implants which may consist of cobalt-chromium-molybdenum (Co-Cr-Mo) alloys have been widely used due to their excellent mechanical properties, corrosion resistance and biocompatibility [4, 101]. However, mechanically assisted corrosion or fretting corrosion of CoCrMo alloys which result in abrasion of oxide film and significant acceleration of degradation of the implant remains as a big concern [8, 80, 37, 102]. Primary focus on CoCrMo alloy has been on the body's reaction to the released particles and corrosion products such as metal ions generated during wear and fretting corrosion process [22, 31, 46, 103]. Elevation in metal ion levels and wear debris have been associated with adverse effects such as pseudotumors [14] and adverse local tissue reactions on patients [15, 32] and lead to high early failure rate or revision of hip implants.

The current one-way perspective of implant-biology interactions may not be complete and can't fully explain corrosion phenomenon reported by recent retrieval studies [66, 69]. Evidence of inflammatory cell-induced (ICI) corrosion of CoCrMo alloy in retrieved hip and knee implants have been reported by Gilbert et al. and the concept that the biological process such as inflammation may influence in vivo corrosion in the absence of mechanical effects has been proposed [66]. Recent study by Laura et al. investigated the clinical relevance of ICI corrosion on CoCr hip implants and reported 59% of the implants show surface damage of ICI

47

corrosion [69]. Previous study by Cadosh et al. have reported osteoclasts induced in corrosion on stainless steel and titanium in vitro [57, 58]. These findings support that the biology (inflammatory cells) induced corrosion may be a significant element missed on the implant-body interaction. Indeed, activated cells during inflammation process are known to release a series of highly reactive chemical species (reactive oxygen species, ROS, NO) (Figure 2.1) that possess high oxidative ability in nature and thus may affect the corrosion performance of metallic biomaterials. However, what chemical species are the main factors in the ICIC process are poorly understood. Recent study by Liu et al. show that the presence of simulated inflammatory species such as hydrogen peroxide ($H_2O_2$) or Fenton reaction ($Fe^{3+}$ and $H_2O_2$) in PBS significantly increase the oxidizing power of the environment and makes the oxide film more defective(Chpater 2) [104].

Another aggressive reactive oxygen species, HClO, is generated by the inflammatory system through respiratory burst and the presence of leukocytes (neutrophils, macrophages and monocytes) in a heme enzyme myeloperoxidase (MPO)-catalyzed reaction [105]. This production of in vivo HClO is associated with innate host defense against microorganisms and is of great importance in killing a series of pathogens [106, 107]. It has also been reported that macrophage cells may produce HClO when stimulated [108, 109]. Estimation of in vivo HClO concentration in neutrophils is as high as 134 mM/min [72]. HClO and its conjugate base hypochlorite ($ClO^-$) are known to be highly oxidative and have been widely used as strong oxidizing agents. It has been reported that HClO/$ClO^-$ is able to oxide $Cr^{3+}$ to $Cr^{6+}$[110], which is highly toxic in vivo. On the other hand, inflammatory cells are known to use acid to attack

invading foreign bodies and create an aggressive low pH microenvironment in vivo. Local pH

during fretting crevice corrosion condition can drop to very low levels [111] and this acidic

environment has been reported to significantly increase the oxidizing power of the solution

with ROS [104]. Thus, cell-released chemical species such as HClO and acid may be involved

in the ICIC processes and accelerate the corrosion of CoCrMo alloy.

Currently, the effect of HClO and acid on the electrochemsitry of CoCrMo alloy is poorly

understood. Thus, the purpose of this study was to investigate the influence of simulated

inflammatory cell-based conditions (HClO, acid) on the corrosion behavior of CoCrMo alloy.

Electrochemical measurements were conduction in simulated inflammatory conditions with

HClO and varied pH. The hypothesis is that the presence of inflammatory cell-based reactive

chemical species in joint fluids will increase the corrosion susceptibility of CoCrMo alloy by

decreasing oxide film impedance or increasing oxidizing power of the environment.

## 3.2 Materials & Methods

**Sample, electrochemical cell:** CoCrMo (ASTM F-1537 high carbon) disks were prepared

by polishing through a series of grits from 240 to 600 grit with wet emery paper before being

mounted into a three electrode corrosion cell. The CoCrMo disk was tested as the working

electrode and the counter electrode and reference electrode were a carbon rod and a

saturated silver-silver chloride (Ag/AgCl) electrode (0.22V vs NHE) respectively. A potentiostat

(Solartron 1280C Potentiostat/Frequency Response Analyzer, Solartron Analytical Inc.,) was

used in open circuit potential (OCP), anodic polarization and Electrochmical impedance

spectroscopy (EIS) tests with software for control and acquisition of electrochemical signals

(Corrware 2.0 for polarization test and Zplot 2.0 for impedance study).

**Simulated inflammatory electrolyte:** There simulated inflammatory solutions including phosphate buffered saline (PBS, Sigma), PBS solution with 0.1 M HClO and acidic PBS solution with 0.1 M HClO (pH 3) were prepared. PBS solution with 0.1 M HClO was created by adding 0.1 M HCl into 0.1 M NaClO modified PBS solution. HCl was used to adjust the pH for the simulated acidic condition.

**Electrochemical measurements**

**OCP tests**: OCP of CoCrMo disks was monitored in three different simulated solutions for around 20 minutes. 0.1 M HCl was added into 0.1 M NaClO modified PBS solution after the start of the test to identify the change in OCP due to the presence of HClO.

**Anodic polarization tests**: Polarization tests were performed from the voltage 30 mV below OCP to +1 V or the potential 1 V above OCP with a scan rate of 1 mV/s after the OCP tests. The corrosion current density ($I_{corr}$) and the corrosion potential ($E_{corr}$) were obtained from the polarization curves.

**EIS analysis**: CoCrMo sample was immersed in simulated inflammatory electrolyte for 20 minutes until OCP reached to a stable level. EIS tests were performed at OCP with 10 mV sinusoidal voltage superimposed at the frequency from 20 kHz to 0.01 Hz. The impedance magnitude and phase angle were calculated from the date at each frequency and were plotted versus frequency for analysis. A modified Randles circuit model was applied to determine electrochemical characteristics of the interface. The standard Randles circuit contains solution

resistor $(R_s)$ in series with a parallel combination of an oxide resistor $(R_{ox})$ and capacitance $(C_{ox})$ of the electrochemical double layer. A constant phase element (CPE) was applied to replace the capacitance element due to the non-ideal behavior of the interface.

In all results, tests were repeated at least 3 times. Only representative plots are presented, however, the behavior observed is consistent across repeated testing.

**Statistical analyses**

Statistical analyses were performed using analysis of variance (ANOVA) methods followed by Tukey's post hoc analysis to assess the significance of simulated inflammatory conditions (HClO, HClO with acid) and pH on OCP, polarization parameters ($E_{corr}$, $I_{corr}$) and modeling parameters ($R_{ox}$, C, $R_s$, alpha) from Randles circuit. One-way ANOVA was used and a p-level of 0.05 was considered significant in all statistical tests.

**3.3 Results**

**3.3.1 Open circuit potential behavior**

The OCP plot of CoCrMo alloy in PBS solutions at different pHs are reported in Figure 3.1A. At pH 7.4, the OCP after 15 minutes' immersion in PBS is about -0.2 V (vs Ag/AgCl) and shifts positively as pH becomes lower. In pH 1 solution, the OCP increases 0.3 V from that in pH 7.4 solution to 0.1 V. Figure 3.1B illustrates how the OCP evolution with time of CoCrMo alloy in PBS solution is affected by the addition of 0.1 M HClO with or without HCl (pH 3). OCP becomes significantly more positive with the addition HClO (P<0.05), showing an increase of at least 1V in both pH 7.4 (0.9 V) and pH 3 (0.85 V) conditions (Figure 3.1C).

### 3.3.2 Polarization behavior

**pH effect in PBS solution**

Anodic potentiodynamic curves of CoCrMo alloy in different pH PBS solutions are shown in Figure 3.2A. The values for $I_{corr}$ and $E_{corr}$ in all tested conditions are presented in Table 3.1. The cathodic reaction at negative voltages range (from -1 V to corrosion potential) is greatly affected by pH. The cathodic reaction at voltage below -700 mV increases as the pH becomes lower. The current density from -1 V to -0.7 V in pH 1 solution is about two orders larger than that is in pH 7.4 solution. Both the zero current potential (corrosion potential) and the corrosion current are pH dependent and increase as solution becomes more acidic (Figure 3.2 B & C, p<0.05). With the decrease pH 7 to 1, corrosion potential jumps from -0.69 V to 0.33 V and corrosion current density increases from $2.2*10^{-6}$ A/cm$^2$ to $21*10^{-6}$ A/cm$^2$. It's interesting to notice that repassivation effect appears in all pH solutions. As the pH gets lower, the transpassive voltage becomes higher. In pH 1 solution, the transpassive voltage is around 0.9 V which is about 0.3 V higher than that is in pH 7.4 solution. As a result, the current density at high voltage range (above 0.6 V) becomes smaller in more acidic PBS solution.

**Effect of Hypochlorous acid at different pHs**

Representative potentiodynamic polarization plots for CoCrMo in PBS solution and PBS solution with 0.1 M HClO at different pHs are shown in Figure 3.2D. Corrosion potential becomes significantly more electropositive (p<0.05) from -0.3 V in PBS only solution to 0.85 V in 0.1 M HClO modified PBS solution. In solution with both acid (pH 3) and HClO, corrosion potential further increases to 0.9 V. Corrosion current density in PBS only solution is 0.11

uA/cm$^2$ while it increases more than 300 times (p<0.05) to 36.9 uA/cm$^2$ in solution with 0.1

M HClO. In acidic solution with HClO, corrosion current density decreases (p<0.05) from that

of HClO alone case to 3.4 uA/cm$^2$ which is still more than 30 times larger than PBS only

condition.

### 3.3.3 Electrochemical impedance spectroscopy behavior

Representative Bode plots obtained from EIS tests for CoCrMo alloy under HClO modified

PBS solutions and different pHs are shown in Figure 3.3. The EIS circuit parameters including

solution resistance, polarization resistance, capacitance and constant phase element

exponent are presented in Figure 3.4. All the values for $R_s$, $R_{ox}$, $CPE_{ox}$, a are presented in Table

3.2.

**pH effect in PBS only solution**

Figure 3.3A and 3.3B shows the representative impedance magnitude and phase angle

response of CoCrMo alloy under different pH PBS solution conditions. As pH gets lower, the

capacitance increases (p<0.05) while no significant difference of oxide resistance is shown.

Solution resistance in pH 1 PBS solution is significantly lower (p<0.05) than that in other pH

conditions. The CPE exponent shows no significant difference between different pH conditions.

(p>0.05).

**HClO effect at different pHs**

The variation in impedance of CoCrMo alloy in PBS solution due to the addition of HClO

and HCl are shown in Figure 3.3C and 3.3D. A large drop in low-frequency impedance (0.02 Hz,

associated with the oxide resistance) and narrowing of the frequency range of the phase angle can be observed in solutions with HClO. The presence of 0.1M HClO decreased the oxide resistance from $4.8*10^5$ Ω to 138 Ω and addition of 0.1 M HClO and HCl (pH 3) decreased it to $1.4*10^4$ Ω ($p<0.05$) (See Table 3.2). Capacitance increased more than 100 times in HClO modified solution (3800 uF/cm$^2$) compared to that in PBS only solution (31 uF/cm$^2$), while further addition of acid to pH 3 decreases it ($p<0.05$) to 236 uF/cm$^2$ which is about 7 times larger compared to the PBS only condition. CPE exponent decreases from 0.90 in PBS solution to 0.81 in PBS solution with both acid (pH 3) and HClO ($p<0.05$).

## 3.4 Discussion

### The effect of pH on CoCrMo electrochemistry

In solutions with HCl, OCP shifts positively with the increases of acidity (Figure 3.1), this is in agreement with the polarization plots (Figure 3.2) where zero current potential increases in more acidic solution. The corrosion current density becomes larger as pH gets lower, indicating a less protective passive layer in lower pH solutions at freely corroding conditions. This result is also supported by EIS results, where the impedance magnitude decreases in lower pH conditions. The capacitance increases in more acidic conditions, which demonstrates a less stable oxide layer. This is in agreement with a previous study [63] where decreased formation and growth of passive layer was found as pH gets lower. Thus, the corrosion susceptibility of CoCrMo alloy in PBS solution increases with decreases of pH.

However, it is worth noticing that the passivation effect of acid on oxide film is observed

54

at more positive voltage range (Figure 3.2A) and passivation character remains even at pH 1. Oxide films at sufficiently positive voltage (higher than 0.6 V) becomes less protective (i.e. the transpassive potential decreases) as pH gets higher. This shows that the oxide film on CoCrMo alloy is both solution chemistry and potential dependent.

The poubaix diagram shows that the passivation region of Cr only occurs at pH>5 region under freely corroding conditions [92], implying an increase in susceptibility of corrosion of Cr in more acidic solution. Addition of acid increases the OCP while it requires higher potential to oxidize Cr(III) to Cr(VI) in more acidic solution. A previous study shows that acid alone favors the dissolution of metal elements ($Cr^{3+}$, $Co^{2+}$) [112]. This indicates that local fretting crevice corrosion, which commonly occurs in modular designed implants, favors the release of metal ions due to more acidic environment.

**The effect of HClO and acid on CoCrMo electrochemistry**

Significant increase of OCP, corrosion potential, corrosion current and large decrease of oxide impedance show that the presence of HClO increases the corrosion susceptibility of CoCrMo alloy, resulting in increased oxidizing power of the solution and a more defective and less stable oxide film on the surface. Further addition of acid increases the impedance and decreases corrosion current, implying the passivation effect of acid on oxide film in HClO modified PBS solution. The passivation effect of acid on CoCrMo alloy has been shown in solutions with other simulated inflammatory species (e.g., $H_2O_2$). It is interesting to notice that the open circuit potential exhibits significant increase to above transpassive range in both $H_2O_2$ (above 0.6 V) and HClO (above 0.85 V) modified solutions when acid is present. This acid-

passivation behavior for ROS under freely corroding conditions may be related to increased surface potential and shows agreement with the results in potentiodynamic tests and the Poubaix diagram [92], implying fundamental changes in oxide structure and chemistry due to HClO and acid.

**Possible involved reactions**

During inflammatory activation, cells are able to release a series of reactive chemical species such as $H_2O_2$, Fenton reagent, NO, peroxynitrite ($ONOO^-$) and acid [113, 114]. These highly oxidative species and related intermediate species are able to accelerate the corrosion of CrCrMo alloy and alter the redox status of inflammatory cells. HClO/ClO$^-$ are known as strong oxidants and previous studies have shown that they are strong enough to oxidize Cr(III) to Cr(VI) over the pH range of 2-10 [110, 115]. Possible oxidation reactions and oxidant generating reactions involving HClO and HCl are [116]:

$$2HClO + 2H^+ + 2e^- \text{---} Cl_2 + H_2O \quad \text{(acidic condition)} \quad\quad 1.63 \text{ V}$$

$$HClO + H^+ + 2e^- \text{---} Cl^- + H_2O \quad \text{(acidic condition)} \quad\quad 1.49 \text{ V}$$

$$ClO^- + H_2O + 2e^- \text{---} Cl^- + 2OH^- \quad\quad\quad 0.9 \text{ V}$$

$$Cl_2 + 2e^- \text{---} 2Cl^- \quad\quad\quad 1.36 \text{ V}$$

$$2Cr(OH)_3 + HClO \text{---} 2HCrO^{4-} + Cl^- + H_2O + 5H^+ \quad \text{Cr(III) to Cr(VI)} \quad \text{--Reaction I}$$
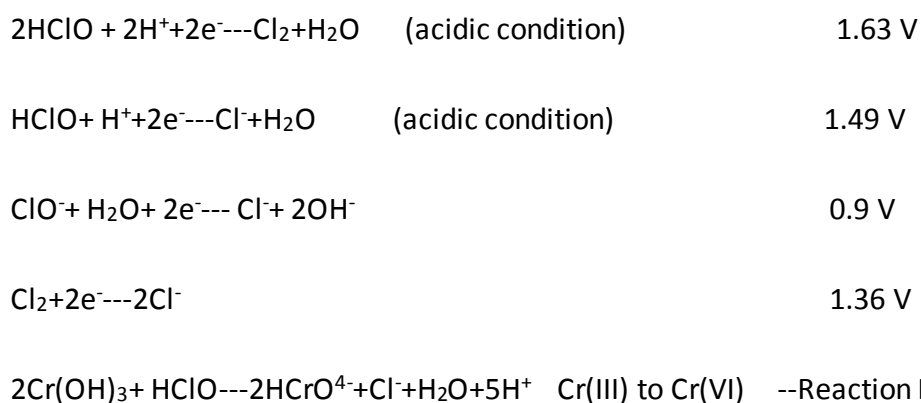
Important production mechanisms for in vivo hydroxyl radical [117] and singlet oxygen [118] are reactions associated with neutrophils that released HClO to interact with superoxide and the reaction of HClO with $H_2O_2$, respectively:

$$HClO + O_2\bullet^- \text{---} OH\bullet + Cl^- + O_2$$

$$HClO + H_2O_2 \text{---} {}^1O_2 + Cl^- + H_2O + H^+$$
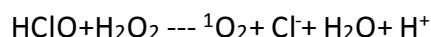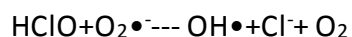
Besides, $OH\bullet$ and ${}^1O_2$ are involved in a series of reactions [68] which will generate other oxygen free radicals such as: $HO_2\bullet$, $O_2\bullet^-$ and increase the oxidizing power of the cellular environment. These radicals, $H_2O_2$, as well as $HClO$ possess higher redox potentials than oxygen reaction and are theoretically able to oxidize metal into a higher valance state and alter the chemistry and structure of oxide film.

Based on the Poubaix diagram of the $Cr/H_2O$ system, the potential required to oxidize $Cr_2O_3$ into $Cr(VI)$ is around 0.3V (VS Ag/AgCl) at pH 7.4 [92]. Our study shows that the OCP at pH 7.4 is as high as 0.8V when $HClO$ is present. Besides, the voltage required for $Cr(III)$ oxidization decreases in higher temperature conditions. Temperature increase is a major clinical sign of inflammation and occurs under hard exercise. Local temperature increases activated area during in vivo inflammatory conditions, which favors the formation of $Cr(VI)$ (Figure 3.5). The concentration of chromium species affects the oxidation reactions of $Cr(III)$. For example, a decrease of chromium concentration from $10^{-6}$ mol/L to $10^{-8}$ mol/L significantly decreases the potential required for $Cr(VI)$ formation [119]. The concentration of in-vivo $Cr(III)$ is unknown and variable. However, as long as there is $Cr(III)$, it is possible that it reacts with the intermediate radical species and will be oxidized into $Cr(VI)$ species. Although $Cr(VI)$ in vivo may not be able to exist for a long time because it will be quickly reduced to the trivalent state, it is those potentially harmful reduction processes such as DNA-damage reactions, that define $Cr(VI)$ as highly toxic in vivo [120, 121]. Meanwhile, $Cr(VI)$ is possible to be stably retained in

the oxide film in the highly oxidative environment created by inflammatory species. Previous XPS studies show the existence of Cr(VI) in oxide layer when the potential is increased to 0.5V [122], which is possible when HClO, $H_2O_2$ or Fenton reaction present [104]. Future XPS work is needed to better understand how the simulated inflammatory conditions affect the CoCrMo oxide.

**Evan's diagram**

Evan's diagram can be applied to illustrate how the presence of acid and HClO affect the OCP and corrosion current result in this study. Open circuit potential is the voltage where the rate of the anodic reactions (metal oxidation) equals to that of the cathodic reactions. Addition of HClO and acid result in significantly accelerated cathodic reactions as well as more defective oxide film which increases the rate of oxidation reactions (Figure 3.6). Further addition of acid increases the passivation of the oxide film, decreasing the rate of metal oxidation, and results in a lower corrosion rate compared to HClO only case. The effect of HClO on CoCrMo alloy is similar to that of of $H_2O_2$ based on the Evan's diagram [104]. However, compared with the results in $H_2O_2$ modified condition, higher OCP and larger increase of corrosion current are shown in PBS solution with HClO, implying a more aggressive corrosion environment in created by the presence of HClO.

**Other reactive chemical species and clinical relevance**

In in vivo joint fluid, inflammatory cells release other strong oxidative chemical species such as nitric oxide (NO), peroxynitrite ($NO_3^-$), hydrogen peroxide ($H_2O_2$) and Fenton Reagent ($Fe^{3+}+H_2O_2$). These reactive chemical species have been shown to significantly alter the oxide

film on CoCrMo surface and increase the corrosion susceptibility of CoCrMo alloy. Recent study has shown significant increases in OCP and change of cathodic reactions in human synovial fluids of high inflammatory level [70], which supports the results in this study and those in $H_2O_2$ and Fenton reagent modified simulated inflammatory conditions (Chapter 2). When ROS are present, physiologically possible potentials on CoCrMo surfaces can reach as high as 0.9 V, a remarkably higher level than -0.1V the research community reported before [123]. Cell viability has been shown to be directly related to the OCP of metallic biomaterials [49, 86, 87] and near 0% cell viability have been reported on CoCrMo alloy when OCP is higher than +500 mV. Thus, the presence of ROS as well as possible release of metal ions ($Cr^{6+}$) through ROS related oxidation reaction are likely to not only induce ICIC corrosion but also to affect the cells and tissues adjacent to the implant. These ROS-based adverse effects may induce cell necrosis in vivo and be related with clinical observations of adverse local tissue reaction [15, 32] and pseudotumors [14] in patients with failed implant. Which chemical species and what cell types and at what concentration are the prime factors in the cell induced corrosion mechanism are as yet to be understood and addition studies of retrieved inflammaed joint fluid will also be helpful.

## 3.5 Conclusion

This study investigated one possible mechanism of inflammatory-cell induced corrosion and the effect of pH on CoCrMo electrochemistry. The presence of HClO, which is an aggressive ROS released by neutrophil MPO during respiratory burst, in PBS solution greatly increases the corrosion susceptibility of CoCrMo alloy. On one hand, it lifts the oxidizing

potential to be as positive as 0.9 V at 0.1 M concentration, a much higher physiologically-possible level than previously reported, significantly increasing the oxidizing power of the solution. One the other hand, it decreases oxide resistance of of the surface and leads to a more defective and less stable oxide film. Increase of pH in HClO modified solution significantly decreases oxide film impedance and results in less protective oxide layer and larger corrosion current. Alternatively, pH 7.4 physiological solutions with HClO was found to be the most corrosive to CoCrMo surface. The addition of HCl alone into PBS increases oxidizing power of the solution, decreases the formation and growth of passive layer and facilitates the corrosion of CoCrMo alloy under freely corroding condition. This study demonstrates that inflammatory conditions may have a pronounced effect on the corrosion of CoCrMo in vivo and forms the basis of our understanding on how HClO, the most bactericidal oxidant known to be produced by the neutrophil, can affect the performance of CoCrMo implants.

A
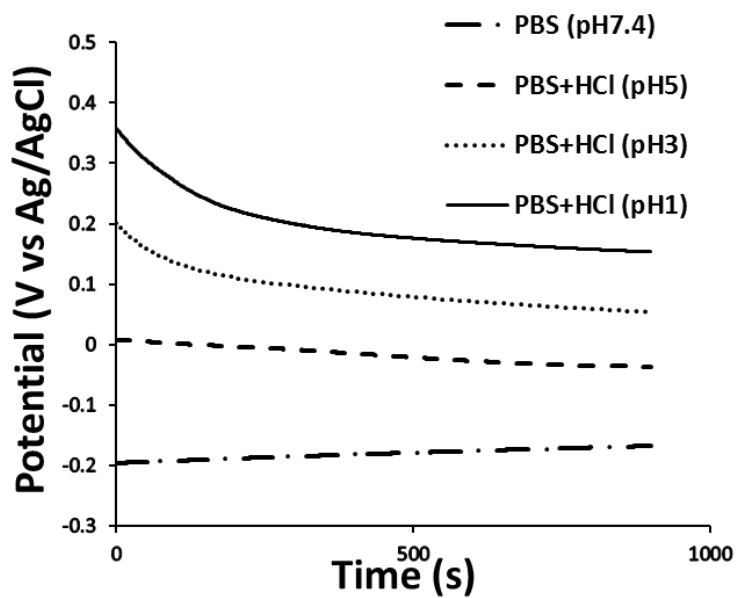


B
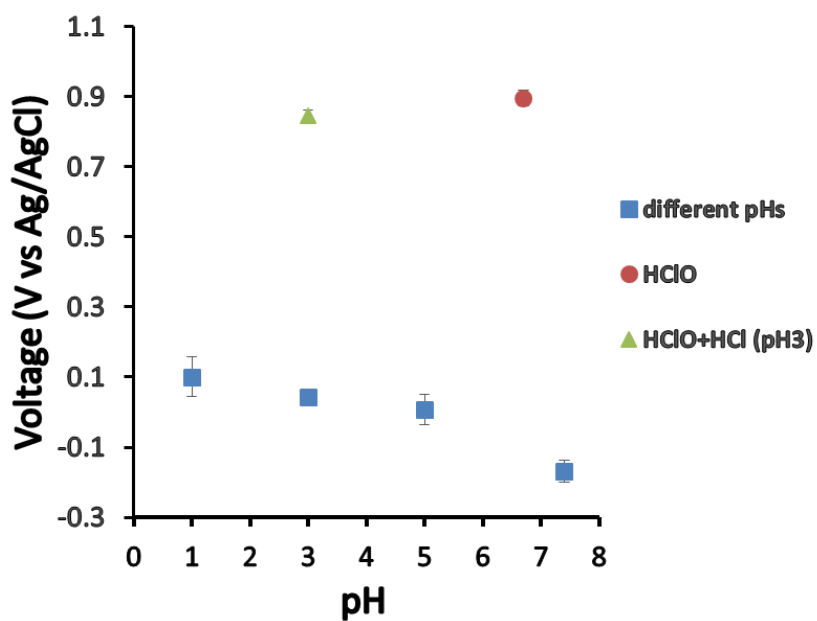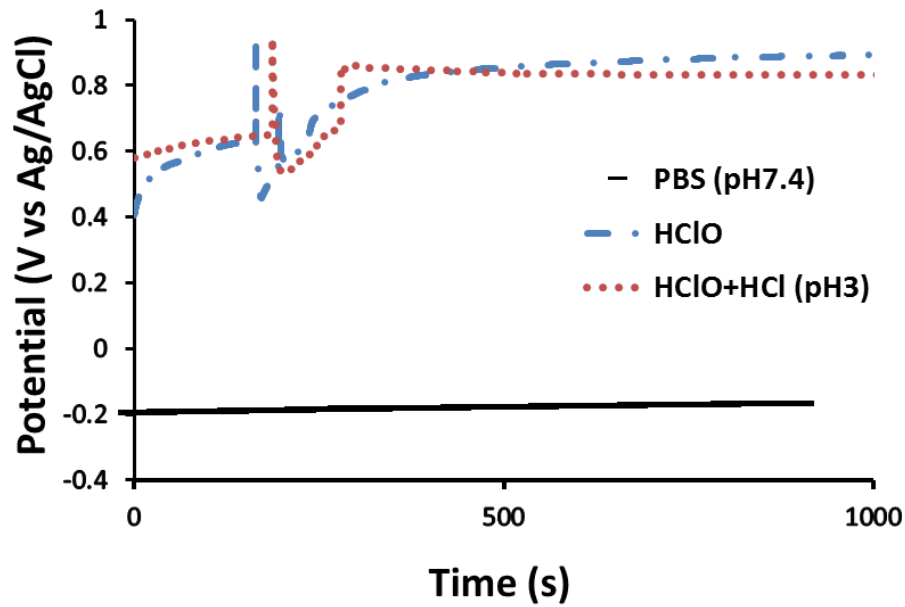
Figure 3.1 Open circuit Potential plots of CoCrMo alloy in PBS solution at different pHs and PBS solution with 0.1M HClO at pH 3 and pH 7.4. A) OCP was raised due to the addition of HCl and shit positively as pH gets lower. B) Summary of OCP in all investigated pH solutions with HClO. OCP increases significantly (p<0.05) due to the presence of HClO. C) OCP vs time evolution in simulated inflammatory conditions with HClO and acid. OCP rises to above 0.85V vs Ag/AgCl in HClO modified solution, creating a highly oxidizing solution for CoCrMo.

A
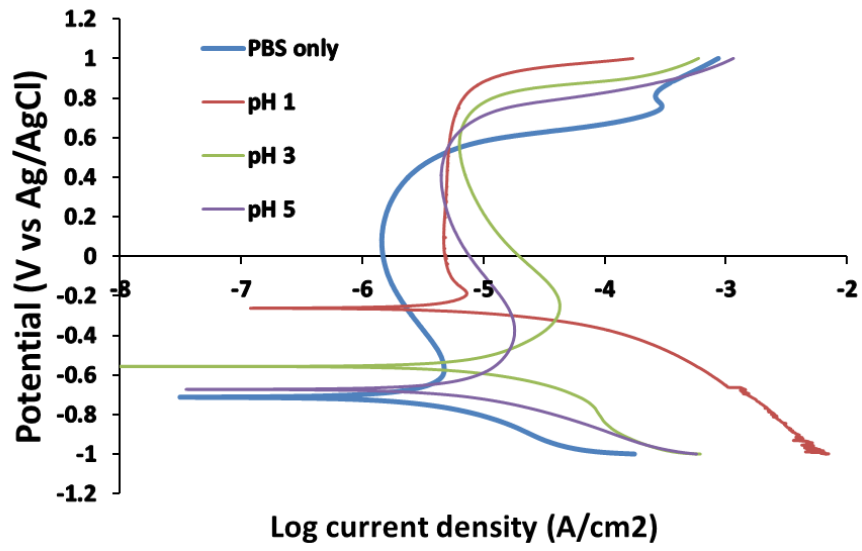


B
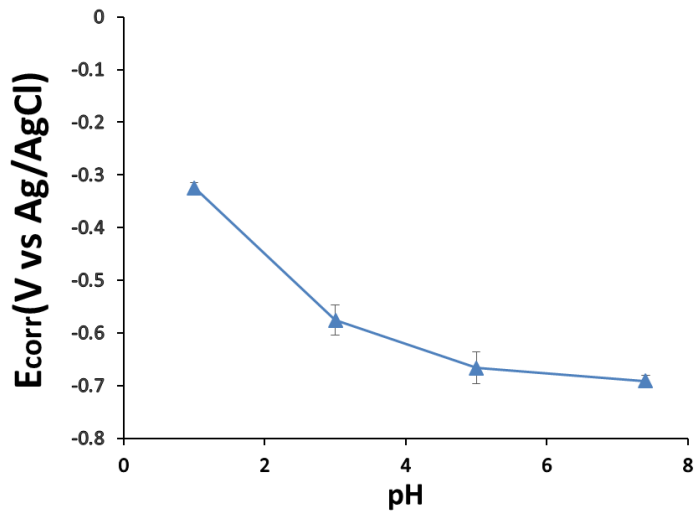


C
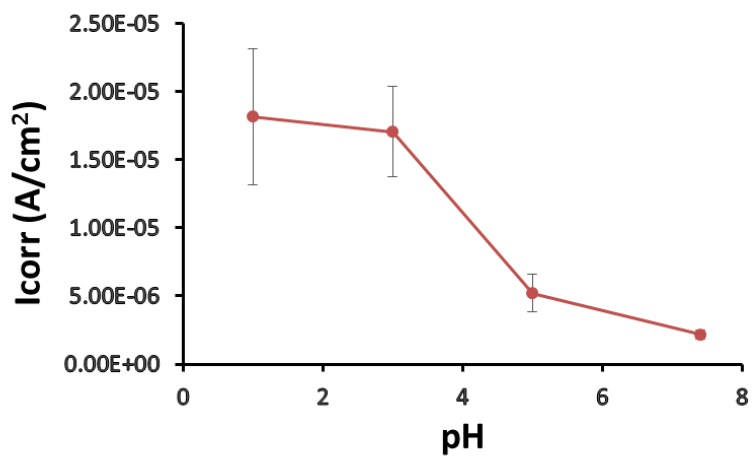
D
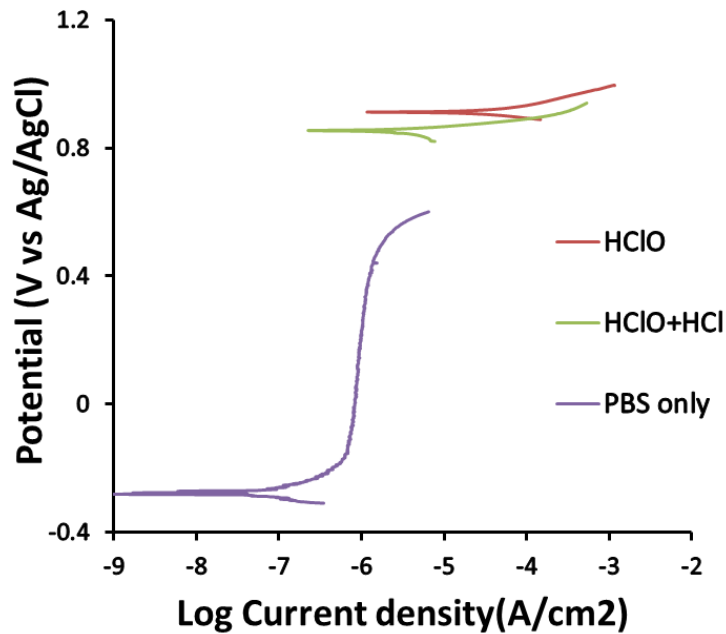


Figure 3.2 A) Potentiodynamic curves of CoCrMo alloy at different pHs in PBS solution. Right

shifts of polarization curve and increase of transpassive voltage are observed with the

decrease of pH. B) Corrosion potential becomes more electropositive as pH gets lower in PBS

solution. C) Corrosion current density shows increasing trend in more acidic PBS solution.

Corrosion current increases from 2.2 uA/cm$^2$ at pH 7.4 to 18.2 uA/cm$^2$ at pH 1 PBS solution. D)

Addition of HClO creates a significant increase in the corrosion currents and lead to changes

in the shape of polarization curve. Acidic shifts of HClO modified PBS solution to pH results in

decreased corrosion rates than in neutral environment. (Values are shown in Table 3.1)
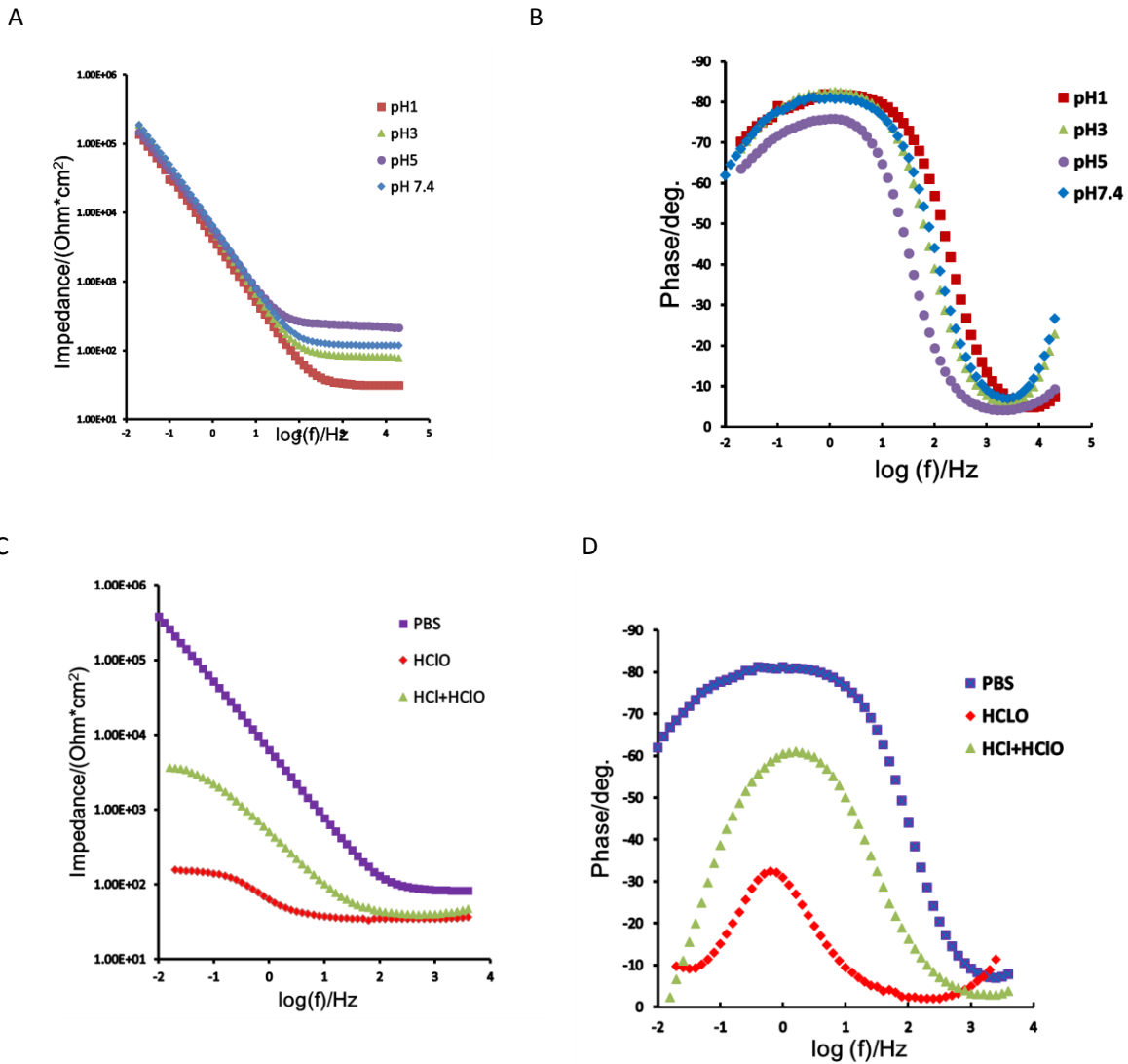
Figure 3.3 Representative Bode Impedance (A) and phase angle (B) plots of CoCrMo alloy in different pH PBS solutions. pH 1 solution shows the smallest impedance magnitude at low frequency (0.01 Hz). Comparison of Bode impedance (C) and phase angle (D) plots in PBS only solution and simulated inflammatory conditions with HClO at pH 3 &7. Decrease of impedance up to 3 orders of magnitude and more depressed phase angle curves were observed in HClO modified solutions. Acidic solution with HClO exhibits increased impedance magnitude than neutral solution with HClO.

A
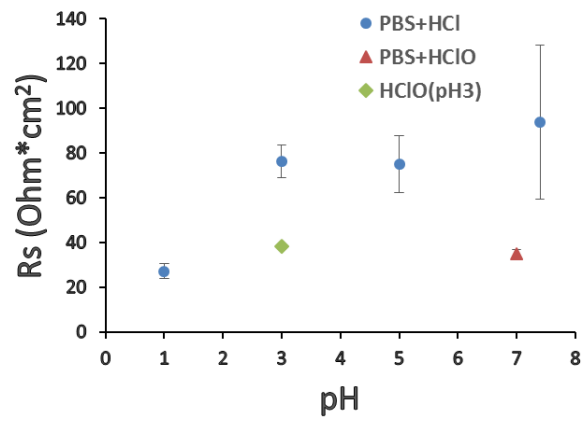


B
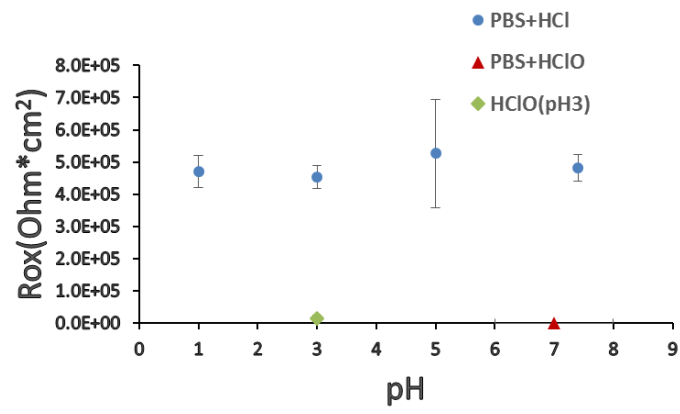


C
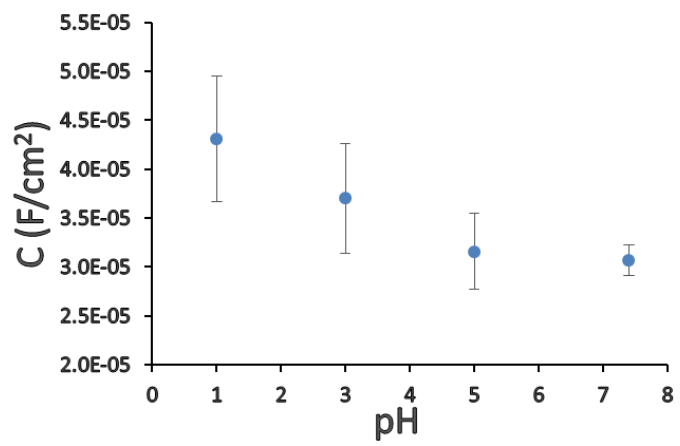
D
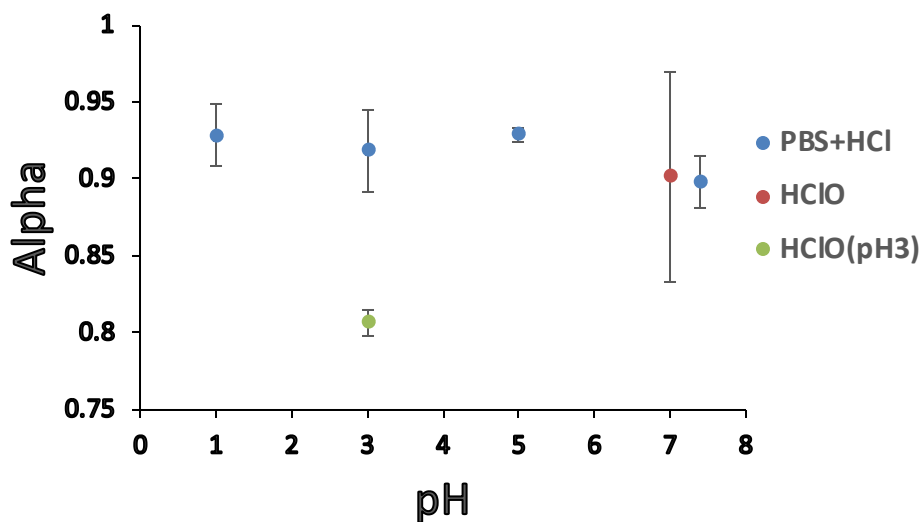


Figure 3.4 Plots of solution resistance, oxide resistance, capacitance and CPE exponent from EIS analysis in different pH conditions. All values are shown in Table II A) Solution resistance shows the smallest value in pH 1 solution. B) Oxide resistance significantly decreases due to the presence of HClO. C) Capacitance increases as pH gets lower. Addition of HClO dramatically increases the capacitance from $10^{-5}$ F/cm$^2$ level in acid modified PBS solutions to $10^{-3}$ F/cm$^2$ level in neutral solution with HClO. (Not shown in the Figure, values are in Table II) D) CPE exponent value is the smallest in acidic solution with HClO.
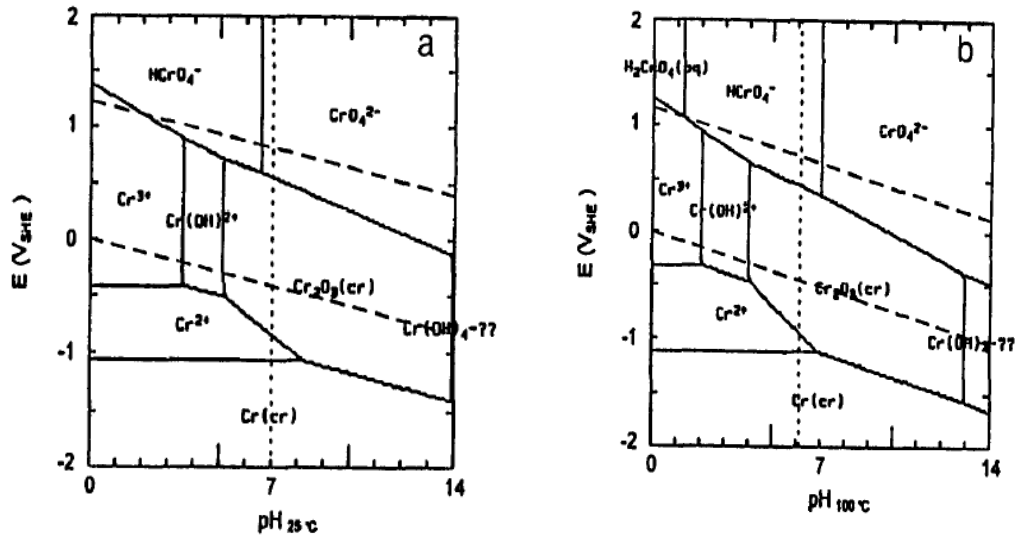
Figure 3.5 Pourbaix diagrams for chromium at different temperatures. (Note: the potential in the Figures is standard hydrogen electrode (SHE), the Ag/AgCl reference electrode used in this study is +0.197 V vs SHE). At 25°C, pH 7, potential for $Cr^{6+}$ formation is 0.6V vs SHE, which is about 0.4V vs Ag/AgCl, while the potential decreases to about 0.2 V VS Ag/AgCl at 100°C.Presence of HClO raised potential to the $Cr^{6+}$ formation range.
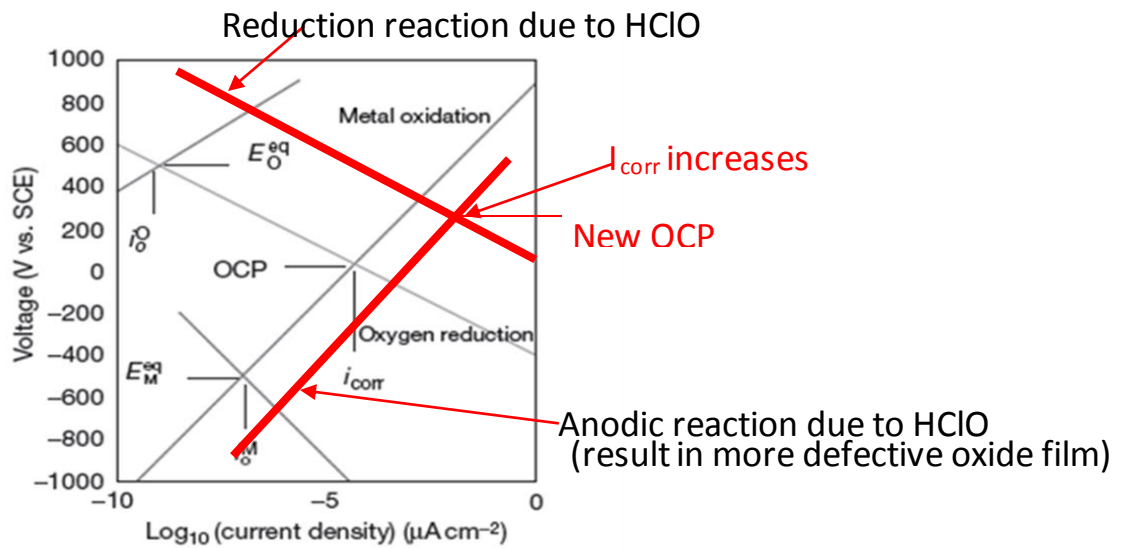
Evan's diagram of possible reaction

Figure 3.6 Significant increase in OCP and corrosion current due to the presence of HClO based on Evan's diagram. Addition of HClO to PBS creates a highly aggressive environment, resulting in larger metal oxidation rates and increased cathodic behavior of CoCrMo alloy.

Table 3.1A

| Electrochemistry parameters | Different pHs | | | |
|---|---|---|---|---|
| | pH 1 | pH 3 | pH 5 | pH 7.4 |
| $E_{corr}$(V) | -0.33$\pm$0.01 | -0.58$\pm$0.03 | -0.66$\pm$0.03 | -0.69$\pm$0.01 |
| $I_{corr}$(uA/cm2) | 18.2$\pm$5.00 | 17.1$\pm$3.31 | 5.2$\pm$1.39 | 2.2$\pm$0.35 |

Table 3.1B

| Electrochemistry parameters | HClO | HClO+HCl (pH 3) | PBS |
|---|---|---|---|
| $E_{corr}$(V) | 0.87$\pm$0.05 | 0.86$\pm$0.00 | -0.26$\pm$0.03 |
| $I_{corr}$(uA/cm2) | 36.9$\pm$9.72 | 3.4$\pm$0.71 | 0.11$\pm$0.02 |

Table 3.1 Electrochemical Test results: Corrosion potential ($E_{corr}$: the potential where the current density changes from cathodic to anodic), Corrosion current density ($I_{corr}$: current density at corrosion potential derived from cathodic extrapolation of the polarization curves). A) Anodic scan started from -1 V to 1V. B) Tests started from 30 mV just below below OCP.

Table 3.2

| Circuit parameters | Different pHs | | | | HClO | HClO+HCl (pH 3) |
|---|---|---|---|---|---|---|
| | pH 1 | pH 3 | pH 5 | pH 7.4 | | |
| $R_s$ ($\Omega$ cm$^2$) | 27.2$\pm$3.2 | 76.3$\pm$7.3 | 75.0$\pm$13.0 | 94.0$\pm$34.4 | 35.1$\pm$1.6 | 38.4 |
| $R_{ox}$ (M$\Omega$ cm$^2$) | 0.472 $\pm$0.05 | 0.45 $\pm$0.03 | 0.53 $\pm$0.17 | 0.48 $\pm$0.04 | (1.4$\pm$0.3)*10$^{-4}$ | 0.014 $\pm$0.01 |
| CPE$_{ox}$ ($\mu$F/cm$^2$) | 43.1$\pm$6.4 | 37.0$\pm$5.7 | 31.6$\pm$3.9 | 30.7$\pm$1.6 | 3800$\pm$1513 | 236$\pm$185 |
| $\alpha$   (%) | 92.8$\pm$2.0 | 91.8$\pm$2.6 | 92.9$\pm$0.5 | 89.8.$\pm$1.7 | 90.1$\pm$0.68 | 80.6$\pm$0.08 |

Table 3.2 Simulated Impedance Parameters found by nonlinear square fitting of the modified Randle's circuit model to the Impedance data.

# Chapter 4 ECAFM study on corrosion behavior of CoCrMo alloy in simulated inflammatory conditions

## 4.1 Introduction

CoCrMo alloys are widely used as biomaterials in dental devices, joint replacements and vascular stents due to its excellent mechanical properties as well as suitable biocompatibility [124-126]. Corrosion resistance has been directly related to the biocompatibility in the past [127]. CoCrMo alloys possess a high degree corrosion resistance due to a spontaneously formed passive oxide film on the surface under normal biological conditions [123, 128]. Surface oxides typically range from 1-10 nm in thickness and protect the bulk alloy from reacting with the biological environment [75, 76]. Thus, the passive films which contact directly with fluid and tissue have been considered highly corrosion resistent in vivo, however, they are actually dynamic and may lose their corrosion protection under specific conditions [77].

Previous studies have shown high early revision rate in hip implants due to adverse local tissue reaction caused by mechanically assisted corrosion which is associated with the use of CoCrMo alloy [129-131]. Mechanical abrasion of surface oxides results in accelerated corrosion of CoCrMo alloy and release of metal ions and metal debris in vivo [8, 14, 15]. On the other hand, these oxide films are highly voltage dependent. Their morphology, composition, thickness as well as impedance have been shown to vary with the surface potential [132, 133] and immersion time [5]. Oxide resistance and capacitance of metallic

biomaterials have been studied at different immersion time and these behaviors have been demonstrated to be time-dependent [83, 84]. It has been known that mechanical abrasion on the surface CoCrMo alloy can negatively shift the potential up to -1V and increase the corrosion rate up to 6 orders of magnitude compared to normal static conditions [11, 85].

Recently, direct cell induced corrosion of CoCrMo alloy has been hypothesized [66, 69]. Once activated, inflammatory cells are able to release reactive oxygen species as well as acid to facilitate the corrosion of CoCrMo alloy. This corrosion mechanism could occur with or without mechanical abrasion on the surface. Physiologically possible potentials of CoCrMo alloy have been found to positively shift from -0.1V up to 0.65V when $H_2O_2$ and Fenton reaction are present under simulated inflammatory conditions. Increase of surface potential into the transpassive potential region have been demonstrated to significantly change surface oxide film chemistry [76], thickness [75], corrosion resistance [132] etc. Release of highly adverse metal ion such as $Cr^{6+}$ is thermodynamically favorable under this condition and XPS studies have shown the existence of $Cr^{6+}$ on the oxide layer at voltages higher than 0.5V in simulated physiological solution [75, 123]. Increase in corrosion susceptibility of CoCrMo alloy in simulated inflammatory conditions has been demonstrated [66]. Addition of $H_2O_2$ into PBS solution significantly increases the corrosion current and decreases corrosion resistance of CoCrMo alloy (Chapter 2 & 3). Positive shifts of open circuit potential of CoCrMo alloy has been directly related to inflammatory level of joint fluid [70]. Thus, in order to better understand the cell-induce corrosion phenomenon, it is of great importance to investigate how inflammatory solution chemistry affects corrosion behavior of CoCrMo alloy. However,

few study has been conducted to directly image how CoCrMo alloy oxide behaves under simulated inflammatory conditions.

To better characterize oxide films, electrochemical atomic force microscopy allows for direct observation of oxide films in biological environment and has been previously applied to investigate titanium [134, 135] and CoCrMo alloy [5, 77]. Electrochemistry experiments can be applied in this ECAFM system to evaluate if surface morphology changes on CoCrMo alloy is related to corresponding electrochemical behavior. The goal of this study was to investigate how oxides on CoCrMo alloy surface behave and how they influence corrosion behavior of CoCrMo alloy under simulated inflammatory conditions. More specifically, voltage, immersion time and solution chemistry effects on oxide morphology, surface roughness and electrochemical behavior were studied.

## 4.2 Materials and Methods

Cast CoCrMo alloy (ASTM F75) with a carbon content of 0.22% by weight was used in this study. This alloy had a carbon content of 0.22% by weight and contains 27-30% Cr, 5-7% Mo, 0.75% Fe, maximum of 1% Ni, Si, and Mg with the balance Co. The samples were 12 mm in diameter and 1mm thick and were ground using a series of silicon carbide abrasive papers (240, 320, 400, and 600 grit). After grinding, the samples were then rinsed with deionized water (DI) ,ethanol and cleaned with DI water in an ultrasonic bath for 10 minutes to remove all traces of silicon carbide particles and polishing compounds. The samples then were polished sequentially using 1, 0.3 and 0.05 um alumina suspensions. After polishing, the samples were again rinsed by DI water, ethanol and were subjected to ultrasonic cleaning.

Appropriate cloth was used at each polishing step.

An AFM (Digital Instruments Nanoscope III Scanning Probe Microscope) was used in this study for capturing images of surface morphology of CoCrMo alloy and conducting data analysis. An electrochemistry (EC) fluid cell was attached to the AFM for in-situ imaging in simulated inflammatory solutions. A three electrode system was used for electrochemistry control and measurements where the CoCrMo disk sample was the working electrode, a platinum (Pt) wire (0.25 mm diameter) was the counter electrode (CE), and a silver (Ag) wire (99.95% purity, 0.127 mm diameter) served as a quasi-reference electrode (QRE). The relative voltage of the silver wire to saturated Ag/AgCl electrode was -0.06V. Thus, it held a reference voltage of +0.137 V with respect to the normal hydrogen electrode (NHE). The schematic illustration of the electrochemical fluid cell and the total ECAFM system were illustrated in Figure 4.1 [134]. CoCrMo alloy sample was attached to a piezoelectric tube of the AFM through a stainless steel magnetic puck (on the bottom of the sample). A thin copper wire was tightly inserted between the magnetic puck and the CoCrMo sample. The copper wire was then connected to the potentiostat and provided electrical contact to the sample. In order to electrically isolate the WE from the AFM, a sheet of thin parafilm (American National Can, Neenah, WI) was placed between the magnetic puck and the piezoelectric tube. After the WE was placed well on the AFM sample station, a glass electrochemical fluid cell (Digital Instruments) was clamped on the top of the CoCrMo disk. The glass EC fluid cell was cleaned by DI water and ethanol before to avoid disturbance from dust on the surface. The EC fluid cell holds a silicon nitride cantilever tip (Nanoprobe SPM tip, Digital Instrument) for surface

scanning and an O-ring to retain fluid on the top of the sample for in-situ imaging. The O-ring has a diameter of 0.75 cm and could contain a solution volume of about 34 uL in the chamber of the EC fluid cell. The quaisi-reference electrode was inserted through a hole in the top of the EC cell and was made to not touch the surface of the WE. Silicone was used to seal the wire and prevent fluid coming out from the hole. All voltages used in this study were referred to the silver quasi-reference electrode. Two ports for fluid output and input were designed in the EC cell. The Pt CE was inserted into the cell through the fluid output port and was made sure to not contact between the CE and sample. About 5 cm of the Pt wire was exposed to the solution in order to avoid limitation of electrochemical reaction at the counter electrode. Both the Ag reference electrode and the Pt counter electrode were connected to the external potentiostat (Solatron 2380).

The solutions used were PBS solution and PBS solution with 30mM $H_2O_2$. A syringe was connected to the fluid input port (Figure 4.1a) and was used to inject solution into the EC fluid cell. Fluid was slowly added into the cell until the inner chamber was just filled and fluid was just about to flow out from the fluid output port. The syringe was removed and the exit tube from the output port was clamped off.

A series of in-situ ECAFM measurements were conducted in freely corroding conditions and potentiostatically held conditions. In freely corroding tests, contact mode deflection/height images were collected every 5 minutes for 2 hours. Open circuit potential (OCP) was first monitored for 20 minutes to make sure that the electrochemical connection was stable and allowed the surface to reach equilibrium at the same time. Deflection and

height images were captured during monitoring of OCP. In the potential-controlled tests, 0.1 V (vs Ag wire) was applied to the CoCrMo sample first and then the potential was incrementally increased to 0.3V, 0.5V, 0.65V. Each potential was held for at least 20 minutes while contact mode deflection and height images were captured. Scanning on the surface started from 20*20 um area and then the scanning range was decreased after a specific area including easily identified grains and carbides was targeted. Direct in-situ surface roughness variation with potential in different solutions was recorded during this experiment. Current measurements were also obtained during potential-held tests using CorrWare software.

## 4.3 Results

### 4.3.1 PBS solution

Figure 4.2 shows AFM behavior of a 8*8 um region of a CoCrMo alloy in PBS solution at different time. It is clear that the surface interacted with PBS solution after immersion. Surface appeared to become less smooth after 30 minutes and more oxide domes were shown after 1 hour. New edge appeared on carbide (Figure 4.2 d-f) and friction images (Figure 4.2 g & h) indicate different chemistry between base alloy and carbide and show variation of chemistry at carbide boundary. Significant increase of surface roughness was observed with time. Surface roughness of this area at 2.5 h was about 1.5 times as large as it was at 0 minute.

Figure 4.3 displays 8*8um contact mode deflection images of a CoCrMo alloy sample in air (Figure 4.3a) and in PBS solution within 2 hours of immersion (Figure 4.3b-d). The oxide film became rougher and small bumps appeared after immersion into PBS solution compared

with it was in air. Surface roughness data shows that surface roughness ($R_a$) increased from

0.8 nm in air to 1.3 nm after 20 minutes in PBS solution (Figure 4.4 trial 1).

Although different $R_a$ values were shown among different samples, increasing trend of

surface roughness with immersion time in PBS solution was consistent. Figure 4.5 shows

relative surface roughness ratio at 30 minute is significantly higher than 1 at the beginning of

the test.

### 4.3.2 Voltage control tests in PBS

Figure 4.6 (a) shows a 8*8 um contact mode deflection image of a CoCrMo sample at

OCP condition in PBS solution. The image was collected after PBS was injected into the EC fluid

cell. Carbides were captured in the center of the figure near the junction of two large scratches

and alloy matrix was clearly identified as well. Figure 4.6 (b-d) displays the ECAFM images of

the same area at elevated potentials from 0.1 V to 0.5 V. At 0.3 V and 0.5 V (Figure 4.6 c & d),

more oxide domes were gradually appearing on the surface and small scratches became

covered due to oxide growing (shown by the arrows). At 0.5 V (Figure 4.6 d), small oxide domes

grew and became larger while the overall surface became less smooth. As shown in Figure 4.6

(e-j), significant changes in surface morphology were captured at 0.65 V within 0.5 h.

Dissolution of alloy matrix was observed first and a large amount of dissolved materials were

shown on the surface (4.6 e-h). Then, carbide dissolution occurred and original surface

features completely disappeared due to oxide transforming and surface dissolution after 20

minutes at 0.65 V. New oxide film formed and large oxide domes became apparent and

gradually covered the total surface (Figure 4.6 i & j). Significant increase of surface roughness

was shown at 0.65V (Figure 4.7) and was in agreement with corresponding ECAFM images. Surface roughness increased from 2 nm to 40 nm within 0.5 h.

Figure 4.8 displays the current information at different voltages during ECAFM tests. It is noticeable that an increase of current density was associated with significant surface morphology changes at higher potential (0.5 V and 0.65 V). At 0.65 V, the current density increased up to 3 orders of magnitude and exhibits time-dependent behavior. It reached the highest value within 5 minutes and then decreased, indicating surface passivation with time. However, the current density level was still high compared to those at lower voltages. It was interesting to notice that the time-dependent current behavior was corresponded to the time-dependent surface morphology transformation. At the beginning of the surface dissolution, the current was the highest and was associated the uniform dissolution of matrix alloy. Following the start of oxide dissolution, new oxide film formation gradually began and current density correspondingly decreased.

Figure 4.9 (a-d) shows a series of smaller scale (5*5 um) contact deflection images of CoCrMo alloy at transpassive voltage ranges. A large carbide with clearly discernable boundary was captured in the center in order to closely observe transpassive behavior of carbide and adjacent matrix. At 0.5 V, both alloy matrix and carbide were undergoing transformation and dissolution. Large oxide dome-shaped structures became apparent after 0.5 hours (Figure 4.9 a-c). The carbide/matrix junctions, grain boundaries and surface defects were preferential sites of dissolution (indicated by circles and arrows in Figure 4.9c and 4.9d). Oxide domes began to appear on carbide and small domes became larger and were grew into

more uniformed shapes after the potential was increased to 0.65 V (Figure 4.9d).

Figure 4.10 (a-k) shows a series of 8*8 um contact mode deflection images of CoCrMo alloy collected in PBS solution at potentials ranging from 0.1 V to 0.75 V. Figure 4.10a displays a scan at OCP condition where a large carbide and several grains were clearly identified and could serve as good reference features for the higher potential scans. No distinct change in surface morphology was observed at 0.1 V (Figure 4.10b). As potential increased to 0.3 V, small remnants of oxide dome at grain boundaries (designated by the circle in Figure 4.10d) were shown, however, no significant change regarding carbide was found. Significant evolution of the surface morphology was observed as the potential further increased to 0.5 V. More dome-shaped structures became apparent on both the alloy matrix and carbide. After 0.5 hour at 0.5 V, dissolution at grain boundaries (Figure 4.10f indicated by the arrows) was discernable. Figure 4.10 g-j shows that, at 0.65 V, significant dissolution at carbide boundaries occurred with the carbide/matrix junction becoming more apparent. Oxide domes on the carbide were transformed and physically enlarged while dissolution of materials on carbide was clearly observed after 1h at 0.65V (Figure 4.10h). At 0.75 V, the surface continued undergoing dissolution with some small grains merging into larger grains and new oxide dome structures. Figure 4.11 shows corresponding current profiles at different voltage. Similar to the result shown before, increase of current density at higher potentials was observed together with drastic surface transformation. Surface roughness information at different anodic potentials was illustrated in Figure 4.12. Initial surface roughness at OCP condition was around 5 nm and increased significantly at the transpassive voltage range (higher than 0.5 V)

and reached 15-20 nm at 0.75 V. It should be noted that the surface roughness changed with the surface morphology and exhibited time-dependent behavior at all potentials.

### 4.3.3 $H_2O_2$+PBS immersion test

Figures 4.13 and 4.14 show sets of 8um by 8um deflection CoCrMo contact mode AFM images in 30 mM $H_2O_2$ modified PBS solution at different immersion times. Rougher surface topography was seen on both carbide and base alloy after 0.5 h and nano-sized oxide domes were present (Figure 4.13 c & d) and swelled with time. Evolution of the carbide surface with time was observed (Figure 4.14 a-d). After 2 hours, surface roughness became about twice as large as it was before immersion (Figure 4.15). Consistent increase of surface roughness with immersion time was shown in all samples.

Original surface roughness varies from samples, however, Figure 4.16 shows that relative $R_a$ ratio shows an increasing trend with immersion time. The $R_a$ ratio at 1.5 h and 2 h are significantly higher ($p < 0.1$) than 1 at the beginning of the test.

### 4.3.4 PBS+$H_2O_2$ voltage control tests

Figure 4.17 shows OCP evolution of a CoCrMo alloy surface in 30 mM $H_2O_2$ modified PBS solution after the fluid was injected into the EC cell. The OCP was around 0.25 V which was in agreement with the results of previous electrochemistry testing in the same solution [66]. Figure 4.18 (a-g) summarizes the ECAFM behavior of a 8*8 um region CoCrMo alloy surface in PBS solution with 30 mM $H_2O_2$. The upper center of the images exhibited bumped surface features and deep scratches which served as reference points during observation of changes

of the surface morphology (Figure 4.18a). No significant transition of surface oxide was observed when the voltage was first increased to just above the OCP value at 0.3 V (Figure 4.18b). Correspondingly, surface roughness stays at around the same value as it was at OCP condition (Figure 4.19) and current density was at a low level (around $10^{-7}$ A/cm$^2$). As the potential was increased further to 0.65 V, noticeable changes of surface morphology occurred, starting with the appearance of many small oxide dome-like structure remnants (Figure 4.18c). Original small scratches were gradually filled and oxide transformation was captured at 0.5 h and depletion of material at grain boundaries was clearly shown (Figure 4.18d). A new oxide film had overgrown the surface and had filled in most of the scratches while small grain boundaries disappeared after 1h (Figure 4.18e-g). Surface roughness increased with time at 0.65 V and reached to about 3 times the value as it was at 0.3 V (Figure 4.19). Significant increase of current density to $10^{-3}$ A/cm$^2$ level was observed once the voltage was increased from 0.3 V to 0.65 V. It exhibited exponential decreasing after 10 minutes and stayed at around $10^{-5}$ A/cm$^2$ level (Figure 4.20).

## 4.4 Discussion

Effect of immersion time on surface topography of CoCrMo alloy in PBS solution was investigated by ECAFM. Increase of surface roughness and oxide domes show growth of the passive film with time. Friction images indicate chemistry changes of the passive film occurs at the same time. Interaction between CoCrMo alloy and solution chemistry was also shown by comparing the AFM image in air and that in PBS solution. A previous study by Hodgson [123] evaluated the effect of immersion time on the general electrochemical behavior of

CoCrMo in NaCl solution using potentiodynamic methods and they found that passive behavior of CoCrMo alloy increased with immersion time due to passive film growth or change in composition of passive film. This study shows similar results and exhibits the dynamics of oxide films at open circuit condition in solution. In PBS solution with $H_2O_2$, significant increase of surface roughness with time and evolution of oxide dome-shape structure exhibit interaction between $H_2O_2$ and CoCrMo alloy. The appearance and development of pit-like structure (Figure 4.13 and 4.14) indicates addition of $H_2O_2$ caused local corrosion attack on CoCrMo alloy. This result is in agreement with study by Hu et al. [136] where they observed initiation of localized corrosion on MP35N alloy after two weeks of exposure in $H_2O_2$ modified PBS solution. Gilbert et al. investigated the effect of $H_2O_2$ on corrosion behavior of CoCrMo alloy and found that corrosion susceptibility of CoCrMo alloy was significantly increased due to the addition of $H_2O_2$ [66].

**Electrochemical information**

Open circuit potential was measured (Figure 4.17) before any voltage controlled ECAFM tests to assess the stability of the testing system. Results show that the three-electrode system was properly set up and well controlled. OCP in PBS solution in the test was at around -0.12 V while it shifted positively to 0.27 V in $H_2O_2$ contained PBS solution. The OCP results are similar to that of previous electrochemistry study where increases of OCP up to around 0.3 V due the addition of $H_2O_2$ was reported [66]. Positive shifts of OCP of CoCrMo alloy in inflammatory joint fluid has been revealed and reactive oxygen species such as $H_2O_2$ are thought to contribute [70]. Based on previous potentiodynamic study, $H_2O_2$ significantly alters the

cathodic behavior of CoCrMo alloy and thus shifts the zero current potential to a more positive region [104].

Current density was simultaneously recorded while ECAFM images were captured at different voltages. In PBS solution, significant increase of current density was observed when potential was increased to above 0.5 V. This result is similar to typical polarization plots for CoCrMo alloy where passivation of oxide occurs in the voltage range from OCP to around 0.4 V and transpassive dissolution occurs at higher voltages. In solutions with $H_2O_2$, similar passive to transpassive corrosion behavior was observed when the voltage was increased from -0.3 V to 0.5 V and current density became larger in the transpassive potential region [104]. It is interesting to notice that in both solutions at controlled voltages, current increased initially and then decreased which indicate the growth of the oxide film after a certain period of time in the voltage controlled test.

**Relationship between surface morphology and electrochemical information**

One goal of this study is to correlate changes in surface morphology with electrochemical behavior of CoCrMo alloy under simulated in vivo conditions. Results of ECAFM imaging and surface roughness measurements show a strong relationship with electrochemistry information, such as current density and voltage.

**In PBS solution**

Figure 4.6 shows typical ECAFM images of CoCrMo surfaces in PBS obtained from anodic potentials above OCP. From OCP to 0.3 V, no significant change of surface was shown due to

already-present protective oxide film. Likewise, the current density was only at $10^{-7}$ A/cm$^2$ level, showing the surface was under passive conditions and was protected by the stable oxide film. Similar phenomena over this potential range were also shown in Figure 9 of ECAFM results of another CoCrMo sample tested from OCP to 0.75V in PBS solution.

Significant changes of surface morphology of CoCrMo alloy in PBS solution were observed as voltage increased to 0.5 V (Figure 4.6, 4.9 and 4.11). Oxide film dissolution and corrosion occurred at this transpassive voltage range. Meanwhile, increase of current density up to 3 orders of magnitude revealed breakdown of oxide film and accelerated corrosion attack on the surface and was in agreement with the results of ECAFM images. As the potential became more positive, current density increased further. Likewise, ECAFM images show that dissolution and depletion of materials at grain and carbide boundaries became more apparent at higher potentials and were in agreement with the increase of current density as well as previous studies of the corrosion mechanism of CoCrMo alloy above transpassive potential [137, 138].

**Simulated inflammatory condition with H$_2$O$_2$**

Another goal of this study was to investigate how oxide film of CoCrMo behaves under simulated inflammatory conditions when H$_2$O$_2$ is present. Previous study showed that OCP shifts positively up to around 0.65 V when Fenton reaction is present [104]. Thus, potential range from OCP to 0.65 V was chosen in ECAFM study when 30 mM H$_2$O$_2$ was present. No significant increase of surface topography was shown when potential increased from OCP to 0.3 V, this was also shown by the surface roughness results (Figure 4.18). Correspondingly,

current density stayed at a low level due to only slight anodic voltage shifts from OCP at 0.3 V. When voltage increased to 0.65 V, dissolution and corrosion attack on the surface was noticeable and current density significantly increased to $10^{-3}$ A/cm$^2$ level. Corrosion attack adjacent to carbide boundaries were observed and grain boundaries became pronounced (Figure 4.18) during the corrosion process. Compared with the current density in PBS solution ($10^{-4}$ A/cm$^2$ level), the current density in solution with $H_2O_2$ is significantly higher. This is in agreement with the result of previous work which showed that $H_2O_2$ increased the current density at anodic polarization potentials. Interestingly, ECAFM images in PBS solution with 30 mM $H_2O_2$ (Figure 4.18 c & d) exhibit different topography surface changes compared to those in PBS only case. Alloy matrix were corroded away and the carbides protruded, which was opposite to the surface evolution observed in PBS only case (Figure 4.6) where new oxide film increased in thickness and gradually covered the carbides. Likewise, surface roughness in $H_2O_2$ cases increased from 1 to 4 nm only at the transpassive potential region, and was a significantly lower increase compared to that in the PBS only case. However, it should be noted that more significant variation in surface roughness was shown in PBS solution with $H_2O_2$ than that in PBS only solution at OCP condition. Thus, it is reasonable to speculate that addition of $H_2O_2$ alters the oxide film on CoCrMo alloy and significantly affects its anodic dissolution behavior. It has been shown that stability of passive oxide film on CoCrMo alloy was decreased due the presence of $H_2O_2$ and cathodic reaction as well as coefficient of friction during fretting corrosion were significantly altered [104]. Future study of surface oxide structure and chemistry (e.g., using x-ray photoelectron spectroscopy) to look at how reactive oxygen species such as $H_2O_2$ affects the oxide film chemistry and composition are being planned.

Reactive inflammatory species released by inflammatory cells such as $H_2O_2$, HClO, possess high oxidative potential and are thought to be involved in the cell induced corrosion mechanism on CoCrMo alloy [66, 69]. With the presence of metal ions such as $Fe^{2+}$, $Fe^{3+}$, $Cr^{3+}$, $Cr^{6+}$, $Co^{2+}$, a series of Fenton-like reactions occur and other highly reactive radical species like $OH^{\cdot}$, $HO_2^{\cdot}$ are generated, further increasing the corrosion susceptibility of CoCrMo alloy [68]. On the other side, the presence of highly oxidative species increases the possibility of metal dissolution from CoCrMo alloy and the presence of $Cr^{6+}$ ions is thermodynamically favorable under simulated inflammatory conditions [66, 92]. Elevated levels of Co ions and Cr ions in patients with metal-on-metal implants have been reported [14]. Inflammatory conditions have been shown to significantly decrease the corrosion resistance of CpTi and Ti6Al4V under cathodic inflammatory conditions [64]. With the presence of both protein and $H_2O_2$, the rate of metal release was far higher than it was in the presence of either specie alone and $H_2O_2$ increased both the rates of the anodic and cathodic reactions of Ti6Al4V alloy [139]. With the increase of inflammation level in human synovial fluids, the corrosion behavior of CoCrMo alloy may be significantly altered [70]. In-vitro studies have also shown that activated inflammatory cells are able to directly corrode stainless steel and titanium [57, 58]. Recent retrieval study has reported in-vivo inflammatory cell-induced corrosion of titanium alloy implant surfaces [96]. In this study, $H_2O_2$ has been shown to alter/increase the corrosion susceptibility of CoCrMo alloy under simulated inflammatory conditions. However, the levels of $H_2O_2$ concentration and at what rate it is released by inflammatory cells in vivo is not known and needs to be further explored.

**Time-dependent behavior**

It is interesting to note that the surface morphology variation with time was in agreement with the time-dependent current density behavior under controlled voltage conditions. For example, Figure 4.6 (e-j) illustrate transient changes of surface morphology of CoCrMo alloy at 0.65 V for 0.5 h. After about 15 minutes, the previous oxide film dissolved and formation of new oxide layer was clearly observed and gradually covered the surface in about 10 minutes. However, as shown by the ECAFM images, this new oxide film was not as dense as the former one and thus it is reasonable to speculate that corrosion resistance was decreased due to the formation of a less protective oxide film. Likewise, the time-dependent current profile (Figure 4.8) is in good agreement with surface morphology evolution at different time periods. Current density increased at first, corresponding to the breakdown of the former oxide film, and then decreased due to the formation of a new oxide layer. However, the current density was still at a significantly higher level than it was at lower potential, indicating that this less dense oxide layer was not as protective as the former one.

These observations are similar to the results of previous polarization and XPS study on CoCrMo alloy by Hodgson et al. [123]. They found strong oxidative dissolution of Cr-oxide film and increase of metal ion release at this voltage region. Meanwhile, their XPS results revealed the existence of a newly formed oxide-film which was thicker and was different in composition from the previous one while it was not highly protective. Thus, it is reasonable to speculate that significant changes in chemistry and structure yielded a less-protective oxide film. A previous EIS study [132] also showed similar results where a decrease of corrosion resistance

and increase of capacitance occurs in the transpassive voltage region. Again, it is interesting to notice that the increase of thickness of the oxide layer was also directly shown by the ECAFM images in this study. Results from this study further demonstrate that susceptibility to corrosion of CoCrMo alloy is affected by a combined effect of oxide thickness, chemistry and structure. Interfering only from variation of one factor is not enough to determine how the corrosion behavior of the oxide changes.

**Preferential sites on dissolution of CoCrMo alloy**

Significant depletion of materials at the boundary between carbides and alloy matrix are shown in Figure 4.9 (a-d) and Figure 4.10 (e-l) and demonstrate that the carbide boundaries are the preferential sites for anodic dissolution and corrosion attack of CoCrMo alloy. This may be due to the chromium leeching of alloy matrix near the carbide/alloy boundary during carbide formation. Bettini et al. [138] studied the influence of metal carbides on dissolution behavior of CoCrMo alloy and found that the matrix areas adjacent to large carbides exhibit lower nobility compared to the matrix. The carbides, therefore, become preferential sites for metal dissolution. During the initiation of localized corrosion and dissolution, the boundary regions behave as an anode while the carbides act as cathodes. Another interesting finding from in this study is the dissolution and morphology change on the carbides during anodic dissolution at high potentials in some cases (Figure 4.10). This phenomenon hasn't been reported before and indicates the heterogeneity of chemistry exists on carbides. Another noticeable site for anodic dissolution of CoCrMo alloy is the grain boundary. As it is shown in Figure 4.10, as potential increases to 0.5 V, grain boundaries became slightly apparent. When

the potential was further increased to 0.75 V, dissolution at the grain boundaries were clearly observed. It is also interesting to note that small carbides exists at some grain boundaries and further contribute to the corrosion attack at these sites. Preferential dissolution at grain boundaries may be attributable to the grain boundary Cr depletion, heterogeneous microstructure and Cr distribution along grain boundary, all of which affect local dissolution of CoCrMo alloy [137].

**4.5 Conclusion**

This study is the first to directly image surface oxide variations during electrochemical testing under simulated inflammatory conditions. Physiologically possible anodic potentials were applied in different solution conditions with or without the presence of $H_2O_2$. Analysis of ECAFM images, surface roughness and potentiostatic polarization information exhibited a correlated relationship between surface morphology and electrochemical behavior of CoCrMo alloy. The following conclusions were reached:

- Surface topography shows variation with immersion time both in PBS solution and PBS solution with $H_2O_2$ at OCP condition. Increase of surface roughness with time indicates interactions between oxide film and solution. More significant increase in surface roughness is shown in PBS solution with $H_2O_2$ compared to PBS only.

- ECAFM images reveal significant surface dissolution and corrosion of oxide on CoCrMo alloy occurs at around 0.5V and are directly related to increased current density at the same potential.

- New oxide formation is observed at the transpssive potential region in PBS solution.

However, it is not highly corrosion protective as the passive oxide film at OCP condition.

- Surface morphology variation, surface roughness and current density exhibit strong time-dependent behavior.

- Carbide boundaries and grain boundaries are preferential sites for oxide dissolution at transpssive potential regions.

- ECAFM images show presence of $H_2O_2$ in PBS solution alters oxide film behavior. Significantly higher current density, positive shifts of OCP and less increase in surface roughness are observed. The results indicate different corrosion reactions occur at SI conditions.

a

Ag reference electrode

fluid cell

AFM tip

fluid

fluid input

Pt counter reference

b

cantilever clip

Ag reference electrode

fluid output

fluid input

fluid cell

O-ring

CoCrMo sample

parafilm barrier

piezoelectric tube

to AFM

RE

WE

CE

potentiostat
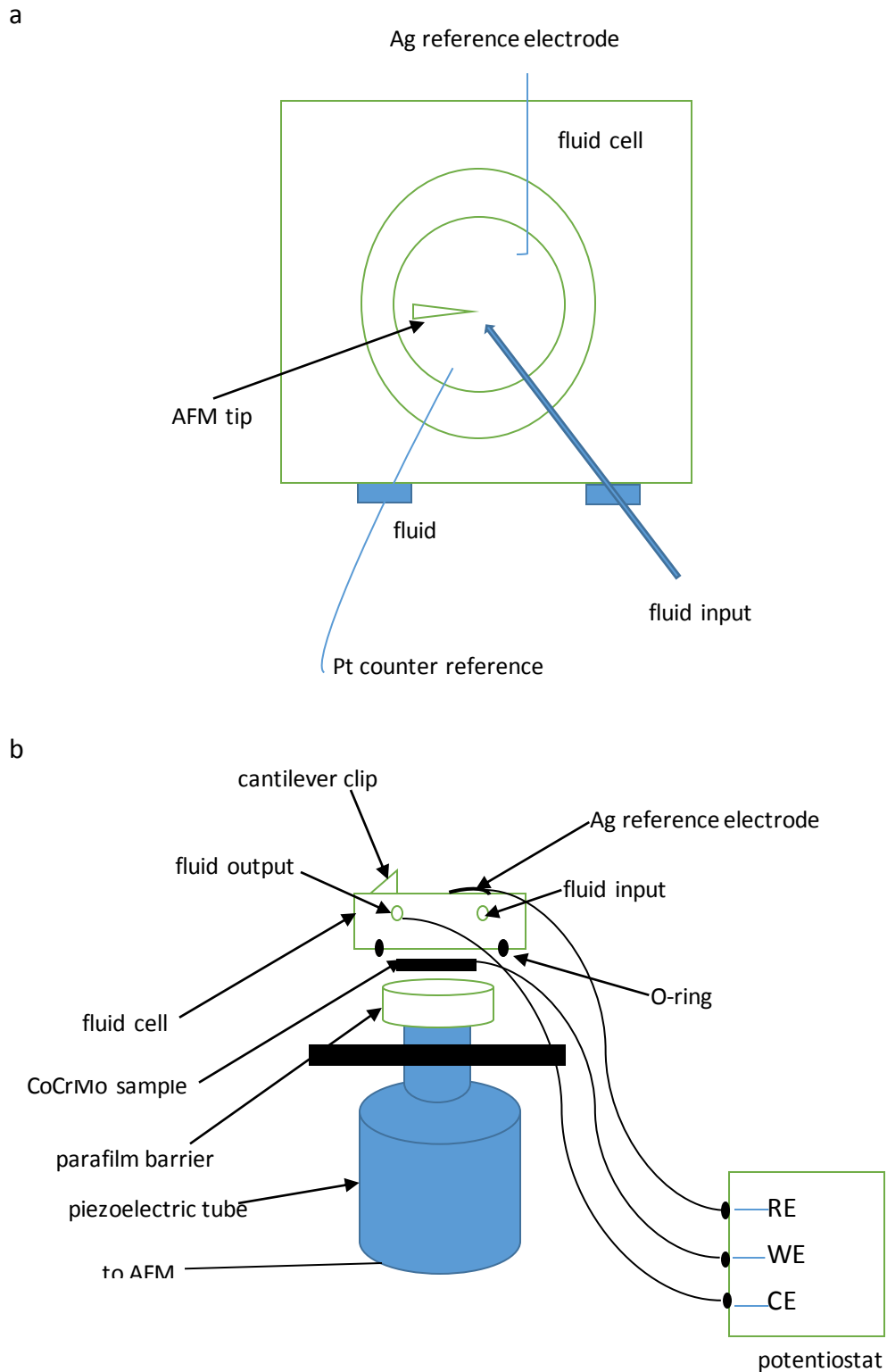
Figure 4.1 Schematic illustration of (a) underside of electrochemical fluid cell and (b) side view

of ECAFM system design; fluid cell in this view is vertically flipped view from (a).
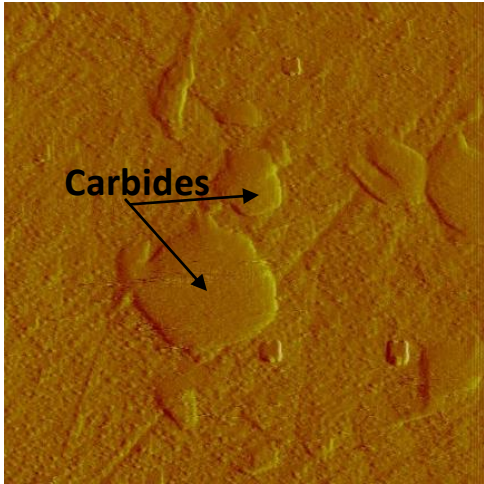
(a) 0 minute
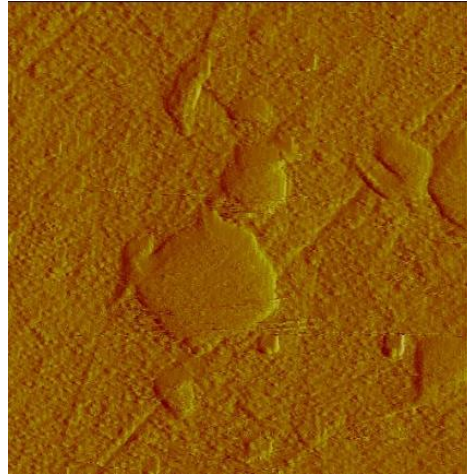
(b) 30 minutes
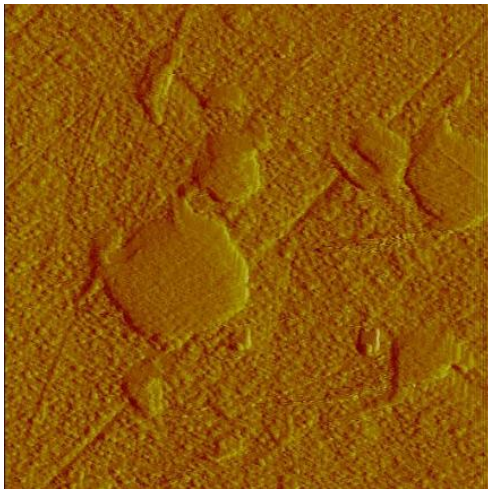
(c) 1h
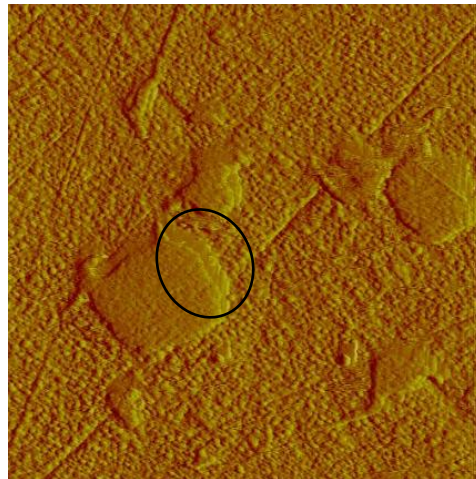
(d) 1.5h
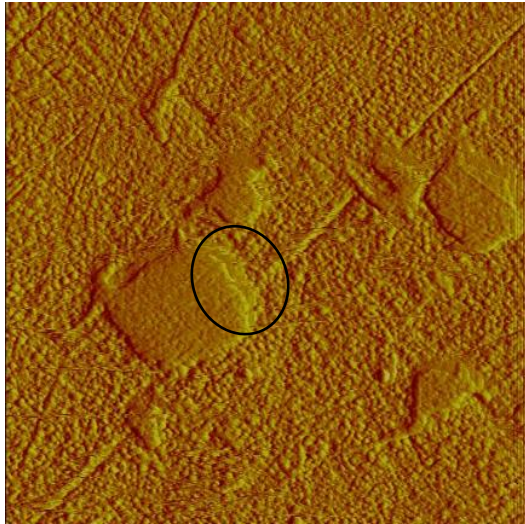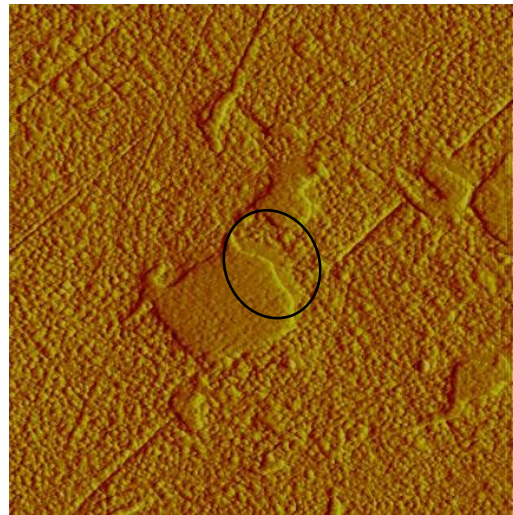
(e) 2h                  (f) 2.5h
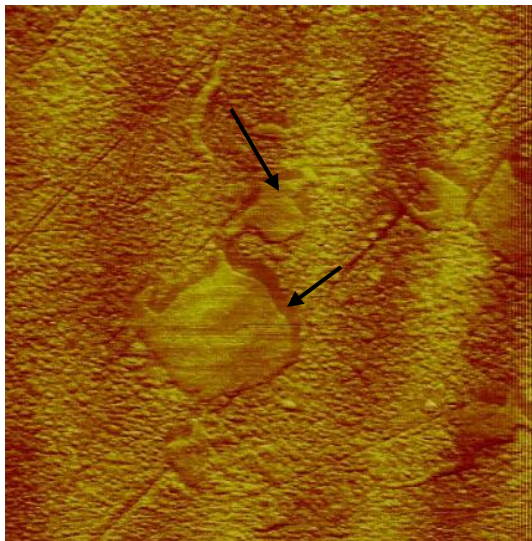
g (Friction image (1.5h))          h (Friction image (2.5h))
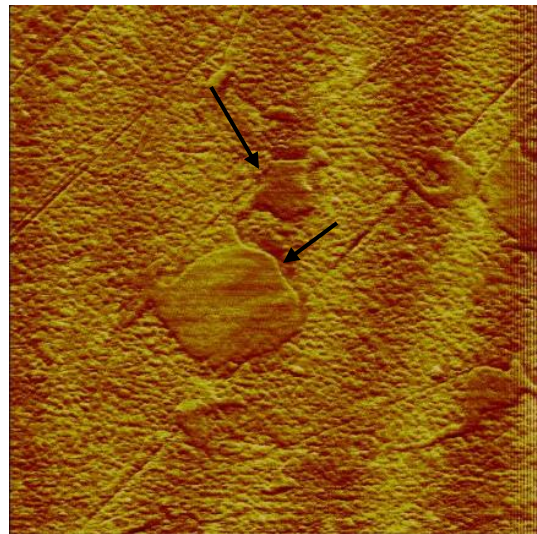
Figure 4.2 AFM deflection images (a-f) and friction images (g&h) for a CoCrMo alloy in PBS solution at different immersion time (8*8 um). Note, the arrows in g and f show chemistry variation between carbide and carbide boundary.
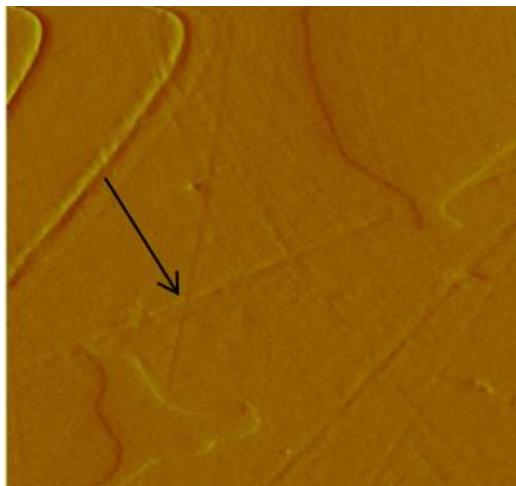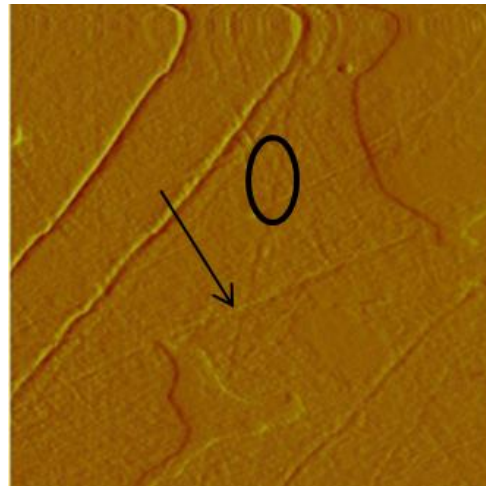
(a) In air( 0 minute)　　　　　　　　　(b) 20 minutes
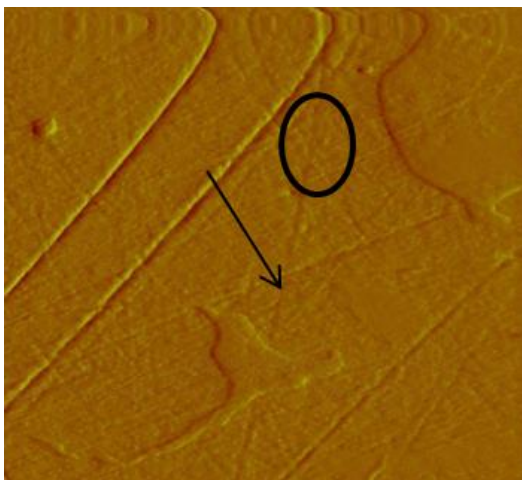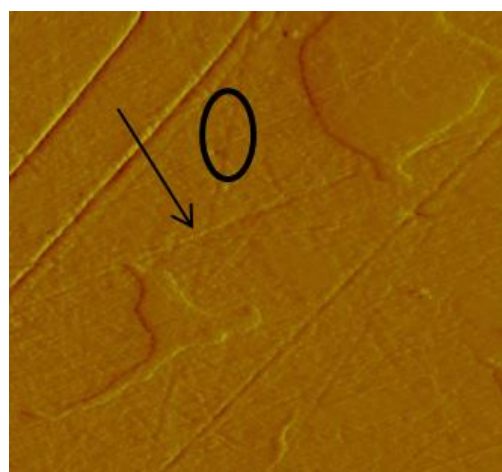
(c) 40 minutes　　　　　　　　　　(d) 2 hours

Figure 4.3. AFM deflection images for a CoCrMo alloy in PBS solution at different immersion time (8*8 um). The arrow and circle show the areas where oxide films become rougher and more scratches show up.
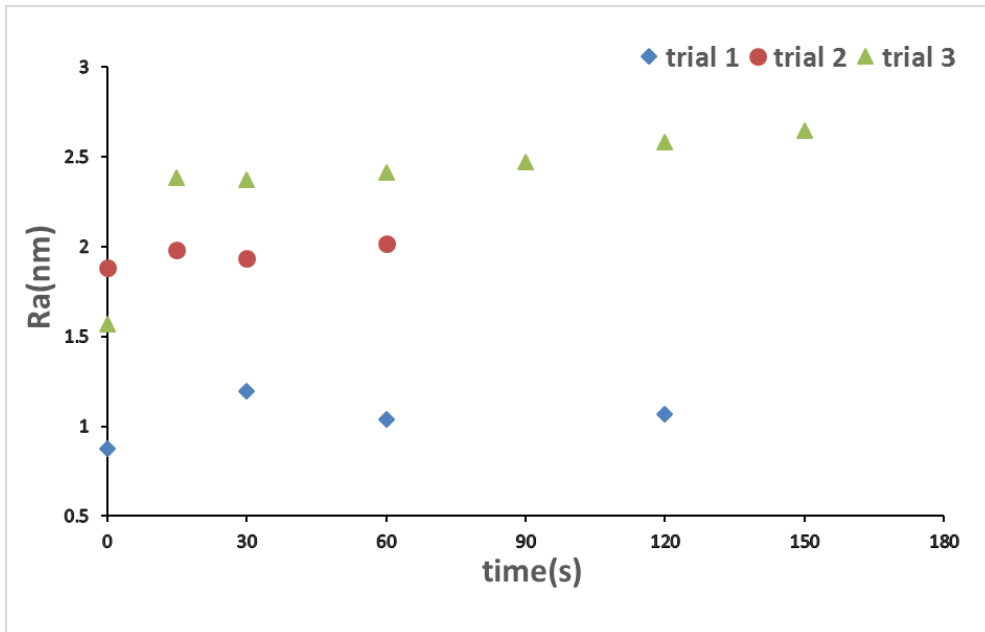
Figure 4.4 Surface roughness of CoCrMo alloy in PBS solution as a function of immersion time

(8*8 um).
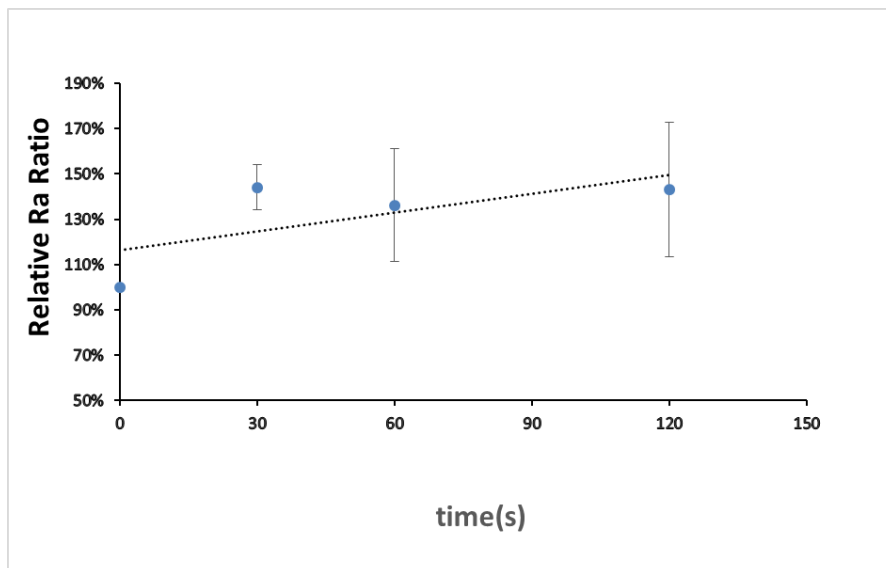


Figure 4.5 Relative $R_a$ ratio of CoCrMo alloy at different immersion time.
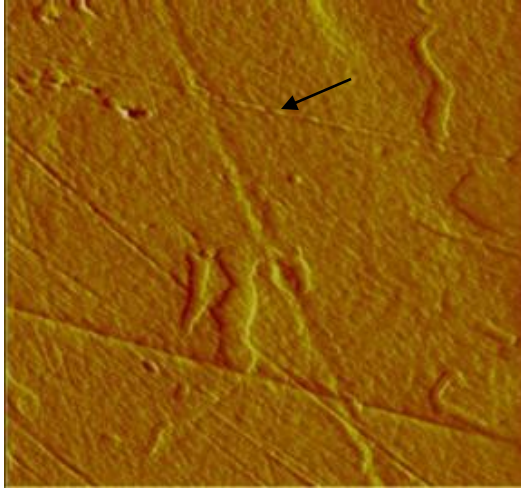
(a) OCP
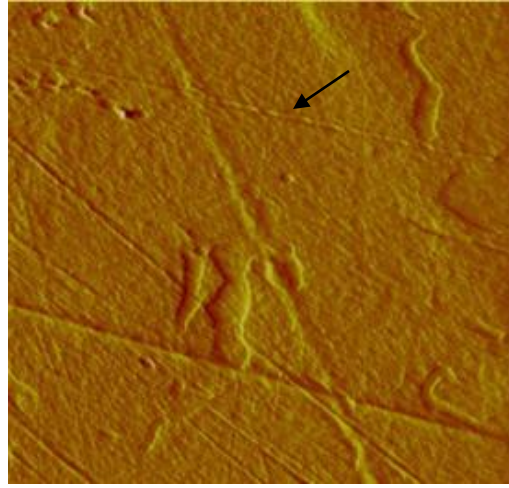
(b) 0.1V (15 minutes)
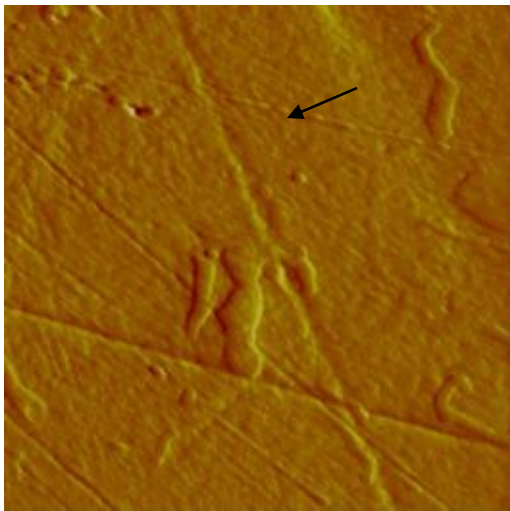
(c) 0.3V(40 minutes)
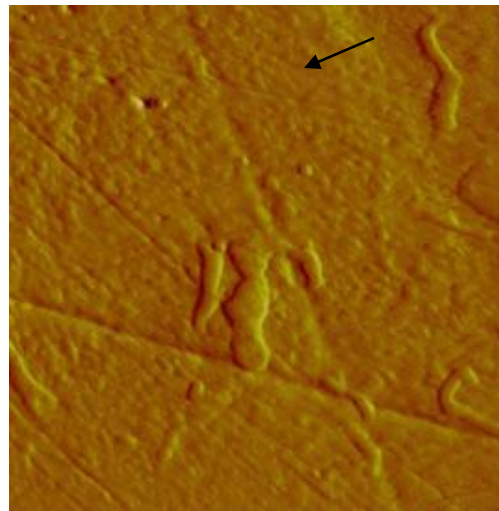
(d) 0.5V (40 minutes)
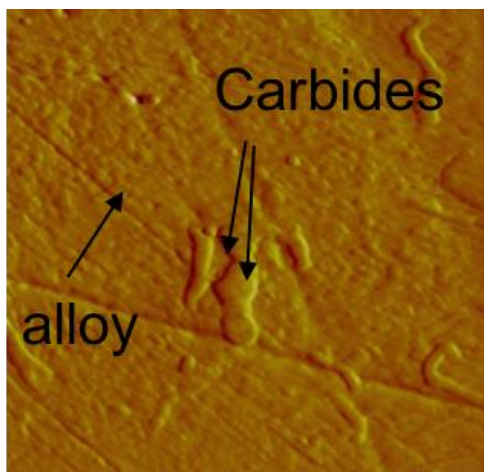
(e) 0.65V 0 minute
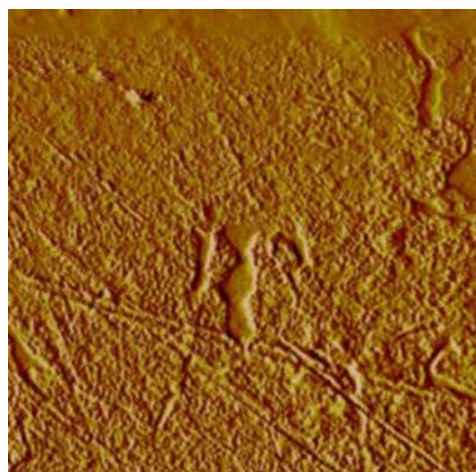

(f) 0.65V 5 minutes
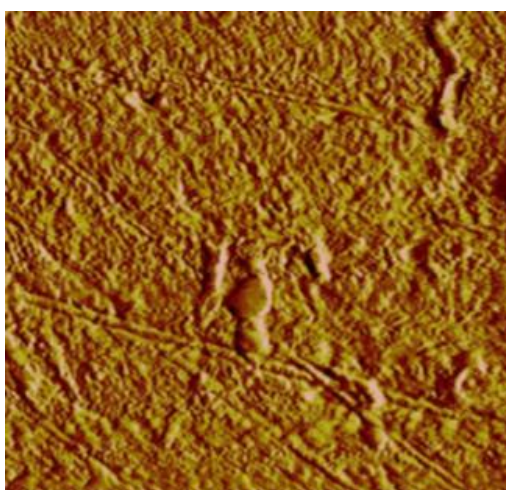

(g) 0.65V 10 minutes
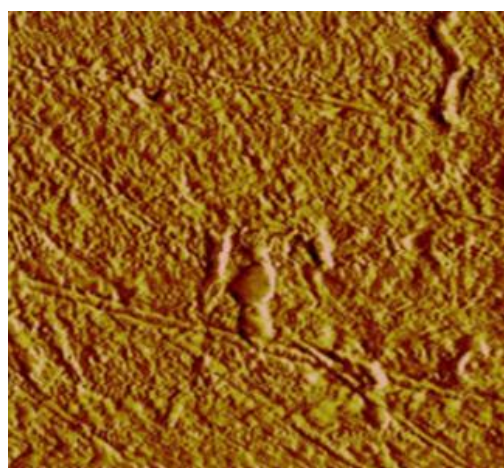

h) 0.65V 15 minutes
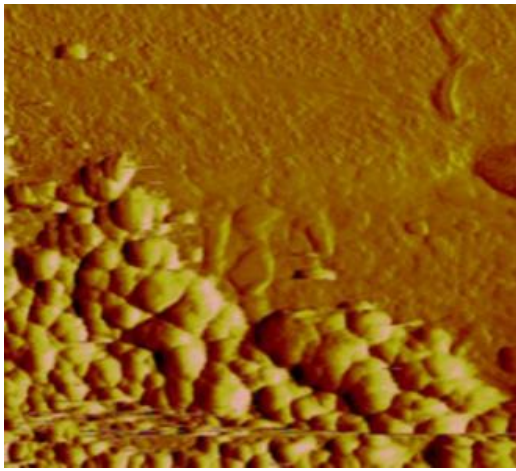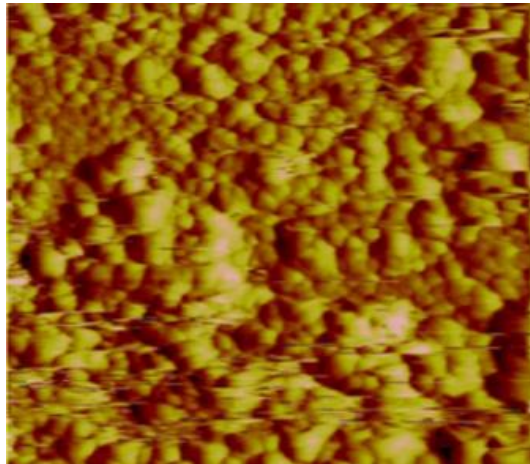
(i)  0.65V 20 minutes        (j)  0.65V 25 minutes

Figure 4.6(a-j) AFM contact mode deflection images of CoCrMo alloy in PBS solution at different voltages (8*8um). Note, arrows in (a-d) show oxide domes appeared on the surface as voltage increases from 0.1 to 0.5V. At 0.65 V (e-j), oxide films kept on dissolving and reforming and significant morphology changes were observed.
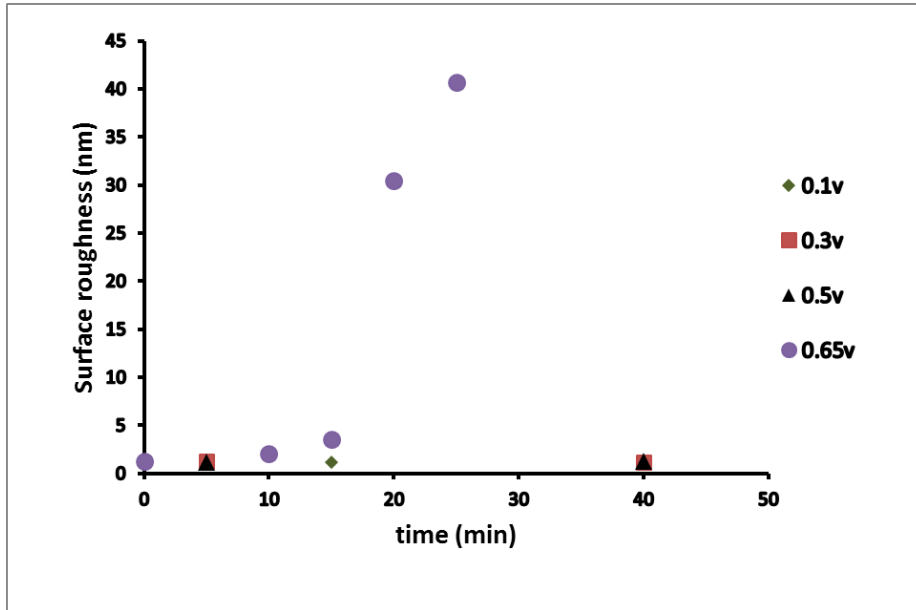
Figure 4.7 Time-dependent surface roughness of CoCrMo alloy at anodic voltages.
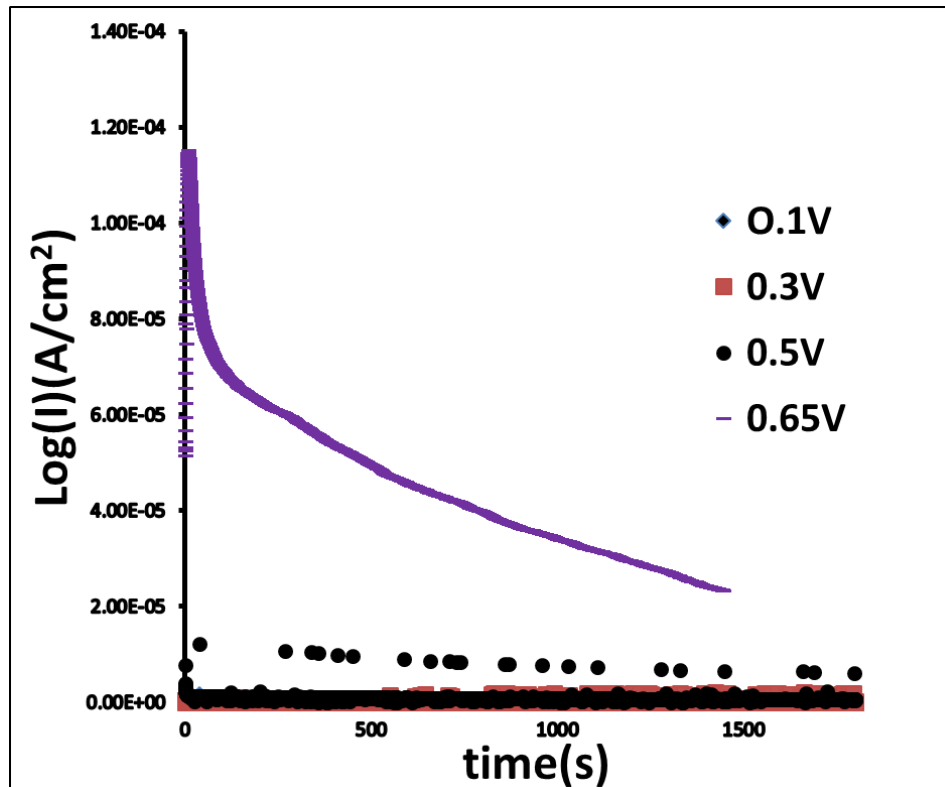


Figure 4.8 Time-dependent current at different voltages in PBS solution. Current density

increases up to 3 orders of magnitude as the voltage increased to 0.65 V.

99
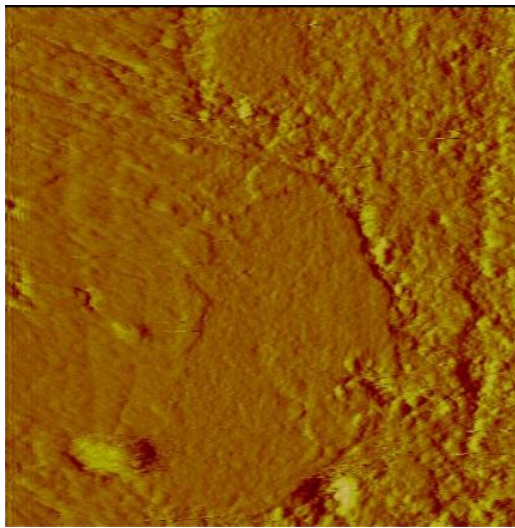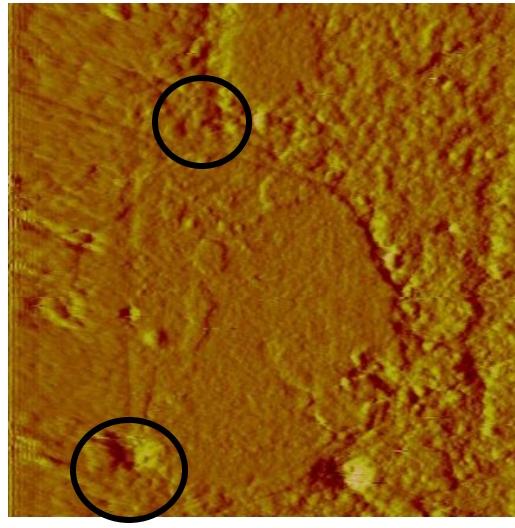
(a) 0.5 V (5 minutes)　　　　　　　　　　　　(b) 0.5V (10 minutes)
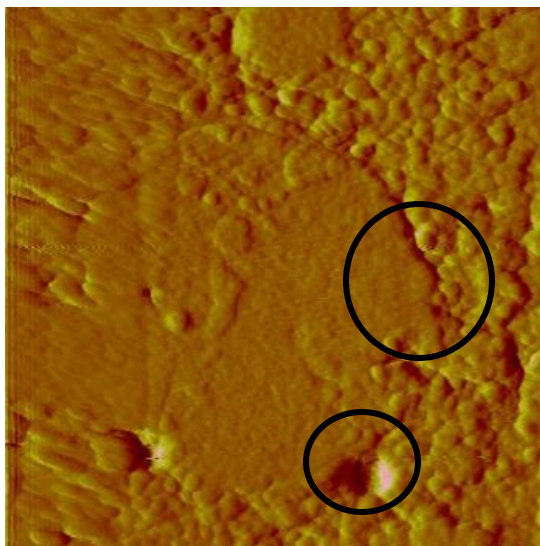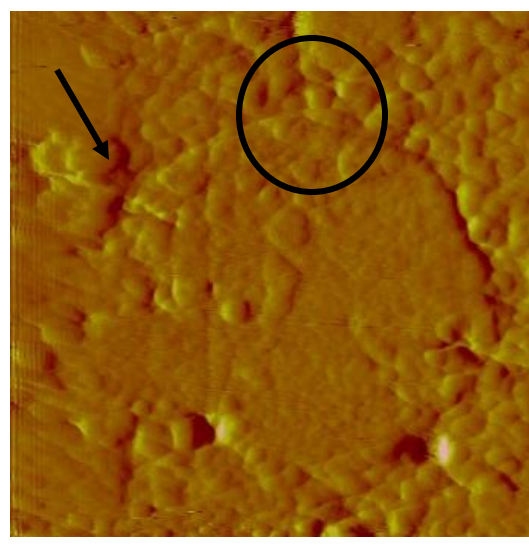
(c ) 0.5V (0.5 h)　　　　　　　　　　　　(d) 0.65V (0.5 h)

Figure 4.9 ECAFM contact mode deflection images of CoCrMo alloy at transpassive voltages in

PBS solution (5*5um)
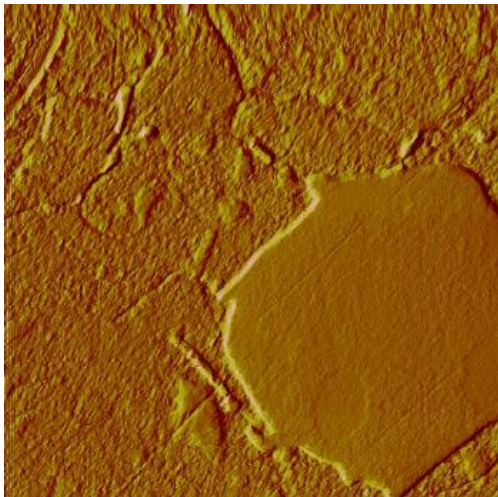
(a) OCP
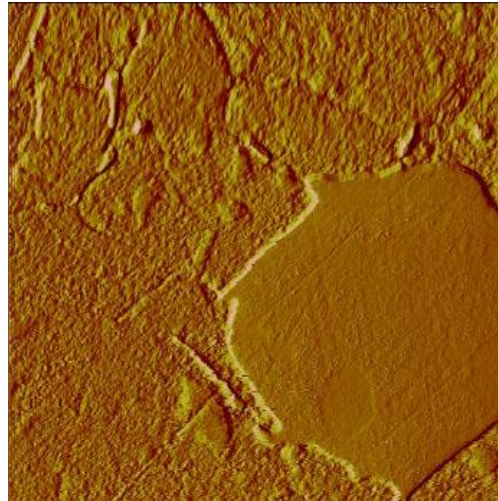
(b) 0.1V 15 minutes
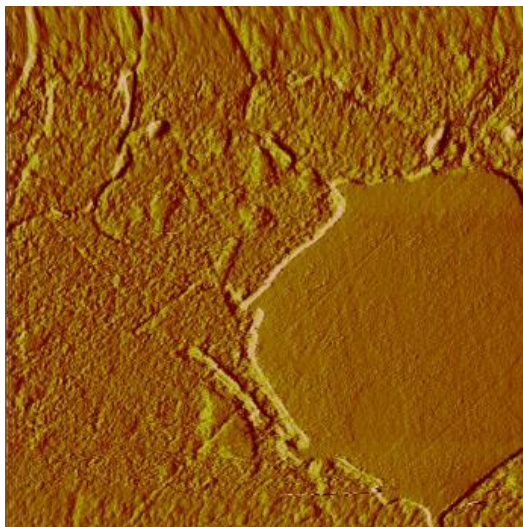
(c) 0.3V
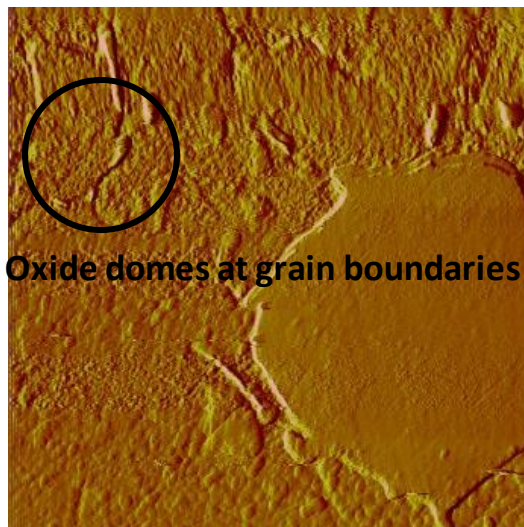
(d) 0.3V 15 minutes

Oxide domes at grain boundaries
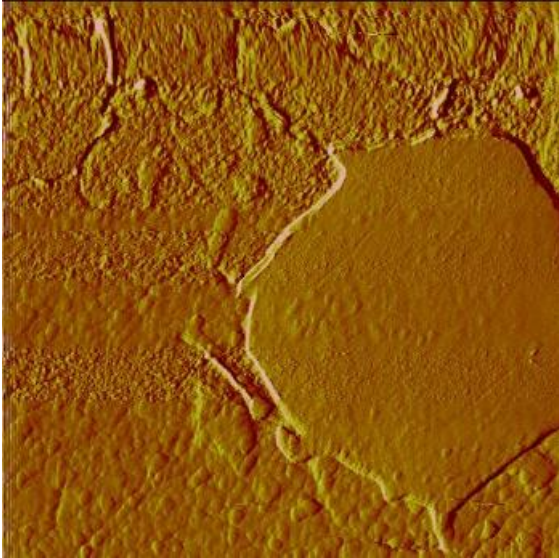
(e) 0.5V 0 minute
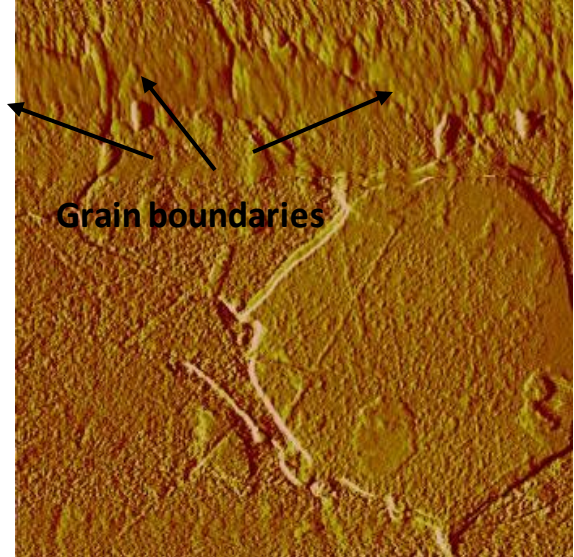

(f) 0.5V 30 minutes
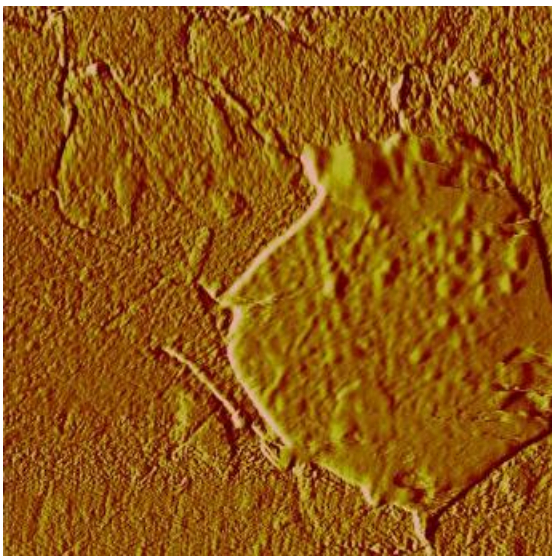

(g) 0.65 0 minute
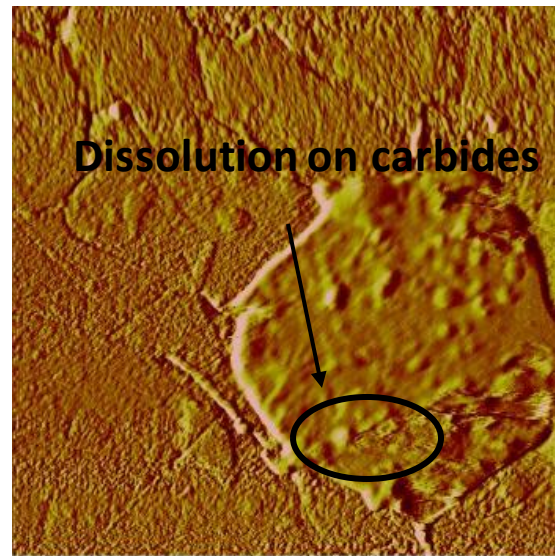

(h) 0.65 5 minutes
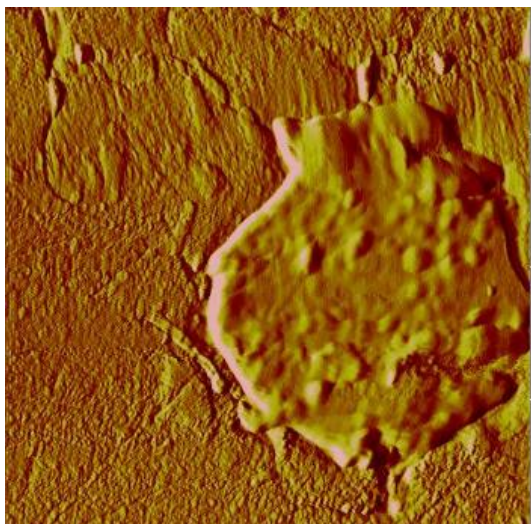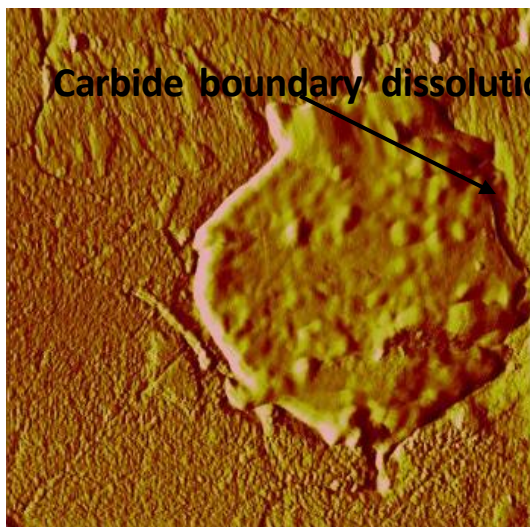
(i) 0.65V 30 minutes          (j) 0.65V 1 h
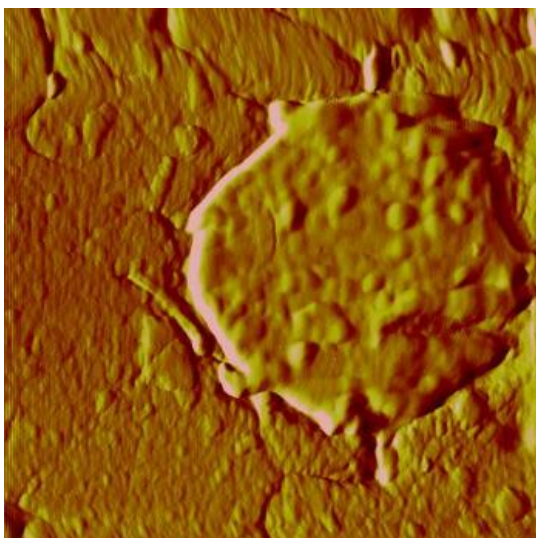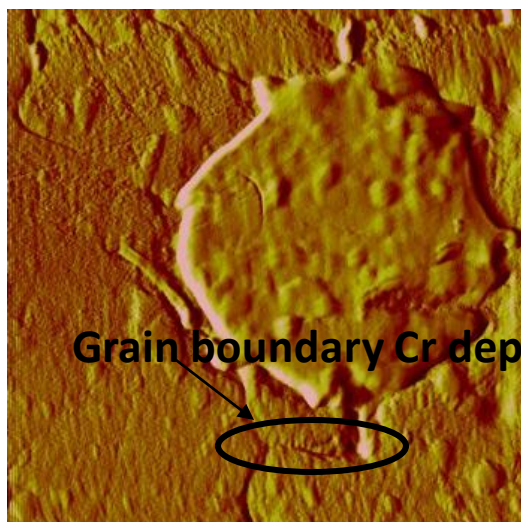
(k) 0.75V 10 minutes          (l) 0.75V 40 minutes

Figure 4.10 ECAFM contact mode deflection images of CoCrMo alloy at different voltages in PBS solution (8*8um). Not, grain boundary depletion of base alloy element was observed (f and l). Dissolution on carbide boundary (j) and carbides (h) were shown.
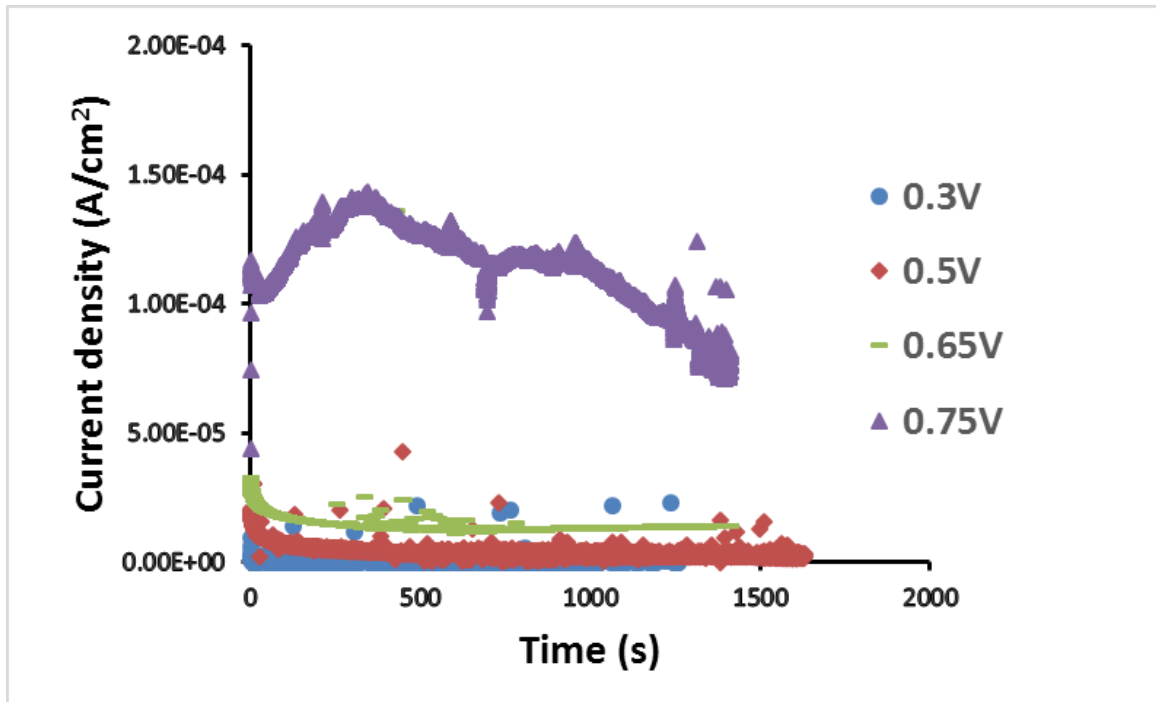
Figure 4.11 Current profiles at different voltages during ECAFM experiments in PBS solution.

Significant increase of current density at voltage above 0.5V were shown.
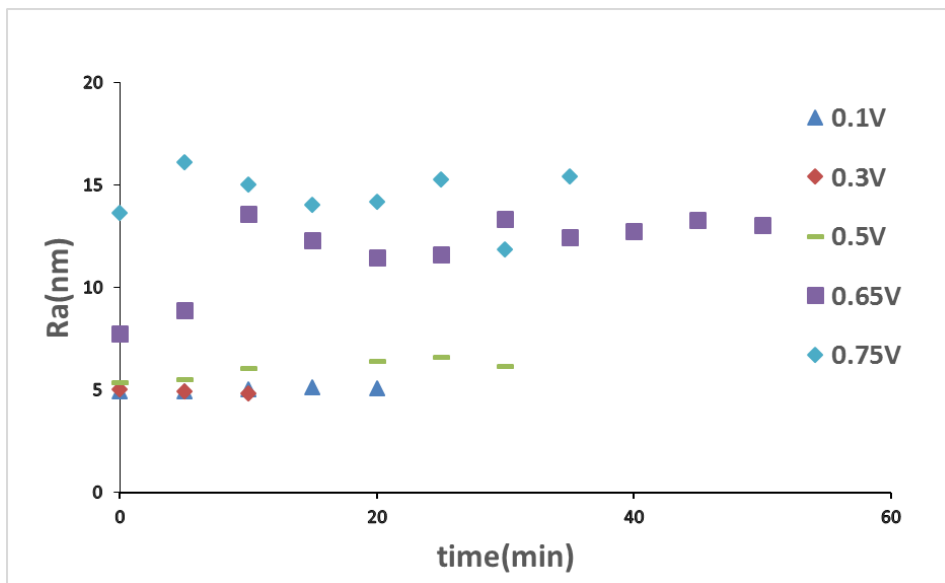


Figure 4.12 Surface roughness of CoCrMo alloy at different potentials in PBS solution. Increase

of surface roughness at transpassive voltages (0.65V and 0.75 V) were shown.
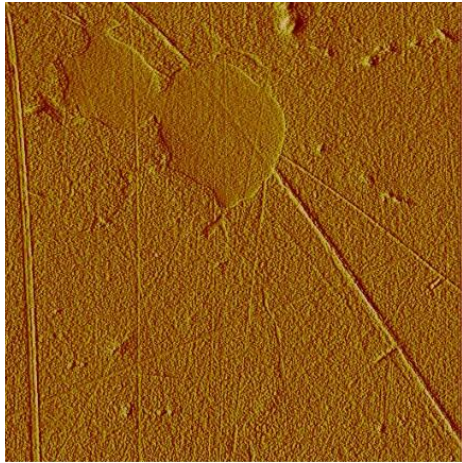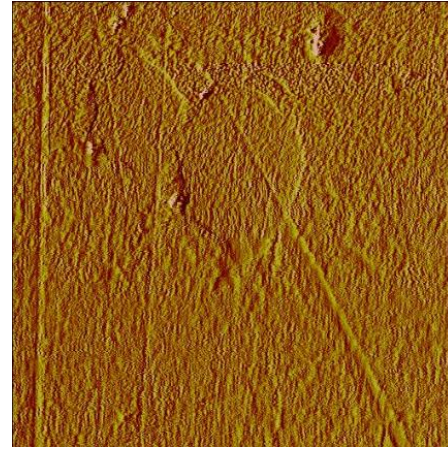
(a) 0 h         (b) 0.5 h
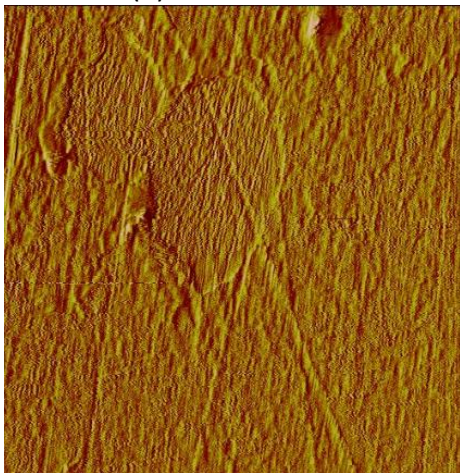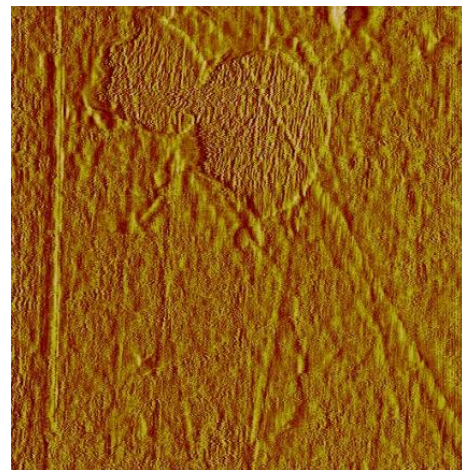
(c) 1 h         (d) 2 h

Figure 4.13 AFM deflection images for a CoCrMo alloy in PBS+30 mM $H_2O_2$ solution at different immersion time (8*8 um). Surface roughness is shown in Figure 7. Note. Stretched images are due to sticking of O-ring.
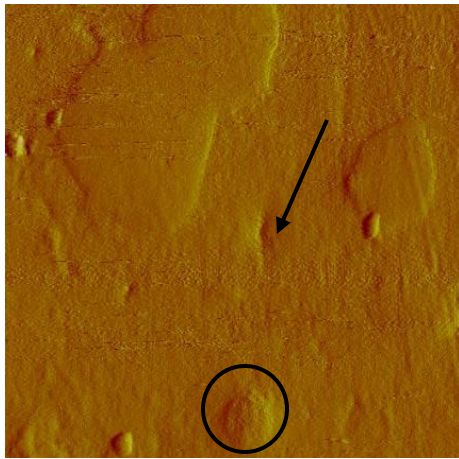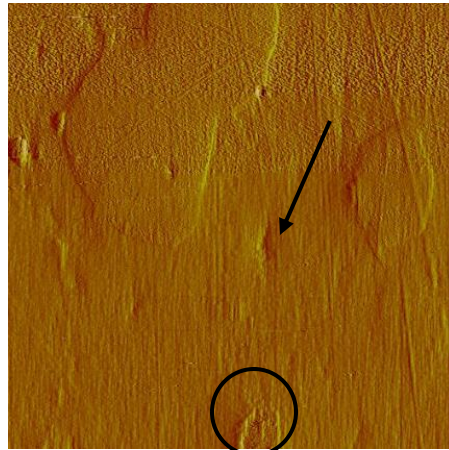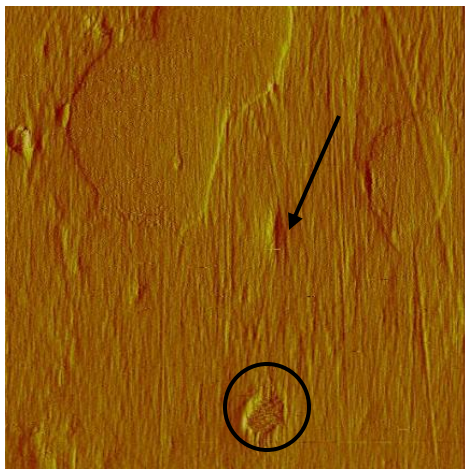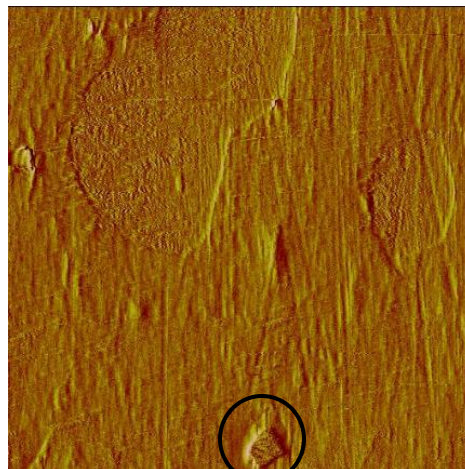
Figure 4.14 AFM deflection images for a CoCrMo alloy in PBS+30mM $H_2O_2$ solution at different immersion time (8*8 um). Surface roughness is shown in Figure 7 (trial 3). Arrows and circles show evolution of a carbide.
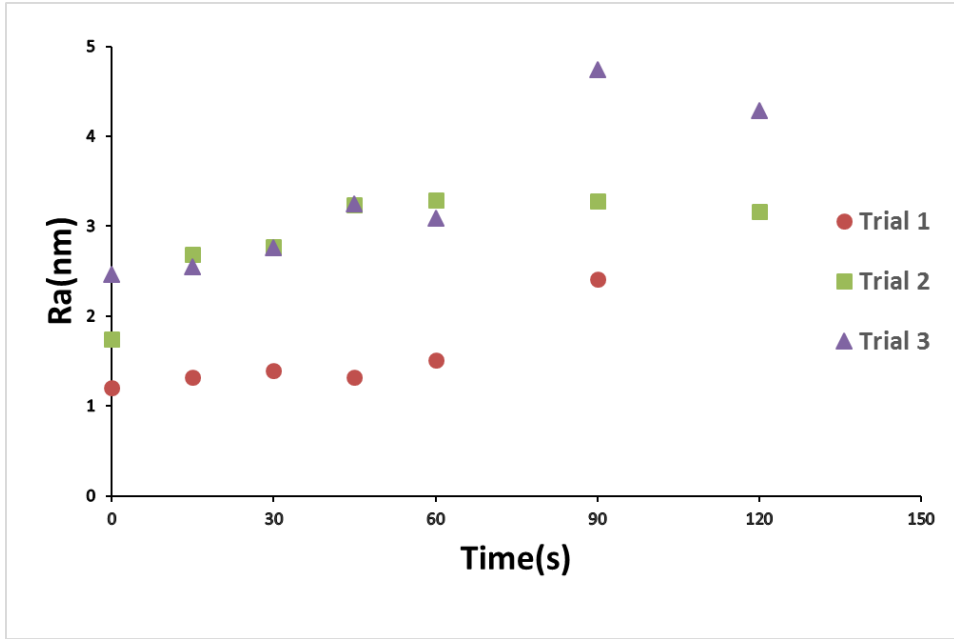
Figure 4.15. Surface roughness of CoCrMo alloy in PBS+30 mM $H_2O_2$ solution as afunction of immersion time (8*8 um).
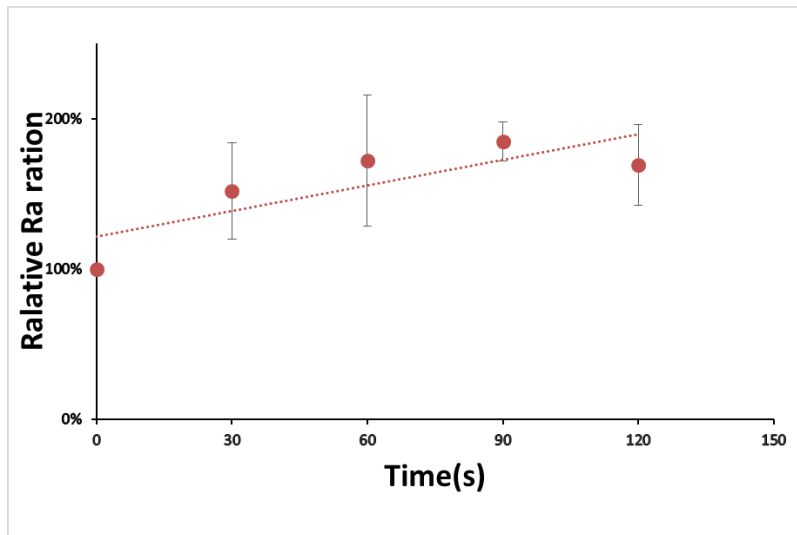


Figure 4.16. Surface roughness ration at different time in simulation inflammatory solution with $H_2O_2$.
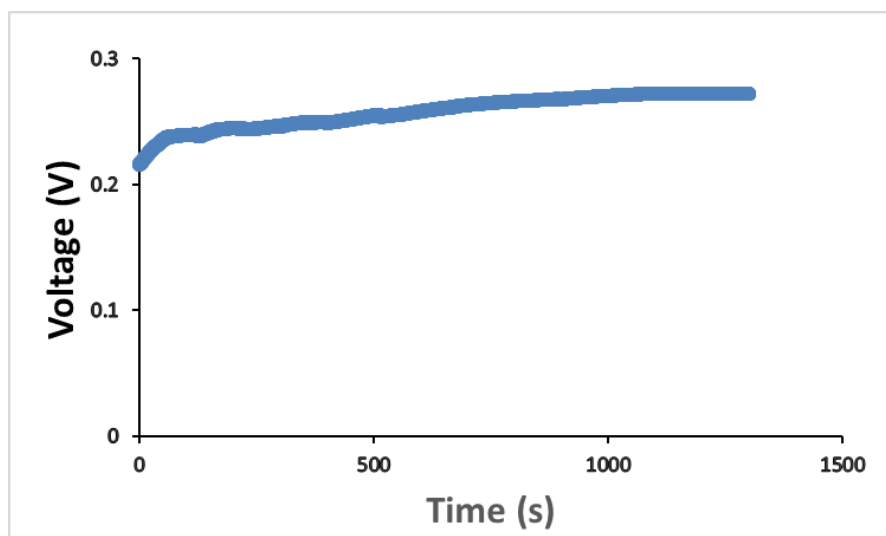
Figure 4.17 OCP of CoCrMo alloy in PBS solution with 30 mM $H_2O_2$.
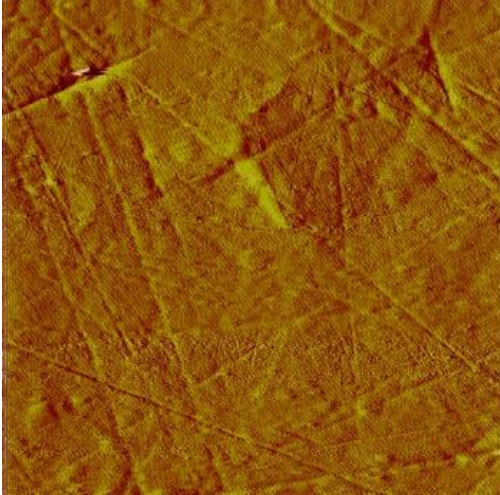
(a)OCP
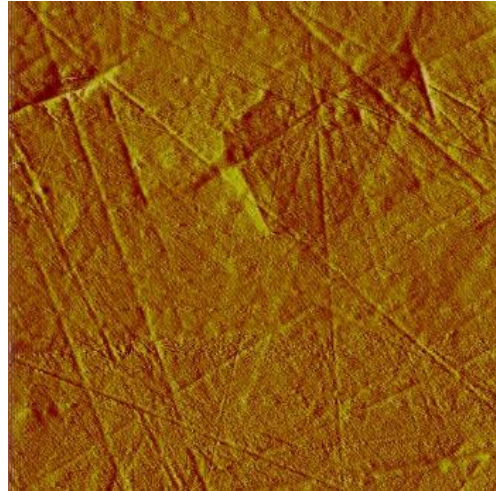

(b) 0.3V
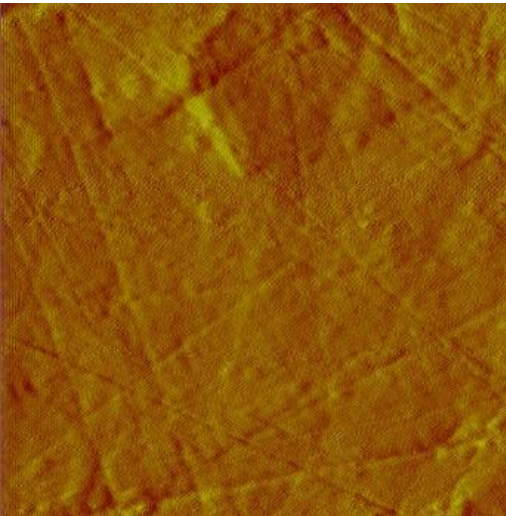

(c) 0.65V (0 minute)
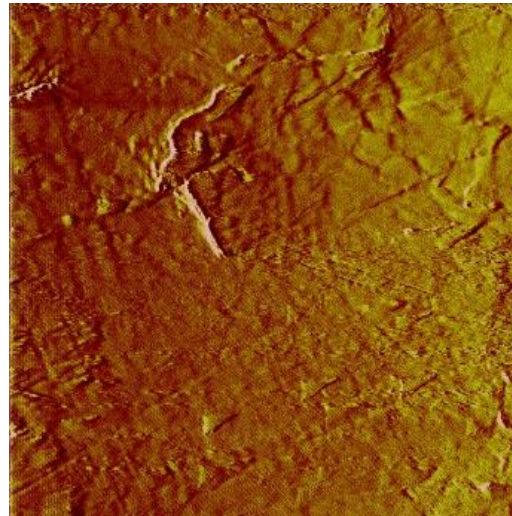

(d) 0.65V (30 minutes)
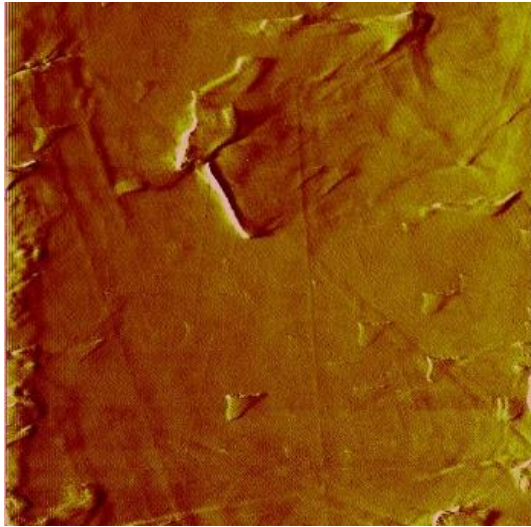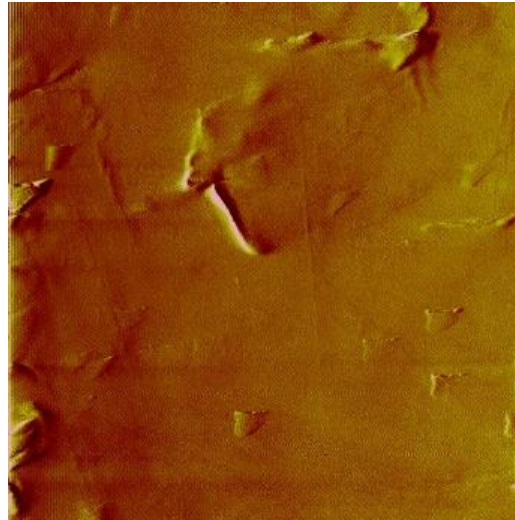
<div align="center">(e) 0.65V (40 minutes)                    (f) 0.65V (1h)</div>
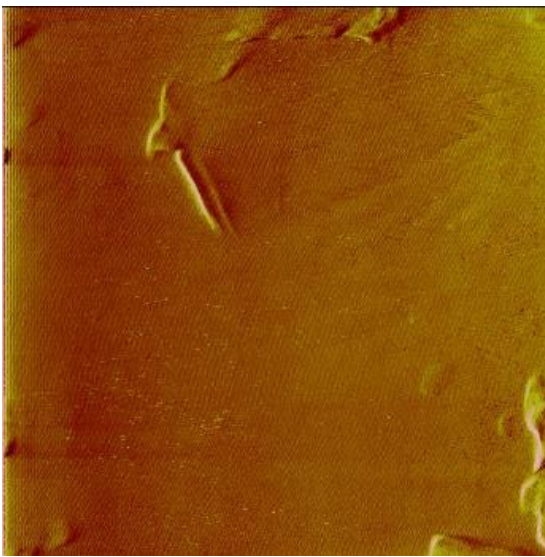


<div align="center">(g) 0.65V (2h)</div>

Figure 4.18 ECAFM contact mode deflection images of CoCrMo alloy at different voltages in PBS solution with 30mM $H_2O_2$.(8*8um). Revolution oxide film dissolution and new oxide formation were observed (c-g) at 0.65 V.
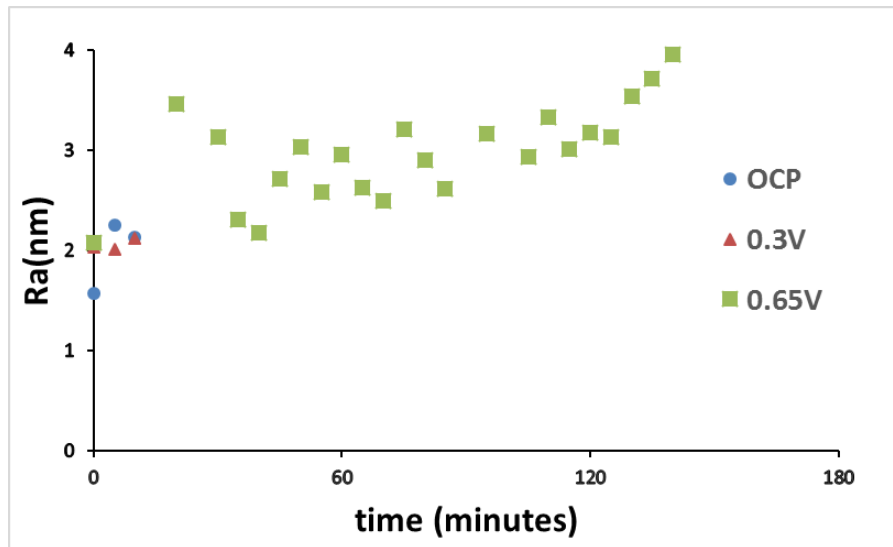
Figure 4.19 Surface roughness of CoCrMo alloy at different voltages in $H_2O_2$ modified PBS solution. Increase of oxide surface roughness were observed as voltage increased to 0.65 V.
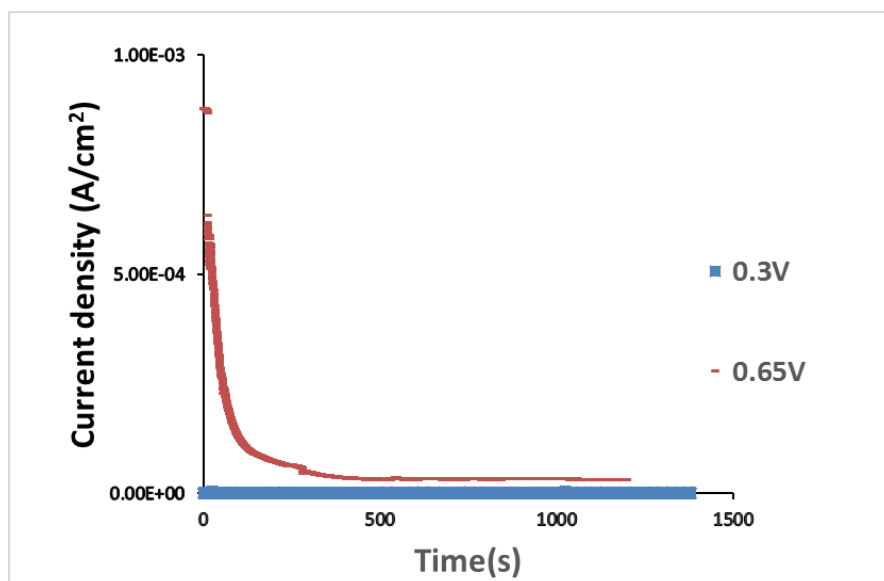


Figure 4.20 Current profiles at different voltages during ECAFM experiment in PBS solution with 30mM $H_2O_2$. Current density increased up to 3 orders of magnitude when the voltage was increased from 0.3 V to 0.65 V.

# Chapter 5 The effect of simulated inflammatory conditions on fretting corrosion of CoCrMo alloy surfaces

## 5.1 Introduction

CoCrMo alloy has been widely used in orthopedic, dental, spinal and cardiovascular devices due to its excellent mechanical properties, corrosion resistance and biocompatibility [4, 5]. CoCrMo alloy owes its high corrosion resistance to the presence of a spontaneously-formed thin passive oxide film on the surface under normal conditions [75, 140, 141]. This passive film is usually only a few nanometers thick and is able to isolate the reactive base metal from the surrounding solution in vivo and becomes a kinetic barrier to active metal dissolution reactions [128, 142]. However, the oxide film losses its protection to corrosion if there is abrasion or other oxide disruption process on the surface of CoCrMo alloy. Once the oxide film is abraded due to fretting or other mechanical disruption, the corrosion rate of base metal significantly increases during repassivation. Moreover, corrosion debris and metal ions are generated and are thought to be associated with adverse local tissue relations [18, 88], adverse reaction to metal debris [15, 16] and pseudotumors [14, 143]. Recently, high early failure rate of hip implants has been directly linked to fretting corrosion of modular taper interfaces. Unfortunately, CoCrMo alloy has been involved in many cases [35, 104, 144]. Therefore, the passive oxide film plays a significant role in determining the fretting corrosion susceptibility of CoCrMo alloy.

Although oxide films contribute to the corrosion resistance of CoCrMo alloy under

normal non-fretting conditions, they are not inert. The morphology, thickness and chemistry of oxides change in solution and depend on the surface potential and solution chemistry. Previous studies have shown that the oxide only forms at voltage higher than -500mV (vs Ag/AgCl) in PBS [5, 81]. The thickness increases almost linearly with potential from 2.2 nm at -0.35V (vs Ag/AgCl) to 3.1nm at 0.25V (vs Ag/AgCl) [75]. At lower potentials, the passive oxide is mainly $Cr_2O_3$. As the potential shifts into the transpassive region, strong thickening and loss of compactness of the oxide, as well as significant change in the composition of oxide film, take place. The oxide film thickness increases to around 9 nm at 0.75 V (vs Ag/AgCl) with Co-oxide and Mo-oxide entering into the outside layer [145]. Chromium oxide begins to dissolve in the transpassive voltage region and Cr (VI) appears in the oxide film at voltages higher than 0.5 V (vs. Ag/AgCl) [123]. These significant voltage-dependent surface changes will alter the corrosion resistance, semiconductor behavior, tribology performance and biocompatibility of CoCrMo alloy. Open circuit potential of CoCrMo alloy stays at -0.3 V to 0.1 V in PBS solution under normal conditions. Fretting corrosion or surface disruption increases oxidation reactions and releases electrons to the metal surface which shifts OCP to more native values. Cathodic excursion of OCP is a common phenomenon for metallic biomaterials under fretting corrosion conditions and depends on surface area, normal load, fretting frequency as well as materials combination. For CoCrMo alloy, the potential shifts as much as -0.8 V at high-speed scratch conditions in PBS [81, 85].

The dynamic oxide film interacts with the complex biological system and therefore the solution chemistry plays a critical role in the oxide film behavior [146] and fretting corrosion

behavior of CoCrMo [10, 82]. Under fretting crevice corrosion conditions, oxygen depletion occurs and pH decreases [8] which affect the corrosion behavior of CoCrMo alloy.

Recently, inflammatory cell-induce corrosion (ICIC) on CoCrMo alloy has been investigated by Gilbert et al. [66]. They found apparent cell-induced corrosion patterns on retrieved implants. Phagocytic cells associated with inflammation release a variety of reactive oxygen-based oxidizing species, so-called ROS, as part of their response to infection, foreign bodies and other inflammation-inducing conditions. ROS released by inflammatory cells include $H_2O_2$, HClO, and hydroxyl radicals amongst others. Some ROS species can engage in Fenton reactions which combine transition metal ions with hydrogen peroxide to generate significant amounts of radical species. These chemical species are hypothesized to have significant effects on the corrosion behavior of titanium and CoCrMo alloy surfaces. Metal ions and chemical species thought to be involved in the corrosion mechanism Include $H_2O_2$ and Fenton reagent ($Fe^{2+}$, $Fe3^+$, $H_2O_2$). Inflammatory cell-based solution chemistry changes significantly alter the corrosion susceptibility of CoCrMo alloy and surface oxide impedance [66]. For example, OCP shifts positively to 0.6 V in Fenton reagents modified PBS solution with a significant increase in corrosion current and decrease of impedance [104]. Large increases of OCP lead to dramatic changes of oxide film and may affect both the corrosion and fretting corrosion behavior of CoCrMo alloy in vivo. Laura et al., have investigated the clinical relevance of ICI corrosion on 100 CoCr alloy hip implants, they found 59% of the implants show evidence of ICI corrosion [69].

In ICIC, inflammatory cells are hypothesized to directly corrode CoCrMo alloy with or

without fretting. However, the ICIC mechanism is poorly understood and how the inflammatory cell-released chemical species affect fretting corrosion behavior of CoCrMo alloy have not been studied. Therefore, the goal of this study is to investigate the effect of simulated inflammatory conditions on fretting corrosion behavior of CoCrMo alloy. Corrosion experiments were conducted to understand how pH and Fenton reagent ($H_2O_2$ & iron ions) affect the static corrosion behavior and fretting corrosion behavior of CoCrMo alloy.

## 5.2 Materials and Methods

The materials used in the experiments were CoCrMo (ASTM F-1537) alloy pins and disks. This pin was cone-shaped and with a flat bottom which had a nominal contact area of about 2 mm$^2$. The true contact area depends on normal load and material hardness. A larger circular geometry disk was mounted into the fretting corrosion cell. Details about the pin-on-disk fretting corrosion system are introduced elsewhere [81]. In the fretting corrosion system, fretting motion was controlled by a high load piezoelectric actuator (Piezosystems Jena, Germany). The electrochemical chamber where the disk was mounted was fixed to an X-Y linear stage (Newport) and connected to the piezoelectric actuator. Linear Z-stage with micrometer screw to adjust the loading arm was designed to achieve the vertical loading control. A multiaxial load cell (MINI 45 F/T, ATI Industrial automation) was mounted under the loading arm and to which the pin sample was attached. A high resolution (1 um) contact DVRT (Microstrain) was used to obtain relative displacement on the pin-on-disk interface.

Pins and disks were prepared through sequential wet sanding to a 600 grit finish, cleaned with ethanol and distilled water. The exposed disk area was circular and fixed at 0.25 cm$^2$ and

controlled by covering the remaining disk area with an acrylic coating material. The pin and disk samples were rigidly mounted in the fretting corrosion system and electrically short circuited to each other to allow for electrochemical measurements from both surfaces. Electrochemical tests were conducted by using a three electrode system where the pin-disk couple was the working electrode, Ag/AgCl reference electrode and carbon counter electrode were used. All electrochemical measurements were obtained through a potentiostat (Solartron 1280C, Solartron Analytical). Mechanical and electrochemical information was obtained using a National Instruments[TM] data acquisition card (NI PCI-6229), Labview[TM] program tool and CorrWare[TM] software.

Three solutions were used to simulate the inflammatory conditions: 1. PBS (phosphate buffered saline) (Sigma, P3813, 0.135 M NaCl, 0.0027 M KCl, 0.01 M $Na_2HPO4$ and 0.002 M $KH_2PO_4$) solution ; 2. PBS (pH 3) solution. pH 3 solution was made by adding hydrochloric acid in PBS with the measurement of a pH meter (Hanna, HI208); 3. PBS with Fenton reagent (0.1 mM $FeCl_3$ and 10 mM $H_2O_2$). Fenton reagent solution was made by mixing 0.1 mM ferric chloride ($FeCl_3$) into PBS first and 30 mM $H_2O_2$ was then added before the measuring of OCP.

**Varied potential tests**

Fixed normal load (6 N), fretting frequency (1.25 Hz) and fretting displacement (50 um) were controlled by the system and applied in this experiment. The potential of the working electrode was varied from -800 mV vs Ag/AgCl to 600 mV vs Ag/AgCl with an increment of +200 mV between each voltage. Potentiostatic tests were conducted at each voltage for 15 minutes to equilibrate the sample surface before initiating the fretting and the

116

current was recorded. Fretting was performed for 150 s at each voltage and the DVRT was connected to capture the displacement information during fretting while load, force and current data was continually collected. After the fretting was stopped, current was continually captured for 5 minutes at each voltage before the next fretting test at higher potential was conducted. At least three samples were tested in each solution.

**Longer-term tests**

Longer-term fretting tests were conducted sequentially in PBS with $H_2O_2$, PBS solution with HCl and $H_2O_2$, PBS solution at 600 mV, and PBS solution with $H_2O_2$ at 600 mV. Fretting was performed for 12 h in PBS with $H_2O_2$ solution and for 1 h in the other three solutions. This potential was selected because it is the OCP of CoCrMo when exposed to simulated inflammatory solution conditions

**Post-test analysis**

Damage of fretting interface was investigated using Scanning Electron Microscope (SEM, JEOL 5600). Fretting areas on pin and disk were measured by digital optical microscope (Hirox 8700).

**Data analysis**

Fretting current was determined by calculating the difference between the current captured during fretting and the baseline current before fretting. Fretting current density was the calculated by averaging the fretting current and dividing by the fretting area (pin fretting area + disk fretting area) obtained from quantitative measurements using the digital optical

microscope. The baseline current density was determined by dividing the baseline current at each voltage by the total exposed area (pin exposed area + disk exposed area). Fretting COF was calculated by averaging the ratio of tangential force to the normal force.

**Statistical analysis**

Analysis of variance (ANOVA) and post hoc comparisons (Tukey's method) were used. A two-way ANOVA statistic was applied to assess the effects of potential and solution on the fretting current density, fretting COF and the work done per fretting cycle at the interface. A p-level of 0.05 was considered significant in all statistical analyses.

**5.3 Results**

Figure 5.1 shows plots of voltage evolution with time of CoCrMo surfaces caused by hand abrasion using emery paper to assess the maximum possible negative potential drop under fast-abrading conditions in different simulated inflammatory solutions. In both PBS and HCl solution (pH 3), surface abrasion caused voltage drops to as negative as -0.8 V (vs. Ag/AgCl) although the starting OCP in acidic solution (pH 3) was more positive. In PBS solutions with 30 mM $H_2O_2$, OCP shifts negatively from 0.3 V (vs. Ag/AgCl) to -0.5 V (vs. Ag/AgCl) due to surface abrasion. In solutions with Fenton's reagent, voltage dropped from 0.5 V (vs. Ag/AgCl) to around -0.2 V (vs. Ag/AgCl) after mechanical abrasion started and did not recover significantly after ceasing abrasion.

Representative raw current density data including baseline current density, fretting current density in a group of fretting corrosion tests for CoCrMo/CoCrMo couple in PBS

solution is shown in Figure 5.2. All currents were recorded under potentiostatic conditions. Static current density variation was recorded before the start of fretting motion at 900 s. The influence of fretting on current can be clearly identified from the sudden deviation of current from the stable baseline current when fretting motion was initiated. The recovery current was recorded and was used to determine if there was self-sustaining corrosion present after fretting for 200 s. It is clear that both the baseline current and fretting current vary due to the change of potential. Current density jumped to a larger anodic value once the fretting was started and became stable (with mean and oscillatory currents corresponding to the motion) during fretting. The detailed relationship between cyclic motion and currents can be seen in Figure 5.2 insert. Current recovered fast after the cessation of fretting and no significant difference was observed between the baseline current and recovery current in all tested conditions.

A summary of the potential versus log current density for both baseline and fretting current densities in different simulated inflammatory solutions including acid or Fenton reagent (see Figure 5.3) shows significant effects of solution on both. It should be noted that different areas were used in calculating fretting current density and baseline current density. For fretting current density, fretted area measured by digital optical microscope after fretting corrosion tests was used while total exposed area was used in determining baseline current density. Baseline current density varies with potential and solution. In PBS and pH 3 solutions, baseline current exhibits similar behavior in terms of general trends. However, current density in pH 3 solution is higher than that in PBS solution at negative voltages, while the opposite

outcome was observed at positive potential range. As potential changes from 0.4 V to 0.6 V, current density increases from 10 uA/cm$^2$ to 27 uA/cm$^2$ in PBS solution, while no significant change was shown in pH 3 solution. In Fenton reagent solution, baseline current was in the scale of mA/cm$^2$ at negative potential range and was at least 10 times larger than it was in PBS and pH 3 solutions. It is also interesting to note that the lowest current density in Fenton reagent solution occurred at 0.4 V, a much higher value than those were in PBS solution (-0.6 V) and pH 3 solution (-0.4 V). Compared with baseline current, fretting current density level was significantly higher in PBS and acidic solutions, it increases by at least 2 orders of magnitude at potential higher than -0.4 V. In Fenton reagent solution, significant rise of current density due to fretting conditions was observed at voltages higher than 0 V.

Figure 5.4 presents the Log current density plot versus potential for different solutions. There were statistically significant effects of both potential and solution on the fretting corrents ($P < 0.05$) based on the 2-way ANOVA. At potentials negative to -0.4 V, no current due to fretting was observed in all solutions. In PBS solution and acid solution, fretting current began to occur at -0.4 V with a value of 125 uA/cm2 and 100 uA/cm$^2$ respectively.

Fretting current density then rises with potential in a linear fashion with a slope of 4.6 mA/V cm$^2$ in PBS solution and 2.9 mA/V cm$^2$ in pH3 solution. Fretting current in PBS solution was the highest among all solutions at all voltages with the highest value of 4.5 mA/cm$^2$ at 0.6 V, while it reached the highest in pH 3 solutions at 0.6 V with a value of 3 mA/cm$^2$. Fretting current density exhibits different behavior in Fenton reagent solution and shows the lowest value among all solutions at all potentials. No fretting current was observed at negative

voltage potentials from -1 V to -0.2 V in Fenton reagent solution. Fretting current began to appear at 0 V with a value of 0.6 mA/cm$^2$ and exhibits an linear relationship with potential, reaching at the highest value (1.5 mA/cm$^2$) at 0.6 V. Trend line of the linear region was extrpolated to the potenital axis to determine the onset potential (Eonset) for fretting corrosion in different solutions. The E$_{onset}$ in Fenton reagent solution is somewhere between -0.2 V and 0 V, a higher value than -0.37 V for PBS solution and -0.41 V for pH 3 solution.

Fretting COF varied significantly (P < 0.05) with solution and potential (Figure 5.5). In PBS and pH 3 solution, fretting COF is in the range from 0.28 to 0.42. Fretting COF exhibits statistically significantly higher values (P < 0.05) from -0.4 V to 0.2 V in PBS solutions compared to that in pH 3 condition. The highest fretting COF in PBS solution is 0.42 at -0.4 V, while fretting COF in pH 3 solution doesn't show significant variations with potential (P > 0.05). Fretting COF in PBS solution increases from 0.32 at -0.8 V to 0.4 at -0.4 V and then decreases to 0.28 with increased potential. Fretting COF shows large variations (0.25-0.5) with potential in Fenton reagent. It shows the highest value of 0.5 at -0.6 V and -0.4 V, decreases to 0.45 at -0.2 V. A large drop of fretting COF to 0.25 occurred at 0 V, after which it increases with a linear fashion to 0.32 at 0.6 V. Fretting COF in Fenton reagent exhibits statistically significantly higher values at potentials from -0.6 V to -0.2 V compared to PBS and acidic solutions.

Representative tangential force at the fretting interface versus displacement at different potentials in different simulated inflammatory solutions (Figure 5.6) show the changes in fretting sliding mechanics with solution and voltage. PBS solution (Figure 5.6A) and pH 3 solution (Figure 5.6B) exhibit similar effective displacement (about 45 μm). However, the

hysteresis loop in PBS solution shows more variation (greater variability in force) at different potentials. At -0.4 V, the tangential force is the highest among all potentials in PBS solutions. Significant variations of hysteresis loop at different potentials are also shown in Fenton reagent (Figure 5.6C).

In Fenton reagent at very negative potentials (-0.4 V and -0.6 V), tangential force is larger than 3 N, a much higher value than is seen in the other conditions evaluated. At more positive potentials, tangential force becomes smaller and effective displacement significantly increases.

Work done during a single cycle of fretting is estimated by calculating the area of the hysteresis loop in the tangential force-displacement plot and is shown in Figure 5.7. In PBS and pH 3 solutions, the work done per cycle of fretting shows similar statistically significant potential variations. In Fenton reagent, work done per cycle exhibits a significant decrease with the increase of potentials from -0.6 V to 0.2 V and then plateaus. Compared with work done in PBS and pH 3 solutions, significantly lower mechanical energy dissipated at the interface is shown in Fenton reagent solution at potentials from -0.4 V to 0.6 V.

OCP and current information from the longer-term fretting corrosion test (Figure 5.8 (a-d)) show a decrease from 0.35 V to 0.2 V due to fretting in PBS solution with $H_2O_2$ and acidic PBS solution with $H_2O_2$ (Figure 5.8a and 5.8b). Fretting current density was as high as $10^{-3}$ A/cm$^2$ (Figure 5.8c and 5.8d), which was more than 100 times higher than the baseline current, showing that fretting of the surface led to faster corrosion of CoCrMo alloy. After fretting in different simulated inflammatory conditions for 15 hours, the current density was $3*10^{-}$

$^3$A/cm$^2$. The current density was at the same level compared with that of short-term fretting corrosion tests at 600 mV in simulated inflammatory conditions.

Figure 5.9 (a-c) shows the representative SEM micrographs of CoCrMo surfaces after fretting tests under potentiostatic conditions from -0.8 V up to 0.6 V. Corrosion damage in PBS solution and Fenton reagent solution is more pronounced than that in acidic solution. Pitting corrosion is observed on the surface after fretting in PBS and Fenton reagent solution. However, no pitting is shown in the acidic solution samples. After long-term fretting corrosion in simulated inflammatory conditions, fretting corrosion surface damage (Figure 5.9e and 5.9f) becomes more severe. Surface dissolution and slip bands are observed and pits are shown in crevice geometry area (Figure 5.9e).

## 5.4 Discussion

The goals of this paper were to assess the effects of simulated inflammatory solutions on the fretting corrosion of CoCrMo alloys. Simulated inflammatory solutions consisted of phosphate buffered saline solutions (PBS) with additions of hydrogen peroxide, acid, or a combination of hydrogen peroxide and iron ions to simulate a Fenton reaction condition. These chemistries are generated during respiratory burst processes associated with immune and inflammatory responses. While the exact levels of these chemistries in vivo are not known, all literature suggests that the range of concentrations investigated is possible at least in local cellular regions [4, 72, 91]. Each solution significantly altered the fretting corrosion performance of CoCrMo when fretted against itself. The electrochemical behavior, the fretting contact mechanics as described by the fretting coefficient of friction and the work per cycle

of fretting, were both affected by solution and potential.

**Effect of acid and potential on CoCrMo electrochemistry and fretting corrosion**

Previous studies have shown that potential of the surface alone greatly influence the morphology [77], thickness [145] and chemistry of CoCrMo oxide films in simulated biological solutions [123]. This study shows that fretting current density, baseline current density, as well as passivation effect were potential-dependent under simulated inflammatory conditions, however, they were also pH dependent. Addition of acid (pH 3) significantly decreased the fretting corrosion current density and indicates that CoCrMo alloy is more fretting corrosion resistant in acidic solution than it is in PBS solution. Oxide formation potential, inferred from the voltage where fretting current starts to appear, was at the same level (around -0.4 V) in acid and PBS solution. This indicates that no protective or little oxide film is formed at or below -0.6 V (vs Ag/Cl) and the surface is under active-passive transition from -0.6 V to -0.4 V. At sufficiently cathodic potential (below -0.6 V), increased cathodic behavior was observed in more acidic solution, showing that acid facilitates cathodic reactions.

Static corrosion behavior based on the baseline current results in this study (Figure 5.3) is generally similar to typical anodic polarization results. It should be noticed that acidic solution shows stronger passivation effect on CoCrMo surface compared to PBS solution. In the normal transpassive region, baseline current density increases significantly with potential in PBS solution while a drop in current density is observed in acidic solution, showing that passivation still exists at 0.6V in acid solution. However, it should also be mentioned that baseline current density in pH 3 solution is larger than that in PBS solution in the normal OCP

124

(-0.3 V-0 V) range, indicating that acid is still more corrosive to CoCrMo surface than PBS under normal static condition. From the SEM micrographs (Figure 5.9), PBS solution and Fenton reagent solution show more severe fretting corrosion damage on the surface than the acid solution, where no pitting was observed. This might be caused by the passivation effect of acid on the oxide film at positive voltage range.

**Effect of Fenton reagents and potential on CoCrMo electrochemistry and fretting corrosion**

Significant amounts of iron may be present in biological proteins (e.g. ferritins) or sequestered in synovial tissues. It may also be present in solid solution in the CoCrMo alloy as was reported in previous retrieval studies [66, 69]. Hydrogen peroxide is a major ROS in living organisms and is known to be released by activated inflammatory cells to attack some biologic targets. Therefore, the presence of Fenton reagent is possible and highly oxidative species such as hydroxyl radical and superoxide can be produced via a variety of Fenton reactions [68]:

$$Fe^{2+}+H_2O_2----Fe^{3+}+ OH\cdot+OH^- \qquad\qquad Fe^{3+}+H_2O_2----Fe^{2+}+ HO_2\cdot+H^+$$

Theses reactive oxygen species increase the oxidizing power of the solution and makes the oxide film more defective [104]. The addition of Fenton reagents significantly alters baseline current behavior and increases corrosion susceptibility of CoCrMo alloy. Baseline current density increased up to 3 orders of magnitude compared with that in PBS solution. The cathodic reactions were largely increased and become dominant at a wider range potentials (below 0.4 V vs Ag/AgCl) (Figure 5.3). Two linear parts with different slopes are observed in the cathodic range (Figure 5.3) of the polarization plot. One is from -0.6 V to 0 V, where current density decreases slightly with increasing potential; the other is from 0 V to 0.4

V with a higher rate of current density drop as potential increases, The former part shows a diffusion-controlled reaction mechanism at negative potentials while the latter part indicates strong passivation occurs from 0 V to 0.4 V in Fenton Reagent solution and is related to the linear increase of oxide film thickness with increase in voltage [85].

Fretting current begins to appear at -0.2 V in Fenton reagent solution, while it starts to occur at round -0.4 V in the other two solutions. This indicates that oxide film becomes less stable in Fenton reagent solution compared to it is in other conditions. Interestingly, based on baseline current plot in Fenton reagent solution, 0 V is where significant drop of cathodic current starts as potential increases. It could be inferred that the protective oxide film starts to form at potential from -0.2 V to 0 V in Fenton reagent solution. Fretting current density shows the highest value in PBS solution and is the lowest in Fenton reagent solution. This also supports the idea that oxide film on CoCrMo in PBS solution is the most protective to corrosion among these solutions while it becomes more defective in solution with Fenton reagent.

**Fretting contact mechanics**

Fretting COF was influenced by both solution chemistry and potential. Results of this study on the Fretting COF of CoCrMo alloy in PBS shows agreement with previous study by Swaminathan et al [81]. Potential chemically and structurally affects the oxide film and influences fretting COF behavior. In acidic solution, fretting COF was lower than that in PBS solution, indicating that acid might alter the oxide film chemistry, thickness and structure. In Fenton reagent, solution chemistry dramatically alters oxide film behavior and fretting COF significantly drops from 0.5 at -0.4 V to 0.25 at 0 V where protective oxide film starts to form.

126

Interestingly, once the oxide film was formed, the fretting COF increases with potential in Fenton reagent solution. This potential-dependent behavior is different from that in acid and PBS solution, showing that potential-dependent friction behavior is significantly altered by Fenton reagent. The reason why fretting COF reaches as high as 0.5 at very negative potential in Fenton reagent solution is probably due to that different oxide layer is formed. It may also be caused by the formation of $H_2$ and $O_2$ from the $H_2O_2$ reactions, which impedes the fretting motion.

Addition of Fenton reagent increases the friction force and results in the decrease of effective displacement at negative voltage range. This could be due to the oxide film change induced by the Fenton reagent or because that the product of Fenton reaction such as $Fe(OH)_3$ precipitates on the surface and affects the fretting motion on the interface. Mechanical work done at the interface is affected by the friction motion and is both potential and solution dependent. The energy dissipated due to mechanical motion in Fenton reagent condition is the lowest among three solutions and this is caused by significant drop of sliding displacements in Fenton reagent condition due to the machine compliance of the test system.

**Fretting corrosion model**

A fretting corrosion model developed previously [81] was used to compare the effect of solution chemistry on the mechanical and electrochemical parameters of fretting corrosion system. Fretting current in this study mainly consists of film formation currents while dissolution reaction current is relative small.

$$I_{\text{film}} = 4 \frac{\rho n F}{M_{\text{w}}} \frac{A_{\text{nom}}}{\Delta} m(E - E^{\text{onset}}) \delta v \qquad \text{Eq.5-1}$$

127

Based on the model, fretting current density increases linearly with potential when potential is higher than the $E^{onset}$ and this shows good agreement with our experimental data. This linear relationship result is also supported by previous high speed scratch test on CoCrMo alloy [85] and anodic oxidation study on titanium alloys [147]. Different increase rates of fretting current density with potential were shown in different simulated inflammatory conditions. Solution chemistry affects the anodization ($m$), oxide properties ($\rho$, $n$, Mw) and friction motion ($\delta$, $\Delta$) and therefore result in different slopes in the linear relationship. The current density-potential slope in PBS is 4.6 mA/cm$^2$*V, a value about twice as large as that is in Fenton reagent solution (2.2 mA/cm$^2$*V). This result also implies that oxide formation is depressed in some level due to the presence of Fenton reagent.

**Longer-term fretting corrosion**

Compared to short term tests, long term fretting corrosion under inflammatory conditions increases the corrosion damage of the surface (Figure 9e and 9f). Retrieval studies show that corrosion on CoCrMo alloy in vivo causes more severe corrosion damage than that is shown in in vitro corrosion studies [66, 96, 148]. Solution chemistry such as inflammatory cell-released species might be an important factor that aggravates corrosion in vivo and it is highly possible that long term fretting corrosion under this condition is able to further increase corrosion damage of the implant.

**In vivo fretting corrosion conditions**

In all experiments presented in this study, different simulated inflammatory conditions were set up to assess how the solution chemistry and inflammatory cell released chemical

species affect the fretting corrosion behavior of CoCrMo alloy. However, these solutions do not completely represent the complicated in-vivo conditions. Additional factors also play significant roles in the fretting corrosion behavior of metallic biomaterials. For example, proteins present on the surface of metallic biomaterials, interacting with other solution chemistry and surface oxide, may affect the fretting corrosion behavior of CoCrMo alloy. Recent study finds that Co (II) and Cr (III) ions released from CoCrMo alloy interact with albumin in solution and increases friction coefficient of CoCrMo alloy [149]. Study shows that biofilm can play a role in forming an effective lubricating film that reduces friction [150]. Other highly oxidative species such as HOCl, which is estimated at a concentration of 0.2 M in neutrophils, might also be an important factor in the cell induced corrosion process and alter the fretting corrosion behavior of CoCrMo alloy. Recent study in our group has shown HOCl significantly increases the corrosion susceptibility of CoCrMo alloy (Chapter 3). Temperature during inflammatory conditions at the fretting interface could be much higher than room temperature. Contact temperature has also been reported to be high in the contact area of an artificial hip joint [151]. Thus, the corrosion rate may be accelerated and the protein activity may be altered as well. Crevice geometry is known to result in more severe corrosion conditions not only including lower pH condition but also oxygen depletion [102]. The voltage of the system in this study is held fixed, however, in vivo potential of the surface could undergo dramatic change depending on solution chemistry, exposed implant areas [152] and fretting motions [81]. How fast the variation of the potential is and how this affects the stability and properties of the oxide film is not fully understood. Previous study has shown that both resistance and capacitance of oxide film is strongly voltage dependent and time-dependent

[123]. Instability of oxide film could result in more severe corrosion damage on the implant. Inflammatory levels in the synovial fluid of patients with hip implants are different [70]. Different concentrations of reactive oxygen species and different pHs are possible, which might significantly alter the Fenton reagent and reactive oxygen species involved as well as the surface potential. Thus, fretting corrosion behavior of the implant and the clinical performance could vary largely among patients.

## 5.5 Conclusions

This study investigated the effect of solution chemistry (acid, $H_2O_2$ and Fenton reagent) and potential on the fretting corrosion behavior of CoCrMo alloy under simulated inflammatory conditions. Mechanical and electrochemical data including static current, fretting current, normal force, fretting COF, fretting displacement were collected during the tests and were used to evaluate how the performance of oxide film on CoCrMo alloy are affected by solution chemistry and potential. Long-term fretting corrosion tests under simulated inflammatory solutions were conducted to assess possible fretting corrosion damage of CoCrMo alloy after long-term implantation. Fretting corrosion model was applied to assess the potential-dependent fretting current behavior and oxide film properties during fretting corrosion. The main findings are summarized below:

- Fretting corrosion behavior of CoCrMo alloy is significantly affected by both solution chemistry and potential. Inflammatory cell based species (Fenton reagent) result in less stable oxide film and increased oxidizing ability of solution, altering the fretting corrosion behavior of CoCrMo alloy.

- Fretting current increases in a linear fashion with potential above oxide formation potential and shows great agreement with the fretting current model. Fretting current is the largest in the PBS solution and smallest in the Fenton reagent solution, indicating less stable oxide film formed in Fenton reagent and acid solution.

- Oxide formation potential varies in different simulated inflammatory solutions. Fenton reagent solution shows the highest oxide formation potential in all solutions and increase in corrosion susceptibility of CoCrMo alloy was found.

- Fretting COF, effective displacement and work done at the interface varies with potential and solution chemistry. High COF in Fenton reagent solution was observed just below the oxide formation potential and is related to the new oxide and solution chemistry.

- Passivation of oxide film is the strongest in acidic solution, where baseline current was the lowest and no pitting corrosion was found. Pitting corrosion was observed in PBS and Fenton reagent solutions.

- Long term fretting corrosion in simulated inflammatory conditions resulted in more sever corrosion damage compared to short-term varied potential tests.
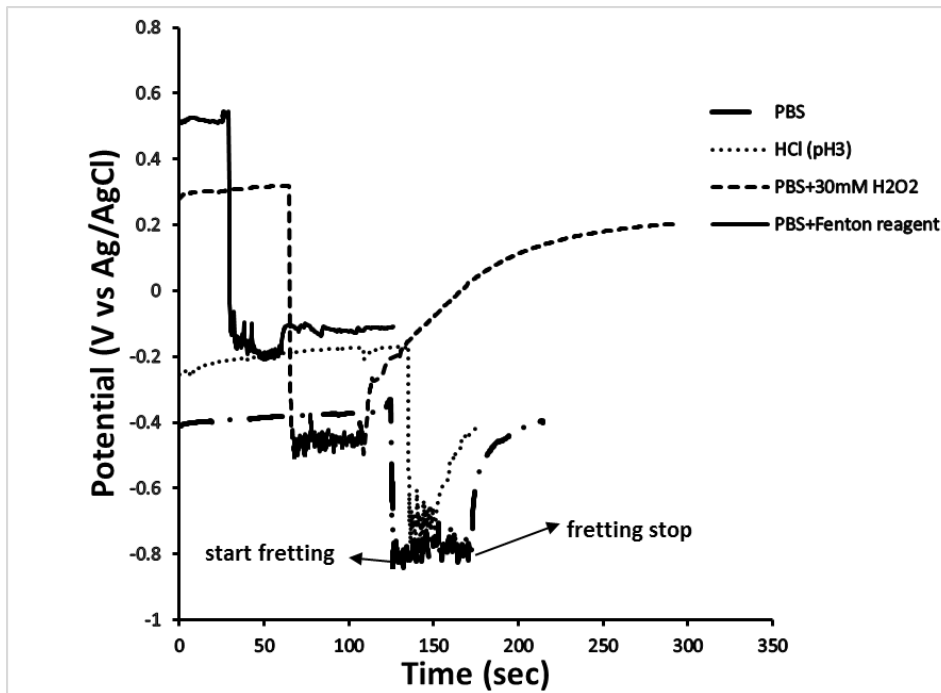
Figure 5.1 OCP variation with time on CoCrMo surface in abrasion tests using an emery paper in different simulated inflammatory solutions. OCP shows at least a drop of 0.5 V due to abrasion in all conditions. OCP during abrasion in PBS solution was the lowest (-0.8 V) while that for solution with Fenton reagent was the highest (-0.2 V) and showed only part of recovery after stop of abrasion. OCP during abrasion stayed at about -0.7 V for pH 3 acidic solution and -0.45 V for PBS solution with 30 mM $H_2O_2$.

132
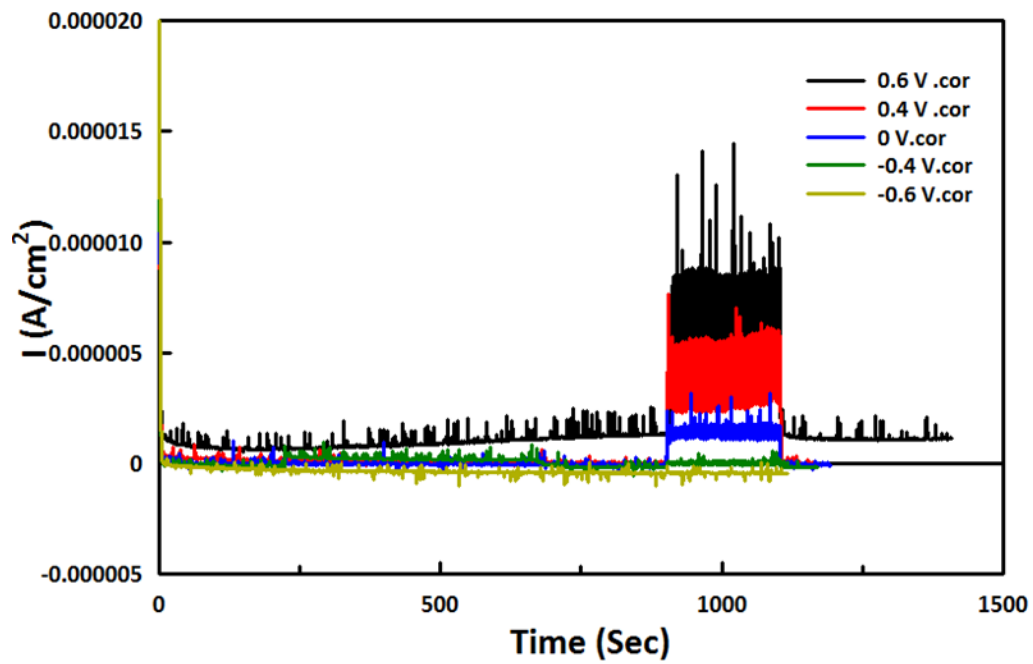
Figure 5.2. Raw current data for fretting corrosion test at different voltages in PBS solution for CoCrMo alloy. Both baseline current and totoal current during fretting beomes more positive with the increase of potential.
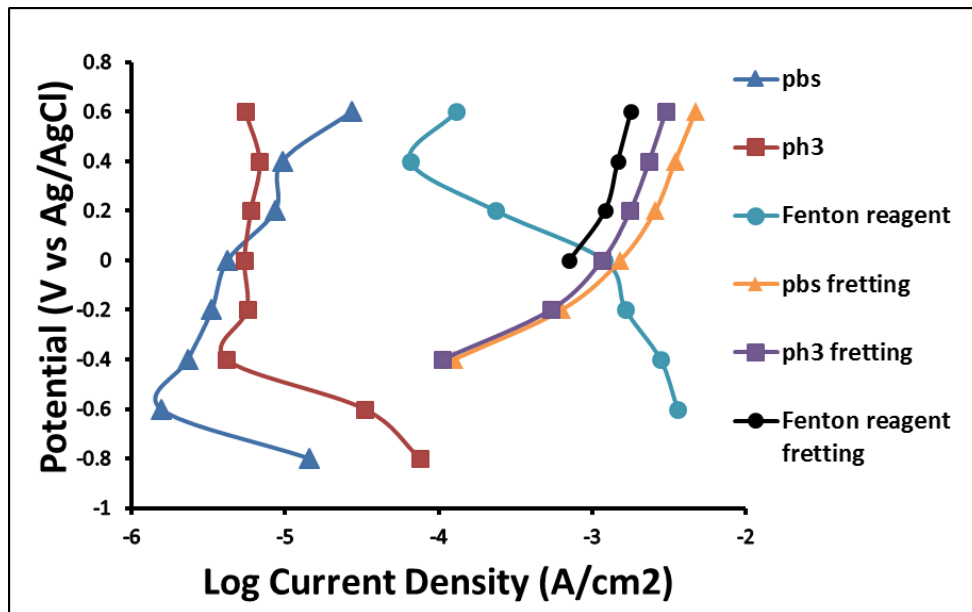
Figure 5.3. Log current density plots at different potentials in simulated inflammatory conditions. Baseline current density and fretting current density are compared. Basline current densities were the highest in Fenton reagent condition compared with those of pH3 and PBS solution. Fretting corrosion current density were about 3 oders of magnitude higher compared with baseline current density in PBS and pH 3 solutions.
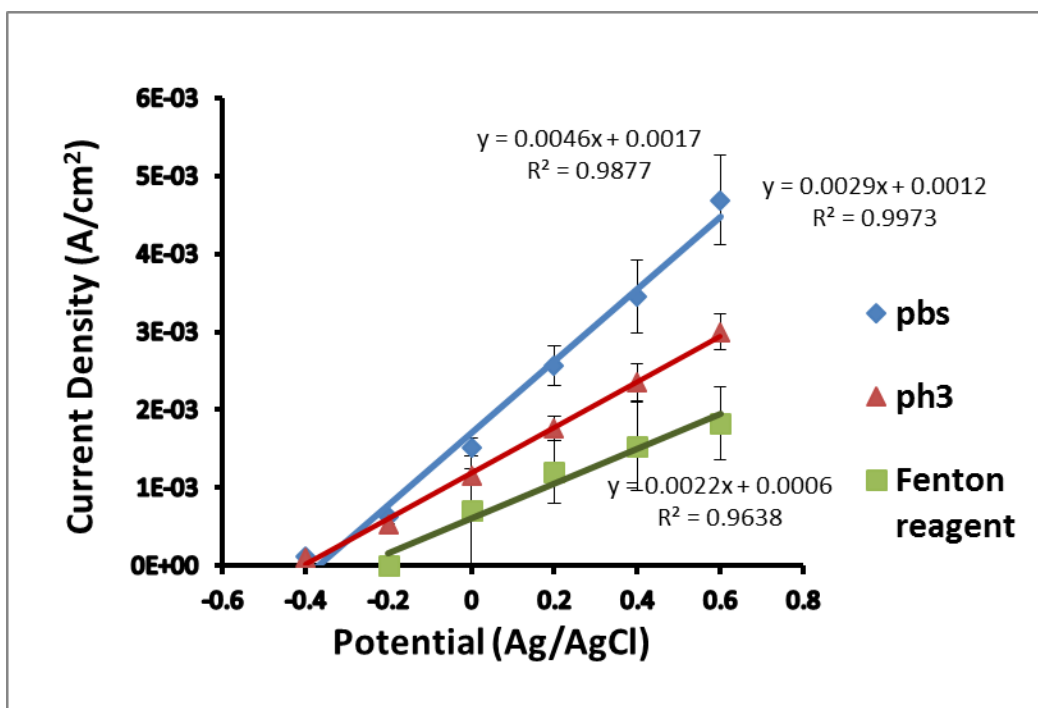
Figure 5.4 Log current density plot versus potential and linear relationship plot in different solutions. Current density increases as potential becomes more positive and different increase rates were observed in different inflammatory conditions. Slop in PBS condition was the largest (4.6 mA/(cm$^2$*V) ) while that in Fenton reagent condition was the lowest (2.2 mA/(cm$^2$*V)).
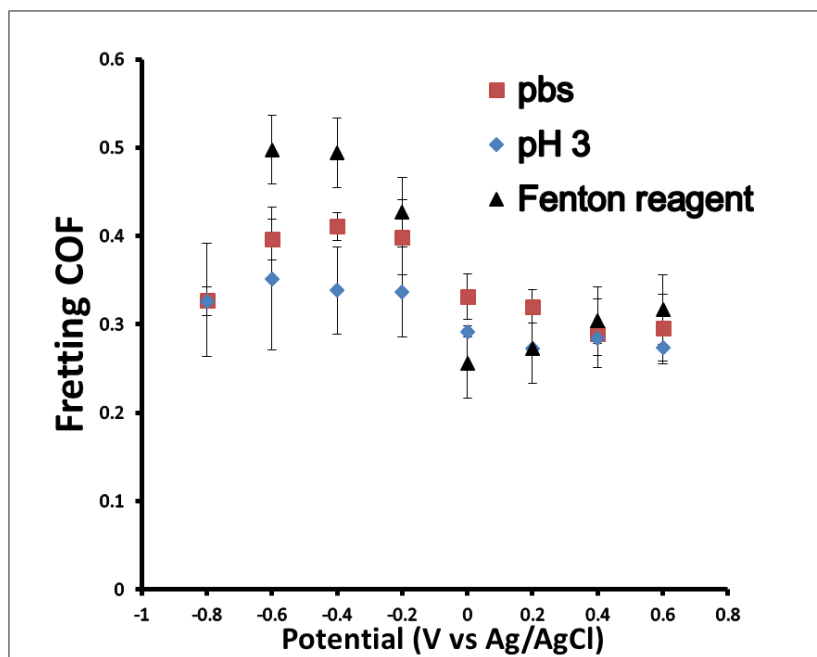
Figure 5.5 Fretting COF variation with potential in different solutions. Similar fretting friction behavior were shown in pH 3 and PBS solutions, while fretting COF in Fenton reagent was significantly higher than those in pH 3 and PBS solutions at -0.6 V and -0.4 V.

A

PBS solution

Tangential force (N)

Displacement (um)

- ◆ -0.6V
- ● -0.4V
- ■ 0V
- ▲ 0.2
- — 0.6V

B

pH 3 solution

Tangential force (N)

Displacement (um)

- ◆ -0.8V
- ■ -0.4V
- ▲ -0.2V
- ✕ 0.2V
- ✳ 0.4V

C

Fenton reagent

Tangential force (N)

Displacement (um)

- ◆ -0.6V
- – -0.4V
- ■ -0.2V
- ● 0.2V
- ▲ 0.6V
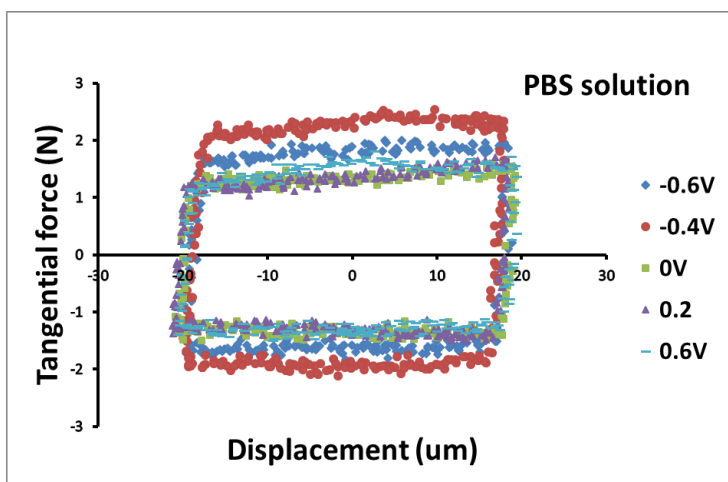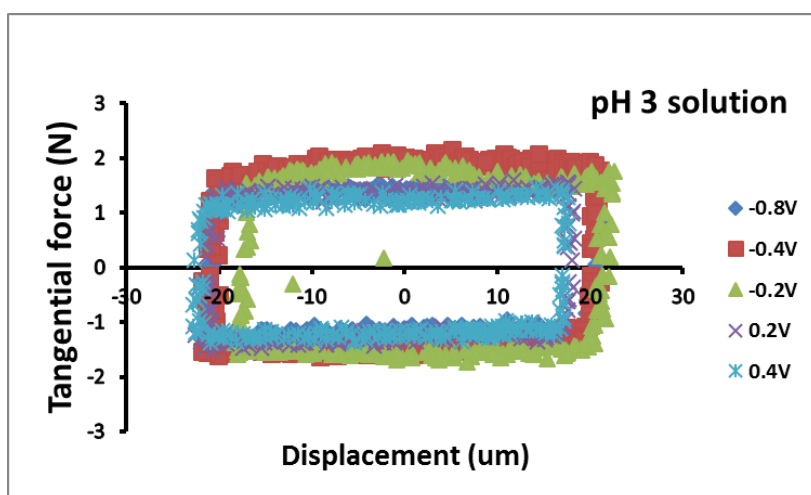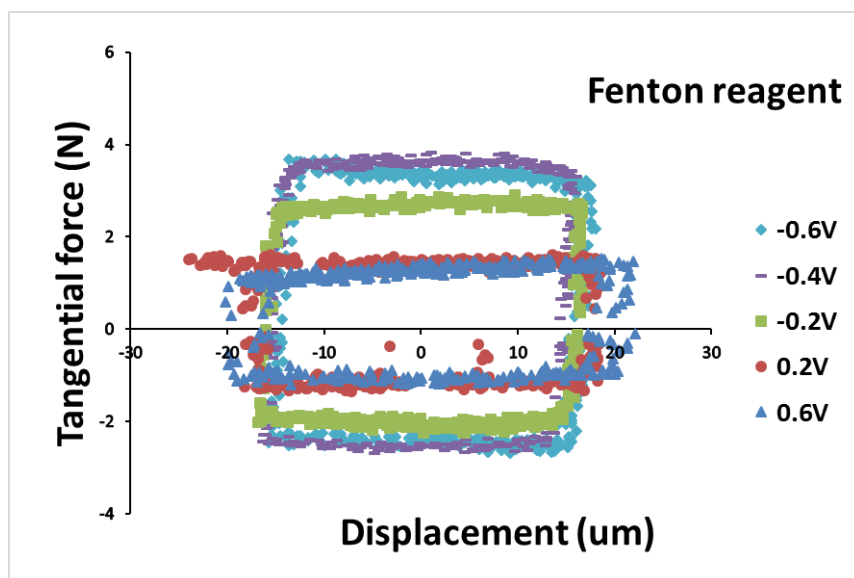
Figure 5.6 Tangential force versus displacement relationship at different potentials in PBS solution (A), pH 3 solution (B) and Fentron reagent solution (C). Tangential force-displacement relationship were voltage dependent and varies with solution. In Fenton reagent condition, displacement was lower at negative voltages compared with that was in other conditions.
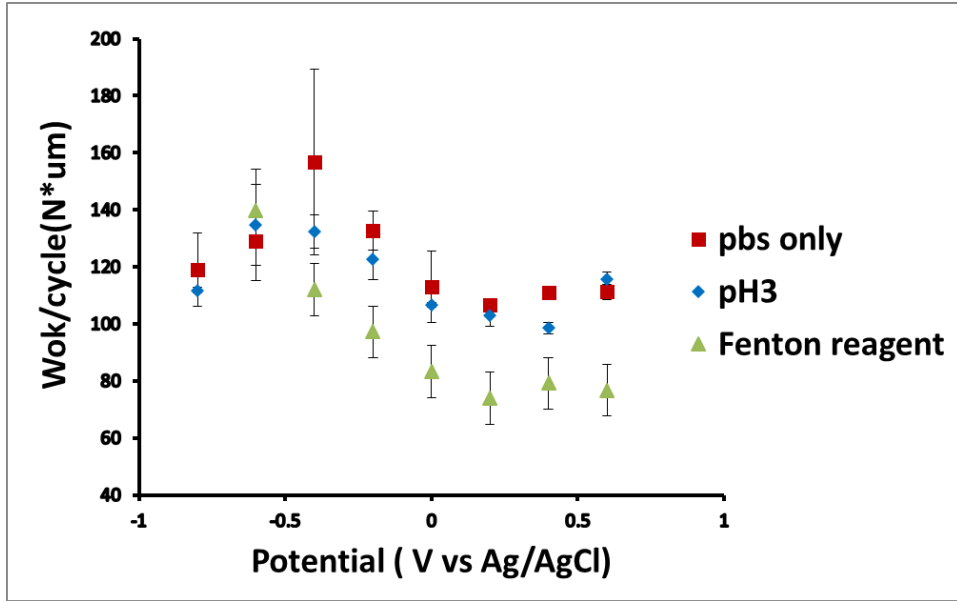
Figure 5.7 Work done per cycle of fretting at the interface at varied potentials in different solutions. Work done per cycle in Feonton reagent condition was significantly lower than that in pH 3 and PBS conditions at voltages higher than -0.6 V.
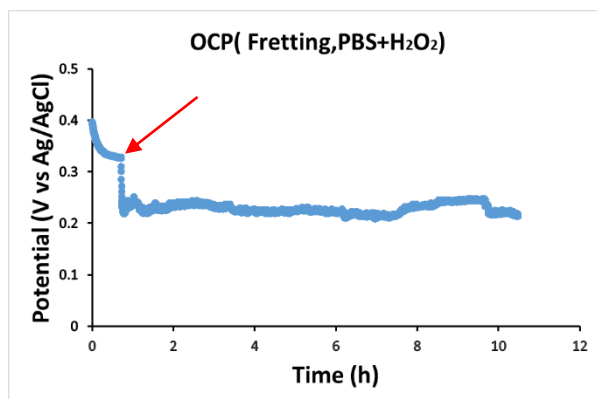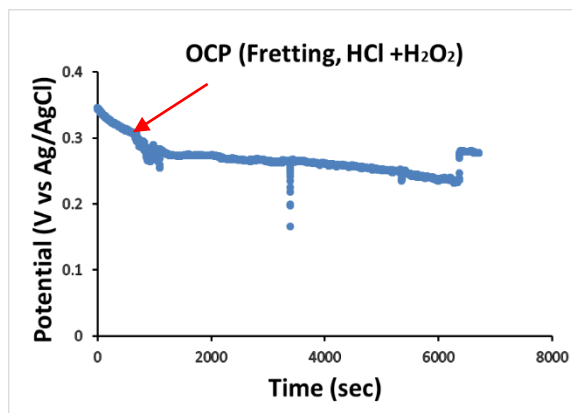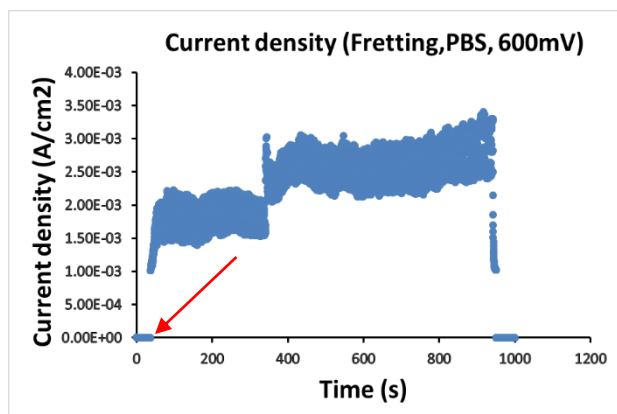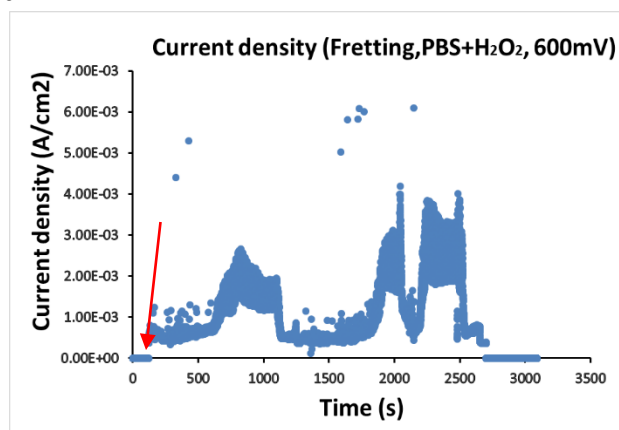
Figure 5.8 (a-d) OCP and current density information of long-term fretting corrosion test. The arrows indicate start of fretting. a) OCP in PBS solution with 30 mM $H_2O_2$; b) OCP in PBS solution with HCl & $H_2O_2$; c) Current density in PBS solution at 600 mV during fretting; d) current density in PBS solution with 30 mM $H_2O_2$ during fretting. Red arrows indicate starting of fretting.
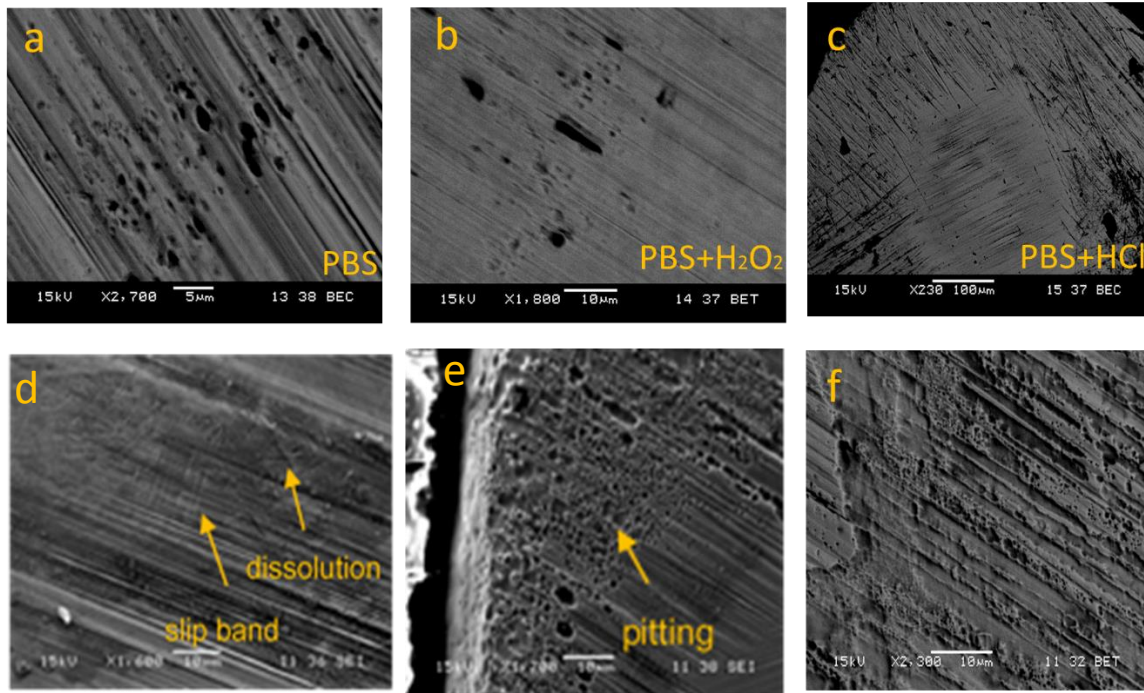
Figure 5.9 SEM micrographs after varied potential fretting corrosion tests (a-c) and long term fretting corrosion test under simulated inflammatory conditions (d-f). a) PBS solution; b) PBS+$H_2O_2$ solution; c) PBS+ HCl solution; d-f) Long-term fretting test. Pitting corrosion were observed after fretting in PBS solution and Fenton reagent solution. Both pitting and surface dissolution were observed after long term fretting corrosion tests.

# Chapter 6 Area effect on voltage shifts during fretting corrosion of Ti6Al4V

## 6.1 Introduction

Mechanically assisted corrosion of metallic biomaterials has been a serious concern in orthopedic implants [33, 80, 102]. It can also occur in other medical devices such as dental implant, spinal implant and cardiovascular stents where mechanical disruption on the metal surface exists [153-156]. During mechanically assisted corrosion, wear or fretting motion on the surface damages the protective passive oxide film and results in the accelerated corrosion of metallic biomaterials. On the other hand, accelerated corrosion, once activated, affects the mechanical motion by altering the surface contact condition [11]. Fretting corrosion occurs at several locations of the hip implants such as the bearing surfaces, modular taper junctions [157] as well as cement-stem interfaces [80, 102, 148]. Diseases such pseudotumor [14, 158, 159], adverse local tissue reactions, adverse reaction to metal debris have been associated with fretting corrosion and cause removal or replacement of the implant. High early failure rate and recent recalls of MoM hip implant devices by Food and Drug Administration (FDA) have raised significant serious concerns about the safely of metallic biomaterials used in hip devices.

While the basic mechanism of fretting crevice corrosion in modular tapers has been studied for a long time and generally well documented [8, 80, 102, 160-164], there are still elements of the process that remain poorly understood in terms of physics, chemistry and

biology. Fretting crevice corrosion occurs in modular taper interfaces when small-scale relative motion between different components happens. During the process, corrosion attack is accelerated due to the disruption of oxide film and pH in the crevice site drops due to the change of solution chemistry resulting from the electrochemical reactions. Meanwhile, release of metallic ions increases and oxide debris is generated and accumulated. Thus, fretting initiated crevice corrosion is possible. This means, under severe conditions, once activated, accelerated corrosion can continue even the fretting motion ceases [33, 165].

The spontaneously formed oxide film layer plays a significant role in protecting metallic biomaterials (Ti-alloy, CoCrMo allys and 316L Stainless Steel alloys) from corrosion and is relatively stable under static conditions. However, these 1-10 nanometers thick oxide films are actually highly dynamic once the environment changes [4, 166-169]. For example, the thickness, chemistry and structure of oxide films are solution-chemistry dependent. Protein on the surface and pH variation affect the properties of the oxide films. Another important factor influencing the oxide film behavior is the surface potential [11]. Previous studies have shown that surface oxide corrosion resistance, capacitance, composition and stability are significantly potential dependent [83, 84]. Under normal conditions, the surface potential of metallic biomaterials is in the range from -0.3 V to 0 V. However, during fretting corrosion process, surface disruption and accelerated corrosion result in burst release of electrons which negatively shifts the surface potential. Fretting corrosion on metallic biomaterials can result in the surface potential becoming negative to -1 V for Ti-alloy and -0.8 V for CoCrMo alloy [11]. In addition, voltage shifts and recovery are time-dependent and appears to be of

an exponential-like form. Previous study have shown negative excursion of the potential could have numerous biological effects such as inducing cell death [86, 87]. Holding potential at more negative than -400 mV (vs Ag/AgCl) can kill cell within 2 h. Thus, in addition to the effects of elevated levels of metallic ions and metal debris, the reduction half-cell could also have significant effects on the biological response during fretting corrosion process.

Cathodic trainsients in electrode potential across the metal-electrolyte interface due to fretting corrosion is affected by oxide conditions and thus is affected by materials combination, solution chemistry as well as fretting motion [170-172]. However, there is very little systematic theory developed to explain this phenomenon. Papageorgiou and Mischler [173] have proposed a model to predict negative potential shifts using Tafel equation, where effect of cathodic reaction and exposed area for reduction on voltage drop have been involved and studied. This approach helps to explain the magnitude of voltage drop due to fretting corrosion, however, the time-course of potential transient and recovery process have not been explained. Also, the conditions of the fretting motion such as normal load, fretting frequency, etc. are not incorporated into this model. Recently, Gilbert et al. [152] have proposed a physical-mathematical model, based on the area-dependent impedance characteristic of the surface and the behavior of the Randle's circuit to model the current return path to predict the extent and time course of the potential excursion resulting from any arbitrary tribocorrosion process. This voltage excursion model is linked to the fretting corrosion equation previously developed by Gilbert et al. so that the effects of mechanical variables (fretting magnitude, frequency, contact stress), and electrochemical variables

associated with fretting corrosion are included.

Thus, the goal of this study is to present experimental assessment of the model with a series of impedance tests and pin-on-disk fretting corrosion tests of Ti-6Al-4V/Ti-6Al-4V couples in phosphate buffered saline (PBS). Electrochemical Impedance Spectroscopy (EIS) tests were used to assess the corrosion resistance and capacitance characteristics of Ti-6Al-4V alloy and the influence of electrode area on them. Comparison of electrode potential drop and related time-dependent behaviour between experimental data and model prediction was conducted. How the variation of electrode area affects the voltage drop during fretting corrosion and voltage recovery after ceasing of fretting motion were investigated.

## 6.2 Theory

The theoretical model for voltage drop during fretting corrosion is developed by Gilbert et al. and is briefly introduced below (details of developing this model are shown elsewhere [152]). The basic idea in this model is that the electrochemical impedance characteristics of the surface of an electrode undergoing tribocorrosion, along with the tribocorrosion currents generated and subsequently returned as reduction reactions at the cathodic area, control the overall potential transient. Several assumptions are made in developing this model:

a. The oxide film thickness increases linearly with the increase of voltage [36].

b. Ionic dissolution reactions are ignored because they are small compared to the oxide film currents.

c. The cathodic surface is assumed to be lumped into a single Randle's circuit, distribution

of current is not incorporated (Figure 6.1).

d. The solution resistance is much lower than the oxide resistance.

e. No ongoing crevice corrosion or other active corrosion process remains during the voltage recovery process after the stop of fretting corrosion.

All tribocorrosion (Film) currents, $I_f$, generated are returned via the Randle's circuit by reduction reactions which are lumped into single parameters. The parameters, $R'_{ox}$, $C'_{ox}$, and $R'_s$ are extrinsic (area dependent) parameters. Based on these assumptions and a constant abrasion rate, the electrode potential transients are expressed as

$$E = -(E_{corr} - V)\frac{KR_{ox}}{(A + R_{ox}K)}\left[-e^{-\frac{t}{\tau_{tribo}}}\right] \qquad \text{Eq. 6-1}$$

$$\tau_{tribo} = \frac{AR_{ox}C_{ox}}{A + R_{ox}K} \qquad \text{Eq. 6-2}$$

E is the voltage drop away from the Open circuit potential, $E_{corr}$. A is the exposed electrode area for current dissipation, $R_{ox}$ is the intrinsic oxide resistance, $C_{ox}$ is the intrinsic capacitance. K is the tribocorrosion admittance (S) and is dependent on material and tribological conditions [8]:

$$K = \frac{\rho n F}{M_w}\frac{A_{nom}}{\Delta}m\frac{d\delta}{dt}$$

Where $\rho$ is the density of the oxide, n is the valence, $M_w$ is the molecular weight of the oxide film, $d\delta/dt$ is the sliding speed, m is the anodization rate for the oxide film (in cm/V). The factor $\Delta$ is the average inter-asperity distance in the sliding direction and $A_{nom}$ is the nominal contact area. The relationship between intrinsic and extrinsic resistances, capacitances are

assumed to be given by:

$$R'_{ox} = \frac{R_{ox}}{A}$$

Eq. 6-3

$$C_{ox}' = C_{ox}A$$

Eq. 6-4

where Rox' is the extrinsic resistance and Cox' is the extrinsic capacitance.

**Voltage recovery from tribocorrosion**

When the fretting corrosion processes are stopped, then the voltage will recover to more positive potentials as the accumulated electrons in the metal from oxidation reactions get dissipated across the interface in reduction reactions. This is like a discharging of the Randle's circuit capacitor which, for constant $R_{ox}$ and $C_{ox}$, will have the form:

$$V - E_{corr} = V_{drop} e^{-\frac{t}{\tau}}$$

Eq. 6-5

Where $V_{drop}$ is the voltage drop just before the stop of fretting corrosion and τ is $R_{ox}C_{ox}$. V is the voltage at any arbitrary time t after fretting motion ceases. These demonstrate that as the overall electrode area increases, the lumped surface resistance and capacitance fall and rise respectively.

**6.3 Materials and Methods**

**Materials**

The materials used in the experimental section were Ti-6Al-4V pin and disk samples (ASTM F-1472). The circular flat-bottom pin had a nominal contact diameter of between 500um and 800um, while the disk area was approximately circular and varied over a range that depended on the experiment, between 0.8 and 6.0 cm$^2$ by covering the remaining disk

147

area with an acrylic coating material. The coating was allowed to dry completely and it was ensured that there is no porosity in the coating (to avoid solution coming in contact with metal surface) before performing the tests. The advantage of having a small isolated test area is that the electrochemical noise (corrosion response from outside the fretting regions) is significantly reduced and high -fidelity current measures can be made. Surfaces were prepared by mechanical polishing to 600 grit and 1.0 um alumina, and cleaned with ethanol and distilled water. The average surface roughness of the pin tip (flat end) was Ra=1.2 um. The samples were immersed in phosphate buffered saline (Sigma, P3813, 0.135 M NaCl, 0.0027 M KCl, 0.01M $Na_2HPO_4$ and 0.002 M $KH_2PO_4$), pH 7.4, and allowed to equilibrate for 1h prior to testing. The experiments were conducted at room temperature.

**Impedance measurement of area dependence**

Electrochemical impedance spectroscopy (EIS) was performed on Ti-6Al-4V disks of 3 different areas (0.8, 2.6, 6.0 $cm^2$) in the absence of fretting. The potential of the disk was held at -0.1 V versus Ag/AgCl (to reflect approximate resting open circuit potential, $E_{corr}$, for Ti-6Al-4V) for 15 minutes for each test after the sample was immersed in PBS for 20min. For EIS measurements, a small sinusoidal voltage (10 mV) was applied to the interface while varying the frequency of input voltage from 20 kHz to 10 mHz. Solution resistance ($R_s$), oxide resistance ($R_{ox}$) and interfacial capacitance (Cox) were obtained by fitting the EIS spectra to the Constant Phase Element (CPE) modified Randle's circuit. Equivalent circuit modeling of all impedance data was performed using a non-linear square fitting software (Zview 2.0, Scribner Associates). Three independent tests per area were performed.

**Electrode potential measurements during pin-on-disk fretting corrosion testing**

Disks and pins were mounted into the fretting corrosion test system which has been introduced in detail before [8]. Fretting frequency, normal load and fretting displacement magnitude were controlled by the test system. Motion was applied by a high load piezoelectric actuator (Piezosystems Jena, Germany). An electrochemical chamber containing the disk was fixed to a motion stage (Newport) and connected to the actuator. A linear Z-stage, where a micrometer screw was used for adjusting the loading arm, was used for load control. The pin was attached to a multiaxial load cell (MINI 45 F/T, ATI Industial Automation) which was mounted under the loading arm. A high resolution (1 μm) contact DVRT (Microstrain) was used for the fretting displacement measurement. A potentiostat (Solatron 1280C, Solartron Analytical) was used for electrochemical measurements. National Instruments data acquisition card (NI PCI-6229) AND LabView 9.0 graphical programming tool were used for data acquisition.

**Effect of area**

To understand how the voltage drop varied with disk area, fretting corrosion tests were performed for disks of 3 different areas (0.25, 1 and 4 cm$^2$) for three times each. Pin-disk couples were allowed to sit at $E_{corr}$ for at least 20 minutes before applying the contact load. After applying a fixed normal load of 5 N, the fretting motion was initiated and a fixed nominal displacement of 50 μm was applied to the interface at a chosen fretting frequency. Fretting was performed for around 150 s and voltage was recorded from the beginning of the test until it recovered to near the starting $E_{corr}$. The voltage drop and time constant was determined

from the voltage during fretting corrosion minus the $E_{corr}$ and the time it took to go 0.63 times the change in voltage. The results from these tests were compared to the model predictions using Eq. 6-1 and Eq. 6-2.

**Statistical analysis**

Data analysis included determination of voltage drop at each area, load and frequency. Voltage drops were calculated by finding the potential at each area and subtracting it from the baseline $E_{corr}$ value prior to the fretting test. Where appropriate, statistical analysis were performed using ANOVA methods and Tukey's post-hoc comparisons, with $p<0.05$ considered significant. Specific results will be utilized to make comparisons with the theoretical model proposed.

**6.4 Results**

**6.4.1 Impedance vs Area**

The impedance of different areas of Ti-6Al-4V surface is shown in Figure 6.2. Three areas (0.8 $cm^2$, 2.6 $cm^2$, 6 $cm^2$) were measured and the impedance is given in Ohms. Clear variation of impedance is observed among different areas. Impedance decreases as area becomes larger over the range of frequencies tests. These scans were used to determine oxide resistance, capacitance, solution resistance, and impedance at 0.01 Hz and the results are shown in Figure 6.3 a-d. Randle's circuit was used in the curve fitting of the impedance scans using Z-view software. A constant phase element was applied to modify the capacitance component due to the non-ideal behavior of the interface. From equations 6-3 & 6-4, the extrinsic resistance

should vary as 1/A while the extrinsic capacitance should increase linearly with area. The area-dependence for these parameters can be clearly seen in the figure as anticipated ($p<0.05$).

### 6.4.2 Voltage shifts during fretting and recovery

An example of how the voltage of the pin and disk electrodes shifts with fretting can be seen in Figure 6.4. This plots shows the open circuit potential for Ti-6Al-4V pin and disk sample prior to fretting, during fretting (2.5 Hz. 50 um at 5 N) and after fretting is ceased. The initial resting OCP in this case is about 180 mV (vs Ag/AgCl). At fretting onset, the potential drops exponentially to about -750 mV (vs Ag/AgCl) and remains there during fretting. When the fretting stops, the OCP immediately begins to recover, again in an exponential fashion where the time constant for recovery is different than that for onset. Figure 4 shows the curve fitting results for the fretting equations for fretting transitions and recovery (Eq. 6-1 & 6-2), respectively. The values used to fit these equations are shown in Table 6.1 and are in reasonable agreement with the values measured for these materials. The difference in the time constant for fretting onset and recovery are related to the fact that during fretting the time constant is dependent on the fretting corrosion admittance (K) while the recovery time constant is simply the product of $R_{ox}$ and $C_{ox}$.

### 6.4.3 Effect of area on voltage drops during fretting corrosion

**Test results for frequency of 0.125 Hz**

The effects of area on the equilibrium voltage drops and the time constants for fretting corrosion (not recovery) seen experimentally at fretting frequency 0.125 Hz are shown in

151

Figure 6.5a and 6.5b. These plots show both measured electrode potential drops (Figure 6.5a) and time constants ($\tau_{tribo}$, Figire 6.5b) versus area and the corresponding values from Eq 6-1 using a single set of selected values of $R_{ox}$, $C_{ox}$, K and $R_s$ for the equation (see Table 6.1). It can be seen that there is reasonable agreement between both the voltage drop and the time constant with area as predicted by Eq. 6.1 & 6.2. Voltage drop values decrease as electrode area becomes larger as expected while time constant during voltage drop exhibits the opposite trend. The difference between the measured values and the constant R and C theory likely relates to the variability in the starting electrode potential, which ranged between -20 mV (for the smallest areas) to -200 mV (for the largest areas). These curves are fit with constant values for the R's, C's and K and do not account for any variation in these parameters with voltage.

**Test results for frequency of 1.25 Hz**

Comparison of voltage drop and time constant between the theory (Eq. 6-1 & 6-2) and experiment results during fretting corrosion at fretting frequency 1.25 Hz are shown in Figure 6.6 a & b. Selected values of $R_{ox}$, $C_{ox}$, K and $R_s$ (see Table 6.1) were used. Significant increase of voltage drop due to the increase of fretting frequency are shown in all tested areas. Electrode potential transients during fretting corrosion decrease as area gets larger and are in the range of -0.4 V and -0.6 V. It can be seen that there is fair agreement between both the voltage drop and the time constant with area as predicted by Eq. 6.1 and 6.2. The difference between the measured values and the constant R and C theory likely relates to the voltage dependence of these parameters, however, while the data and theory do not overlay one

another in these plots, the trends shown by both the experiment and the theory are consistent. When each individual potential transient used to make these plots are fit with Eq. 6.1 and 6.2, the Rox's and Cox's vary with both area and voltage (See Fig. 6.6 c & d). These are plots of the mean and standard deviation of the $R_{ox}$ and $C_{ox}$ used in the best fit versus the potential reached during fretting (which was more negative for smaller electrodes). These data imply that a single set of constant $R_{ox}$ and $C_{ox}$ may not be best for the overall performance, but that voltage-dependent values may be more suitable for wide ranging potentials.

## 6.4.4 Effect of voltage recovery after fretting corrosion

The effect of area on the voltage recovery time constant after ceasing of fretting corrosion experimentally are shown in Figure 6.7. Significant differences ($p<0.05$) are observed between 1 cm$^2$ and 4 cm$^2$, while no significant differences are shown between other groups. The time constant of 4 cm$^2$ is significantly smaller than that of 1 cm$^2$. Based on the Randle's circuit model, the recovery time constant equals to the product of intrinsic R and C and should remain unchanged assuming the intrinsic parameters are constant. This result indicates that intrinsic R and C are voltage dependent. Different voltage conditions during voltage recovery among different electrode areas affects both intrinsic and extrinsic R and C.

## 6.5 Discussion

This work has shown that voltage variation on surfaces of Ti-6Al-4V alloy undergoing fretting corrosion of their oxide films under freely corroding conditions are influenced by the overall electrode area available for reduction, the impedance characteristics of the surface as

well as the conditions of oxide abrasion (e.g., fretting frequency). The mechanics of the tribo-electrochemical interface and the materials dependence are accounted for in this model. The theoretical underpinning of these responses is able to describe and predict the voltage behavior both in terms of the magnitudes of the shifts but also in the time course of the changes seen. When Randle's circuit behavior is coupled with the fretting current equation previously described [11], the resultant expression can predict the behavior of the voltage in terms of the magnitude of the shift and the time course of the changes. Additionally, once the open circuit potential versus time during the fretting process, V (t), is known, the fretting currents can be obtained. Indeed, it is possible to use the measured voltages to make direct measurement of tribocorrosion currents.

Cathodic electrode potential excursions increased when the cathodic area decreased because the extrinsic resistance of the surface rose. Voltage drops also increased when the fretting frequency increases (faster surface oxide abrasion). Normal load on the surface is another important factor influencing the voltage drop by affecting the surface fretting condition. Increasing loads to a certain of level could lead to a decrease in the voltage drop when sticking of the fretting interface occurs [11]. Details of how the fretting frequency and normal load affect the voltage drop is described elsewhere [81]. The maximum voltage drop is limited by $V_0$, the onset voltage for oxide formation.

The solution resistance did not significantly alter the voltage transient behavior because terms containing Rs were much smaller than other parameters due to the ionic concentration in the solution (isotonic saline). Typically, Rs is on the order of 10 to 100 $\Omega$ while Rox is in the

$10^5$ to $10^6$ $\Omega$ range, and K is typically in the $10^{-5}$ to $10^{-6}$ S range. Thus, terms containing Rs are typically three orders of magnitude smaller than other terms in the equations developed and therefore do not significantly contribute to the response. However, when solution resistance is large (i.e., dilute aqueous solutions, distilled water), then Rs may play a role and therefore has been included here.

The solution to the Randle's circuit differential equation due to the fretting current equation, Equation 6.1, presents some interesting observations worth mentioning. The equation has a pre-exponential term and a time constant for the transient response which arises from assumed constant tribological conditions and constant resistances. This approach allows for direct linkage to be made between the mechanics of the process and the electrochemistry. Additionally, the time constant for tribocorrosion is shown to be sensitive to the mechanics, impedance and area, as was seen in the experimental results. It increases with area, $R_{ox}$ and $C_{ox}$ and decreases with increasing K.

The time constant for the voltage recovery after fretting corrosion $\tau$ is theoretically independent of area and voltage. However, different of voltage recovery time constant was observed in this study. $\tau$ is expressed as the product of R and C:

$$\tau = RC = \frac{\rho l}{A} \frac{\varepsilon \varepsilon_o A}{l} = \rho \varepsilon \varepsilon_o$$

where $\rho$ is the electrical resistivity of the material, $\varepsilon$ is the relative static permittivity of the material, $\varepsilon_o$ is the electric constant ($\varepsilon_0 \approx 8.854 \times 10^{-12}$ F·m$^{-1}$). Thus, the electrical resistivity or the relative static permittivity of the oxide film may vary with voltage. Previous studies [36, 38] have shown that voltage alters not only the thickness of the oxide but also the oxide film

chemistry, valence and defect density. These changes of oxide during voltage recovery could result in variation of electrical resistivity and permittivity of the oxide film.

There are limitations to the models presented in this study. First, the ideal Randle's circuit (with constant R's and C) is a first order simplified approximation of a much more complicated and voltage-dependent surface. Even though, the resultant potential transients were reasonably good approximations of the experimental results.

The concepts of voltage-dependent circuit elements could be applied to replace the constant R and C values in the equation. As voltage becomes more negative, the resistance of the oxide decreases and the capacitance increases [83]. One explanation for this is to apply the Tafel element, Mott-Schottky concept (for the capacitance of the oxide) and assume the cathodic reactions are activation limited [152]. The Tafel-element/constant capacitance and Tafel/Mott Schottky discharging models were better able to describe the potential recovery.

Another limitation of this study is that the fretting equation used assumed that the fretting speed is slow enough such that the repassivation reactions happen much faster than abrasion of new oxide. Thus, the rate of repassivation is governed by the slower abrasion rate. At high abrasion sliding speeds this assumption will not hold. However, since oxide repassivation reactions under potentiostatic conditions occur in the millisecond range, fretting speeds would need to be much higher than those presented here to violate this assumption.

The assumption was also made that only film forming oxidation currents were at play.

156

Where there are significant ionic currents present that contribute to the film currents, adjustments to the model will be needed. Additionally, the byproducts of the oxidation and reduction reactions may alter local solution chemistry which can alter oxide film properties and structure. These effects have not been accounted for in this model.

Eq.1 also predicts that the time constant for potential transients during fretting will approach zero as the area of the cathode approaches zero. However, this is not likely to be the case. The model does not deal with cases where the abraded area is a significant fraction of the total area. In this case, the bare abraded surface would contribute significantly to the voltage response deviating away from the theory presented.

This effort attempts to model the links between fretting corrosion processes (mechanics and electrochemistry), impedance, and geometry and the potential drops observed. Linkage of these factors has important consequences. One direct consequence is that the amount of corrosion that occurs during oxide abrasion depends on the amount of oxide repassivated. This analysis shows that as the potential becomes more negative, the amount of oxide repassivating decreases and the amount of oxidation currents generated also goes down. Thus, the relationship between mechanical sources of material loss and electrochemical sources cannot be decoupled or summed algebraically. Rather, the cathodic area and its properties will affect the process.

Additionally, voltage changes on metallic biomaterial surfaces have been shown to impact redox reactions may occur at the surface and that living cells cultured on these surfaces under cathodic bias can rapidly die [87]. Thus, implants in the body that are subject to

157

mechanically assisted corrosion will have similar voltage drops that may result in conditions that adversely affect the local biological environment and may contribute to local cell death. The results of this work can provide estimates of the cathodic surface area needed to keep implants from developing potentials below the threshold for impact on cells, and may be helpful for designing against some of the biological effects of tribocorrosion.

## 6.6 Conclusions

This study has conducted experiments to evaluate and demonstrate the validity of a theory for predicting the voltage shifts observed in mechanically assisted corrosion processes for oxide-film covered alloys. The voltage drop depends on the surface and solution impedance characteristics, the area of the electrode, the material and the mechanical conditions giving rise to the oxide film abrasion. The theory predicts all of the voltage-time behaviors seen in such systems. The time-course of the voltage change during onset as well as recovery were shown to be predicted by the model where the time constant during voltage drop was dependent on the electrode area. As electrode area increases, cathodic excursion during fretting corrosion decreases while the voltage drop time constants increases. As fretting frequency increases, voltage drop during fretting corrosion becomes larger. This model can be used to estimate voltage drops in metallic implants (or other structures) being subjected to mechanically assisted corrosion mechanisms and provides a tool to better understand and model tribocorrosion behavior.
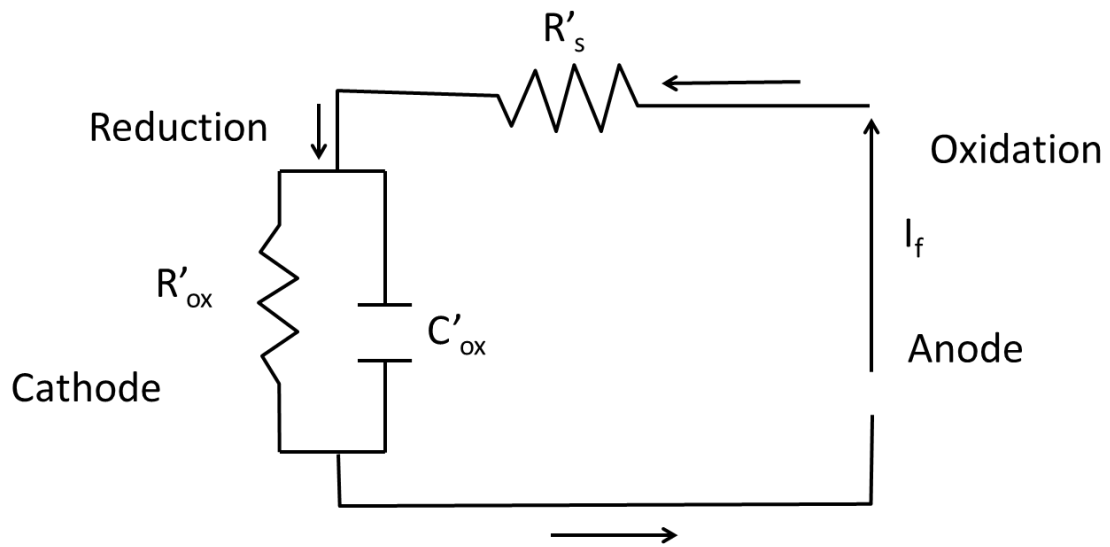
Figure 6.1 Schematic of the Randle's Circuit approximation for the electrode area where

tribocorrosion currents are returned at the cathode during a freely corroding process.
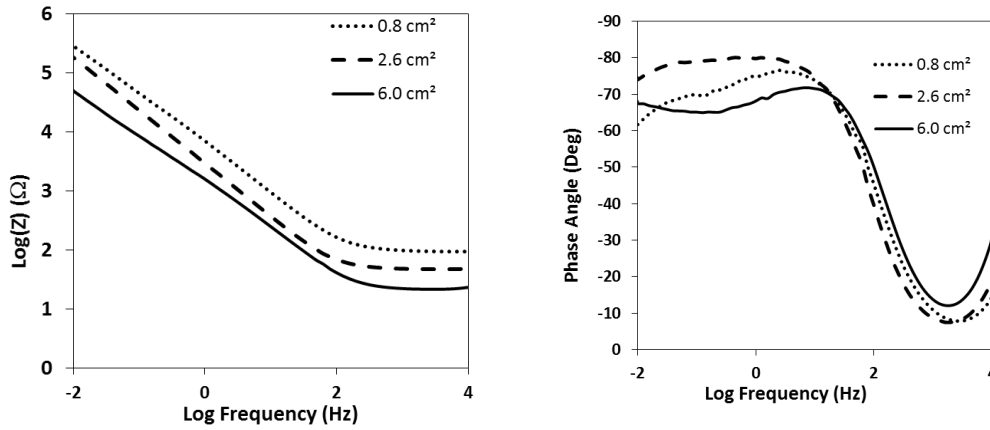
Figure 6.2 Experimentally-determined impedance of Ti-6Al-4V in phosphate buffered saline (PBS) at three different electrode areas. Electrodes were planar and polished to 1 um with areas of 0.8, 2.6, and 6 cm$^2$. Note the systematic drop in impedance with increasing electrode area.
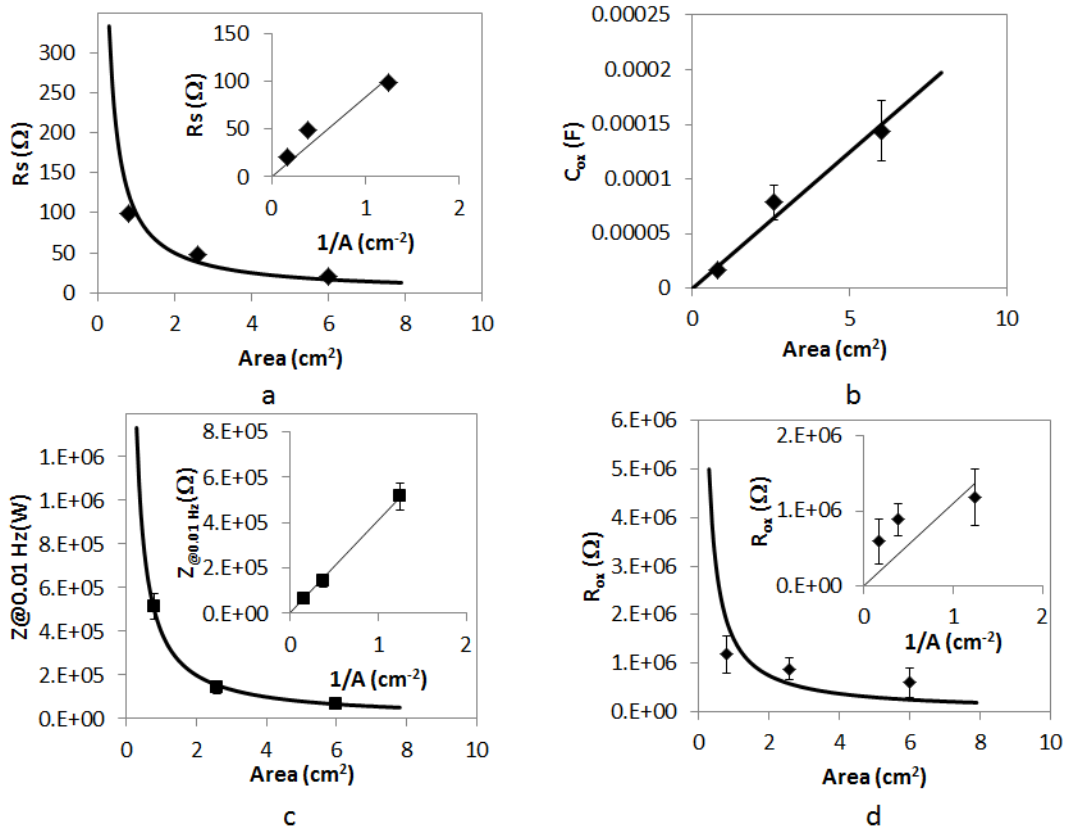
Figure 6.3 a-d. At fretting frequency of 0.125Hz, summary of electrical parameters for the Randle's circuit based on the impedance measurements of Ti-6Al-4V at different electrode areas. Extrinsic resistances (R's and R'ox) vary with the reciprocal of area while extrinsic capacitance varies directly and linearly with area as expected. a) R's – solution resistance, b) C'ox – capacitance, c) Z@0.01Hz impedance magnitude at 0.01 Hz, and d) R'ox – oxide resistance. Inset plots show R's plotted against 1/A. These plots approximately show the area dependence expected from the impedance tests.

161
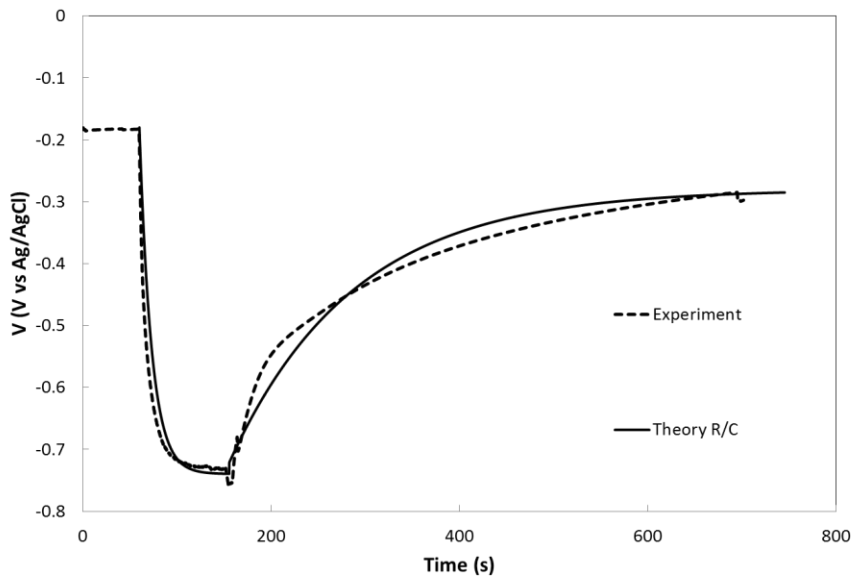
Figure 6.4 Electrode potential transient response of Ti-6Al-4V subject to fretting corrosion and recovery. The theory prediction is shown in the dashed line applying Eq.6-1 and Eq.6-2. The values for all parameters used in these plots are listed in Table 6.1

a.
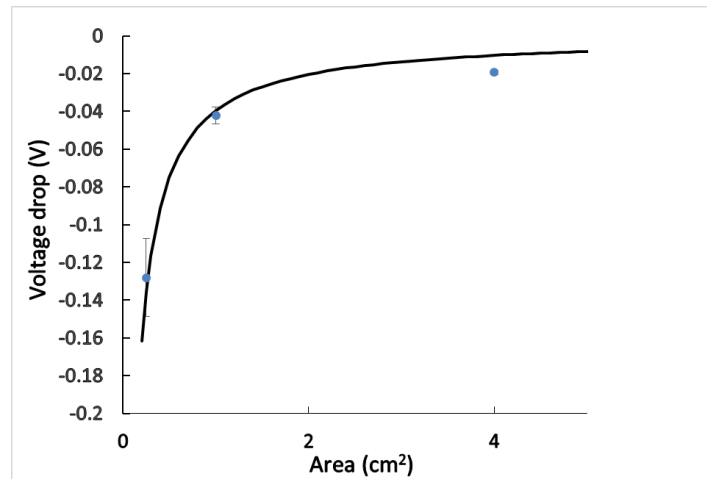


b
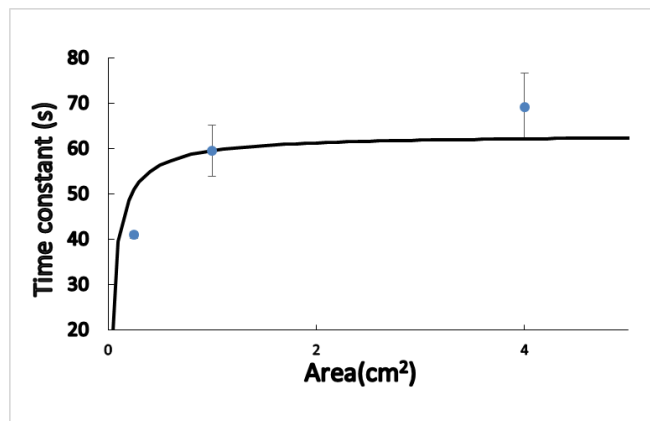


Figure 6.5 Plots of a) the voltage drop and b) the time constant for fretting corrosion onset resulting from fretting corrosion tests of Ti-6Al-4V with three different total electrode areas at fretting frequency 0.125Hz. The conditions for fretting were held fixed (e.g., load, sliding distance, sliding speed), n=3 for each area. The predicted values for the time constant and the voltage drop based on Eq. 1 are also shown. Values used are in Table 6.1.
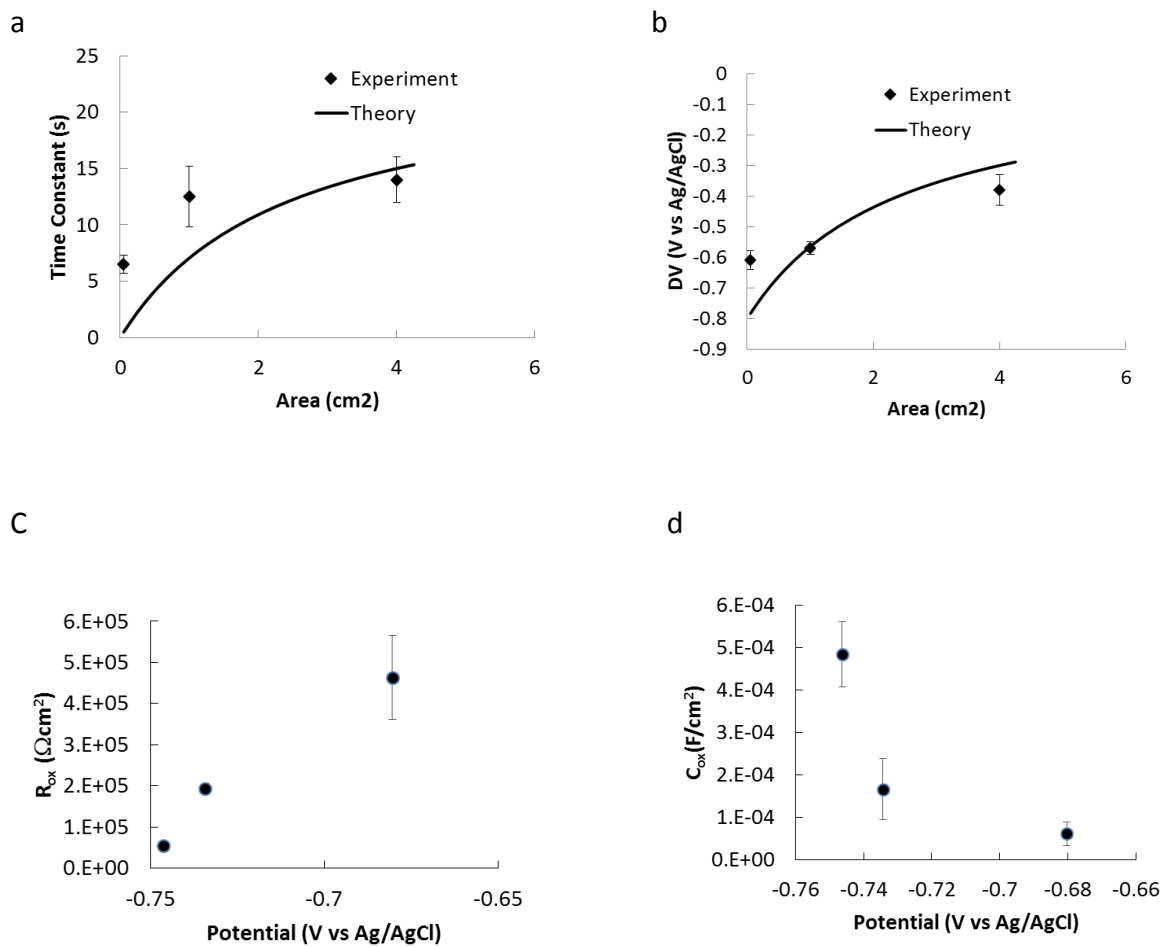
Figure 6.6 Plots of a) the time constant for fretting corrosion onset, and b) the voltage drop resulting from fretting corrosion tests of Ti-6Al-4V with three different total electrode areas at fretting frequency 1.25Hz. The conditions for fretting were held fixed (e.g., load, sliding distance, sliding speed), n=3 for each area. The predicted values for the time constant and the voltage drop based on Eq. 1 are also shown. Values used are in Table 1. Also shown are average and standard deviations for c) $R_{ox}$ and d) $C_{ox}$ used to get best fits to each individual potential transient curve at each area. Note that these are intrinsic values yet they appear to vary with the potential attained in each experiment indicating that R and C are sensitive to the voltage conditions.
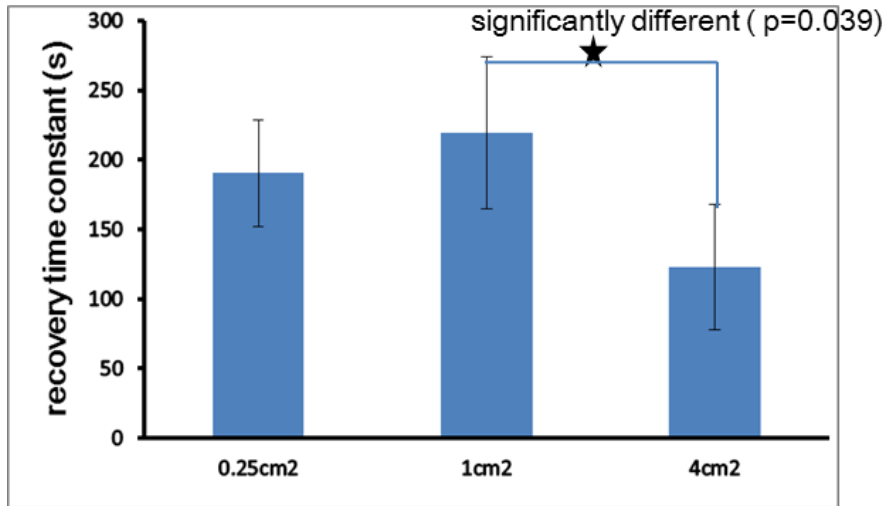
Figure 6.7 Voltage recovery time constant after ceasing of fretting corrosion for different areas

at fretting frequency of 1.25Hz.

Table 6.1

Summary of defined variables and their values for specific figures. Values were either known from the literature, determined from experiment, or adjusted to obtain the best fit of the theory with the data.

| Table 6.1: Parameters and Values | | | Figure | | | |
|---|---|---|---|---|---|---|
| Parameter | Definition | Unit | 3 | 4 | 5 | 6 |
| $R_s$ | Intrinsic Solution Resistance | $\Omega cm^2$ | 100 | 100 | 100 | 100 |
| $R_{ox}$ | Intrinsic Oxide Resistance | $\Omega cm^2$ | 1.50E+06 | 1.20E+06 | 3.00E+04 | 8.00E+05 |
| $C_{ox}$ | Intrinsic Oxide Capacitance | $F/cm^2$ | 2.50E-05 | 1.10E-04 | 6.00E-05 | 3.00E-05 |
| A | Total Area | $cm^2$ | | 1.0 | | |
| Dt | Time Increment | S | | 0.1 | | |
| K | Fretting Corrosion Admittance | S | | 7.74E-06 | 2.00E-06 | 3.00E-06 |
| $E_{corr}$ | Open Circuit Potential at Rest | V | | -0.18/-0.28 | -0.1 | -0.2 |
| $V_o$ | Oxide Formation Onset Voltage | V | | -0.8 | -1.0 | -1.0 |
| M | Anodization Rate | cm/V | | 1.80E-07 | | |
| d | Sliding Speed (2) | cm/s | | 0.05 | | |
| Δ | Average Interasperity Distance | Cm | | 0.05 | | |

# Chapter 7 Synthesis of results

Recent report of inflammatory cell-induced corrosion mechanism of CoCrMo alloy challenged traditional understanding of the relationship between corrosion and biology in hip implant systems. To better understand the role biology may play in the corrosion of CoCrMo based-hip implant devices, this study explored the mechanism of inflammatory cell induced corrosion on CoCrMo alloy and investigated how simulated inflammatory conditions and Fenton chemistry affect the electrochemistry behavior, oxide film behavior and fretting corrosion behavior of CoCrMo alloy. The hypothesis is that the presence of inflammatory cells-based reactive oxygen species, acid and Fenton chemistry in joint fluid alter the corrosion resistance of oxide film and increase the oxidizing power of the solution to affect the corrosion and fretting corrosion behavior of CoCrMo alloy.

In Chapter 2, electrochemical corrosion tests found that the corrosion susceptibility of CoCrMo alloy can be significantly increased by inflammatory cell released ROS such as $H_2O_2$ and Fenton reaction. These inflammatory cell based chemicals have been shown to create a highly corrosive environment at physiologically possible concentrations. Presence of $H_2O_2$ and Fenton reaction increase the oxidizing power of the solution and significantly increase the cathodic behavior of CoCrMo alloy. Meanwhile, these reactive chemical species decreased the impedance of oxide film and led to a more defective and less stable oxide. This combination effect, as hypothesized, resulted in a significant increase in the corrosion current and more positive open circuit potential. One major finding of this study is that physiologically possible potential of CoCrMo alloy has been shown to be as positive as 0.65 V, a much higher level than

167

previously thought. OCP increased to around 0.65 V in Fenton chemistry modified PBS solution at pH 7 or PBS solution with 30 mM $H_2O_2$ at pH 1. Increase of OCP to 0.65 V brings Cr ions to +6 state and could potentially lead to adverse local tissue reactions due to the toxicity of $Cr^{6+}$ in vivo. Interestingly, in 30 mM $H_2O_2$ modified PBS solution, decreases in pH increased corrosion resistance of CoCrMo alloy, which is counter in counterintuitive in that lower pH solutions are normally associated with increase in corrosion susceptibility. Thus, pH 7.4 physiological solution with $H_2O_2$ is the most corrosive to CoCrMo alloy.

In chapter 3, the effect of HClO, an important and aggressive ROS released by neutrophil myeloperoxidase (MPO) during respiratory burst, and hydrochloric acid on corrosion behavior of CoCrMo alloy was investigated. Corrosion susceptibility of CoCrMo alloy was significantly increased in simulated inflammatory solution when 0.1 M HClO was added. Open circuit potential significantly increased from -0.1 V to 0.9 V, where $Cr^{6+}$ generation was thermodynamically favored. Corrosion current density in HClO modified solution increased more than 300 times compared to PBS-only solution, while significant decrease of impedance magnitude was observed in simulated inflammatory solution with HClO. HClO exhibited similar effect on CoCrMo electrochemistry as $H_2O_2$. It increased the oxidizing power of the solution, damaged the oxide film and facilitated the corrosion of CoCrMo alloy. Interestingly, pH 7.4 physiological solution with HClO was found to be more corrosive than more acidic PBS solution with HClO. This " acid-passivation" effect was similar to that of $H_2O_2$. The presence of acid alone increased the oxidizing power of the solution, decreased the formation and growth of the passive oxide layer and resulted in a more aggressive (corrosive) environment for

CoCrMo alloy.

In chapter 4, the effect of simulated inflammatory solution with $H_2O_2$ on oxide of CoCrMo alloy was investigated by electrochemical atomic force microscopy (ECAFM). Physiologically possible anodic potentials reported in Chapter 2 & Chapter 3 were applied in physiological solutions with or without $H_2O_2$. ECAFM images showed that the presence of $H_2O_2$ in PBS solution altered the oxide behavior and indicated different corrosion reactions occurred in simulated inflammatory solutions. ECAFM images, surface roughness and polarization results demonstrate a correlated relationship between surface morphology and electrochemical behavior of CoCrMo alloy. Significant surface dissolution and corrosion of oxide on CoCrMo alloy were observed with increase of corrosion current density as potential was increased to 0.5 V or higher, which are physiologically possible potentials when $H_2O_2$, acid, Fenton chemistry or HClO are present. New oxide film formation was observation at transpassive potentials, however, the new oxide is not as corrosion protective as the passive film at OCP condition in PBS. Surface morphology variation, surface roughness and current density exhibited strong time-dependent behavior. Carbide boundaries and grain boundaries were observed to be preferential sites for oxide dissolution at transpassive potential. This study indicated both voltage and simulated inflammatory solution altered the corrosion behavior of CoCrMo alloy. Significant corrosion of CoCrMo alloy can happen at sufficiently positive physiologically possible potentials.

In chapter 5, the effect of simulated inflammatory conditions and potential on the fretting corrosion behavior of CoCrMo alloy was studied. Cell-based ($H_2O_2$, acid and Fenton

reaction) and implant-based (acid) solution chemistry were applied in this study to represent possible simulated inflammatory conditions. Fretting corrosion behavior of CoCrMo alloy were significantly affected by both solution chemistry and potential. Presence of Fenton chemistry resulted in less stable oxide film and increased oxidizing ability of solution. Oxide formation potential varied in different solutions and was the most positive under Fenton chemistry modified PBS solution, indicating increase in corrosion susceptibility of CoCrMo alloy when $H_2O_2$ and iron ions were present. Fretting current density was the largest in PBS solution and smallest in the Fenton reagent solution, showing less stable oxide film in physiological solution with Fenton chemistry. Fretting current density increased in a linear fashion with potential above oxide formation potentials for all solutions, but with different slopes and shows great agreement with the fretting corrosion model developed by Gilbert et al. before. Fretting COF, effective displacement and work done per fretting cycle at the interface were both potential and solution chemistry dependent. Interestingly, high fretting COF was observed just below the oxide formation potential in Fenton chemistry modified solution, indicating a change in frictional behavior due to the formation of new oxide. Pitting corrosion damage was shown in PBS and Fenton chemistry cases. Passivation of oxide films was the strongest in acidic solution, where no pitting corrosion was observed. Longer-term fretting corrosion in simulated inflammatory conditions resulted in more sever corrosion damage compared to shorter-term tests.

In Chapter 6, the effect of electrode area and impedance characteristics on the voltage drop during fretting corrosion of Ti6Al4V was investigated. Experiment results showed good

agreement with the impedance-based fretting corrosion model in predicting the time-dependent voltage excursion behavior during fretting corrosion process. Increase of electrode area leads to decrease of cathodic voltage excursion and increase of voltage drop time constant. This study has shown that the fretting corrosion model can be applied in estimating voltage drops in metallic biomaterials being subjected to fretting corrosion and provides useful tool to better understanding the nature of voltage excursion due to fretting corrosion for metallic biomaterials.

In conclusion, this study has explored the role of possible reactive chemical species released by inflammatory cells on the corrosion of CoCrMo alloy and has shown inflammatory cell released ROS such as $H_2O_2$, HClO, Fenton chemistry and acid increase oxidizing power of physiologically simulated solution, decrease oxide film impedance and significant increase in corrosion susceptibility of CoCrMo alloy. These reactive chemicals are able to create a highly corrosive environments and demonstrate at least part of the hypothesized mechanism of inflammatory cell-induced corrosion. Oxide film plays an important role in the corrosion behavior of CoCrMo alloy. Morphology, surface roughness and friction behavior of oxide film are directly associated with electrochemical corrosion behavior of CoCrMo alloy and have been shown to be significantly altered by the presence of simulated inflammatory species such as $H_2O_2$. Direct oxide dissolution and reformation were observed by ECAFM under physiologically possible potentials when simulated inflammatory species present. Fretting corrosion behavior of CoCrMo alloy is significantly altered by simulated inflammatory solution with Fenton chemistry. Oxide film was significantly altered by the combined effect of fretting

motion and aggressive chemical species, which led to different oxide formation potentials, fretting COF and fretting corrosion rates under simulated inflammatory conditions. This study has systematically demonstrated that inflammatory cell-based species play a significant role in CoCrMo electrochemistry and represented a major step in our understanding of the hypothesized cell-induced corrosion mechanism and the interaction between biology and corrosion. The role of biological response on the corrosion behavior of metallic biomaterials should be carefully considered and better understood. The immune system and the solution chemistry it develops may be the missing link between current in vitro corrosion studies, which can't completely duplicate all the corrosion modes on retrieved implants, and actual implant corrosion in vivo.

# Chapter 8 Conclusions

This study explored the mechanism of inflammatory cell induced corrosion. Several important finding were made on how simulated inflammatory conditions and Fenton chemistry affect the electrochemistry, oxide film and fretting corrosion of CoCrMo alloy. The key findings are summarized below:

- The corrosion susceptibility of CoCrMo alloy can be significantly increased by simulated inflammatory cell released reactive oxygen species ($H_2O_2$ acid, HClO) and Fenton reactions. These chemicals are similar to what is expected to occur under phagocytic cells during activation and demonstrate at least part of the mechanism of inflammatory cell induced corrosion.

- Addition of reactive oxygen species ($H_2O_2$, Fenton reagent and HClO) increased the oxidizing power of the solution and decreased the impedance of surface on CoCrMo alloy.

- Physiologically possible potential of CoCrMo alloy was found to be as positive as 0.9 V when HClO presents. The level is 0.8 V higher than what was thought before.

- In $H_2O_2$ or HClO inflammatory conditions, decrease of acidity significantly increased the corrosion susceptibility of CoCrMo alloy.

- ECAFM study showed that simulated inflammatory condition ($H_2O_2$) and potential significantly altered oxide film behavior (surface roughness, topography, corrosion resistance).

- Variation of surface roughness, corrosion resistance were related with potential and time-dependent oxide film topography.

- Fretting corrosion behavior of CoCrMo alloy was significantly affected by both solution chemistry and potential.

- Simulated inflammatory conditions (Fenton reaction) led to less stable oxide film and increased oxidizing ability of solution, altering the fretting corrosion behavior of CoCrMo alloy.

- Cathodic electrode potential excursion during fretting corrosion depends on the surface and solution impedance characteristics and the area of the electrode.

# Chapter 9 Future study

This dissertation answered many questions associated with the mechanism of inflammatory cell-induced corrosion on CoCrMo alloy and was the first effort to explore the effects of biological processes on the corrosion and fretting corrosion behavior of metallic biomaterials. There still remain a series of significant and interesting aspects to be investigated in order to better understand the ICIC mechanism and its possible effects on patients. This chapter describes several future studies related to the topic of this thesis. Some proposed studies aim at providing supplemental information associated the work presented in previous chapters, while the others suggest new directions on the ICIC topic. Some suggestions for future efforts are listed as below:

Joint fluid

All tests in this study were conducted in simulated inflammatory solutions to investigate which chemical species were mainly responsible for ICIC. In vivo joint fluid is more complicated and contains a variety of chemicals and proteins. Thus, the corrosion behavior of CoCrMo alloy may differ in joint fluid and should be better understood. A previous study has shown that the inflammation degree of joint fluid affects electrochemistry of CoCrMo alloy. It is important to conduct electrochemistry, surface characterization and fretting corrosion tests on CoCrMo alloy in joint fluid. Meanwhile, to characterize the constituents of joint fluid from patients is meaningful and will provide valuable guidance in preparation simulated solution for in vitro corrosion tests.

Cell-materials interaction

Another proposed study is to investigate the inflammatory cell-CoCrMo alloy interaction and duplicate the ICIC damage on CoCrMo alloy in vitro. Currently, it is unknown what types of cells are involved in the ICIC process and what local environment created by inflammatory cells is to induce CoCrMo alloy corrosion. Thus, cell culture experiments on CoCrMo alloy may provide valuable information to the answers of these questions. Different types of inflammatory cells can be used in this study to determine the cell types responsible for ICIC. This study can be used to monitor the time inflammatory cells need to induce CoCrMo alloy and this is directly related to the clinical performance of the implants.

XPS study

Another suggested study is to use X-ray photoelectron spectroscopy (XPS) to investigate the chemistry of oxide film on CoCrMo surface. It has been shown in this study that simulated inflammatory species are able to positively shift the surface potential about 1V to as high as 0.9V, which brings the oxide into transpassive voltage region. Under sufficiently positive potentials, metal element in oxides may be oxidized into high valance state and be retained in the oxide or released into the solution [75]. It is known that some metal ions, such as Cr, is highly toxic at high valance state ($Cr^{6+}$) and is undesired in vivo. Thus, this study will provide meaningful information on possible release of highly toxic metal ions by CoCrMo-based implants.

Metal ions concentrations

It has been shown that implantation of CoCrMo alloy increase metal ion concentrations in joint fluid, some metal ions (Co, Cr) are dangerous beyond a certain level of concentrations. Thus, it is important to study how simulated inflammatory solutions affect the metal ions release of CoCrMo alloy and know what concentrations and which valance states the metal ions are in solutions. Simulated inflammatory solutions significantly increases corrosion susceptibility of CoCrMo alloy, changes the oxide film behavior and may significantly influence the release of metal ions from oxide. This information can also be used to speculate on reactions associated with oxide film and, together with XPS technique, may provide better understanding of the possible influences ICIC has on the implant and joint fluid system.

Long-term tests

Currently, the time inflammatory cells needed for ICIC is unknown. All experiments in this study were shot-term tests which may not be able to reveal what actually happens to implant long-term after implantation. Long-term corrosion and fretting corrosion tests under simulated inflammatory conditions or joint fluid will provide supplemental valuable information for better understanding long-term corrosion performance of CoCrMo alloy after implantation. The corrosion damage is probably more sever after long-term attack by cells and fretting motions, which may lead to same damage modes observed from retrieval study.

Reactive nitrogen species

This dissertation has investigated the effect of a series of possible inflammatory cell-based reactive chemical species, including H2O2, HCl, HClO and Fenton chemistry on the corrosion behavior of CoCrMo alloy. Other important reactive chemical species released by

177

activated inflammatory cells and have high strong oxidative ability are nitric oxide (NO) and peroxynitrite ($NO_3^-$). Previous studies reported that macrophages and their released NO altered oxide film of CoCrMo alloy [59]. Thus, it is important to study how simulated inflammatory solutions with reactive nitrogen species affect the electrochemistry and oxide film behavior of CoCrMo alloy and exam their possible roles in the ICIC mechanism.

ICIC on titanium

Recently, ICIC has been reported on retrieved titanium implants. Similar to CoCrMo alloy, titanium alloy may be attacked by activated cells in vivo. The effect of $H_2O_2$ on corrosion of titanium alloy has been studied for a long time and is well documented. However, how other reactive chemical species released by inflammatory cells influence the corrosion susceptibility of titanium alloy is poorly understood. Thus, to perform corrosion tests, ECAFM test and fretting corrosion tests on titanium alloy under simulated inflammatory solutions will provide answer to this question and may be able to duplicate ICIC damage similar to what has been observed on retrieved titanium implants.

Fretting COF variation with voltage

Fretting corrosion tests in this study has shown that fretting COF on CoCrMo alloy is voltage and solution chemistry depended. However, why this occurs is poorly understood. Fretting COF affects fretting motion and corrosion behavior of hip implants and is of significance in selection of material in hip and knee implants. ECAFM study with friction mode combined with varied potential tests will reveal the reasons of variation in COF at different potentials at nano-scale level and may provide useful suggestions for alloy processing and

improving fretting corrosion performance of CoCrMo alloy.

# Chapter 10 Bibliography

[1] Richards RG, Moriarty TF, Miclau T, McClellan RT, Grainger DW. Advances in biomaterials and surface technologies. Journal of Orthopaedic Trauma. 2012; 26(12):703-707.

[2] Bashinskaya B, Zimmerman RM, Walcott BP, Antoci V. Arthroplasty utilization in the United States is predicted by age-specific population groups. ISRN Orthopedics. 2012.

[3] Pramanik S, Agarwal AK, Rai KN. Chronology of total hip joint replacement and materials development. Trends in Biomaterials & Artificial Organs. 2005; 19(1):15-26.

[4] Gilbert JL. Electrochemical behavior of metals in the biological milieu. In: Healy KE, Ducheyne P, Kirkpatrick CJ, editors. Comprehensive Biomaterials. Elsevier Press; Chapter 13; 2011.

[5] Megremis SJ. The mechanical, electrochemical, and morphological characteristics of passivating oxide films covering cobalt-chromium-molybdenum alloys: A study of five microstructures. Ph.D thesis, Northwestern University. 2001.

[6] Hoffman EE, Lin A, Liao Y, Marks LD. Grain Boundary Assisted Crevice Corrosion in CoCrMo Alloys. Corrosion. 2016; 72(11):1445-1461.

[7] Dowson D. Tribological principles in metal-on-metal hip joint design. Proceedings of the Institution of Mechanical Engineers, Part H: Journal of Engineering in Medicine. 2006; 220(2):161-171.

[8] Jacobs JJ, Gilbert JL, Urban RM. Current concepts review-corrosion of metal orthopaedic implants. Journal of Bone and Joint Surgery, American Volume. 1998; 80(2):268-282.

[9] Lucas LC, Buchanan RA, Lemons JE, Griffin CD. Susceptibility of surgical cobalt-base alloy

to pitting corrosion. Journal of Biomedical Materials Research. 1982; 16(6):799-810.

[10] Contu F, Elsener B, Böhni H. Corrosion behaviour of CoCrMo implant alloy during fretting in bovine serum. Corrosion Science. 2005; 47(8):1863-1875.

[11] Swaminathan V, Gilbert JL. Fretting corrosion of CoCrMo and Ti6Al4V interfaces. Biomaterials. 2012; 33(22):5487-503.

[12] Panigrahi P, Liao Y, Mathew MT, Fischer A, Wimmer MA, Jacobs JJ, Marks LD. Intergranular pitting corrosion of CoCrMo biomedical implant alloy. Journal of Biomedical Materials Research Part B: Applied Biomaterials. 2014; 102(4):850-859.

[13] Okazaki Y, Gotoh E. Comparison of metal release from various metallic biomaterials in vitro. Biomaterials. 2005; 26(1):11-21.

[14] Kwon YM, Ostlere SJ, McLardy-Smith P, Athanasou NA, Gill HS, Murray DW. "Asymptomatic" pseudotumors after metal-on-metal hip resurfacing arthroplasty: prevalence and metal ion study. The Journal of Arthroplasty. 2011; 26(4):511-518.

[15] Keegan GM, Learmonth ID, Case CP. Orthopaedic metals and their potential toxicity in the arthroplasty patient. Bone and Joint Journal. 2007; 89(5):567-573.

[16] Velard F, Braux J, Amedee J, Laquerriere P. Inflammatory cell response to calcium phosphate biomaterial particles: an overview. Acta Biomaterialia. 2013; 9(2):4956-4963.

[17] McKenzie L, Vale L, Stearns S, McCormack K. Metal on metal hip resurfacing arthroplasty. The European Journal of Health Economics. 2003; 4(2):122-129.

[18] Matusiewicz H. Potential release of in vivo trace metals from metallic medical implants in the human body: from ions to nanoparticles−a systematic analytical review. Bcta biomaterialia. 2014; 10(6):2379-2403.

[19] US Food and Drug administration- Recalls specific to Metal-on-Metal Him implants.

Available from:

http://www.fda.gov/MedicalDevices/ProductsandMedicalProcedures/ImplantsandProstheti

cs/MetalonMetalHipImplants/ucm241770.htm, pg updated: 01/17/2013.

[20] US Food and Drug Administration- Styker initiates voluntary product recall of

rejuvenate and ABG II modular-neck stems.

Available from: http://www.fda.gov/Safety/Recalls/ucm311043.htm, pg updated: 7/9/2012

[21] Jacobs JJ, Hallab NJ, Urban RM, Wimmer MA. Wear particles. Journal of Bone and Joint

Surgery, American Volume. 2006; 88(2):99-102.

[22] Ingham E, Fisher J. Biological reactions to wear debris in total joint replacement.

Proceedings of the Institution of Mechanical Engineers, Part H: Journal of Engineering in

Medicine. 2000; 214(1):21-37.

[23] Catelas I, Petit A, Vali H, Fragiskatos C, Meilleur R, Zukor DJ, Antoniou J, Huk OL.

Quantitative analysis of macrophage apoptosis vs. necrosis induced by cobalt and chromium

ions in vitro. Biomaterials. 2005; 26(15):2441-2453.

[24] Howie DW, Vernon-Roberts B. Synovial macrophage response to aluminium oxide ceramic

and cobalt-chrome alloy wear particles in rats. Biomaterials. 1988; 9(5):442-448.

[25] Haynes DR, Crotti TN, Haywood MR. Corrosion of and changes in biological effects of

cobalt chrome alloy and 316L stainless steel prosthetic particles with age. Journal of

Biomedical Materials Research. 2000; 49(2):167-175.

[26] Adala R, Chakravarthy M, Srinivas V, Pai S. Orthopaedic surgery in a patient with metal

sensitivity. Journal of Cutaneous and Aesthetic Surgery. 2011; 4(1):67.

[27] Thyssen JP, Jakobsen SS, Engkilde K, Johansen JD, Søballe K, Menné T. The association between metal allergy, total hip arthroplasty, and revision: A case-control study. Acta Orthopaedica. 2009; 80(6):646-652.

[28] Colognato R, Bonelli A, Ponti J, Farina M, Bergamaschi E, Sabbioni E, Migliore L. Comparative genotoxicity of cobalt nanoparticles and ions on human peripheral leukocytes in vitro. Mutagenesis. 2008; 23(5):377-82.

[29] Behl B, Papageorgiou I, Brown C, Hall R, Tipper JL, Fisher J, Ingham E. Biological effects of cobalt-chromium nanoparticles and ions on dural fibroblasts and dural epithelial cells. Biomaterials. 2013; 34(14):3547-3558.

[30] Posada OM, Gilmour D, Tate RJ, Grant MH. CoCr wear particles generated from CoCr alloy metal-on-metal hip replacements, and cobalt ions stimulate apoptosis and expression of general toxicology-related genes in monocyte-like U937 cells. Toxicology and Applied Pharmacology. 2014; 281(1):125-135.

[31] Gibon E, Amanatullah DF, Loi F, Pajarinen J, Nabeshima A, Yao Z, Hamadouche M, Goodman SB. The biological response to orthopaedic implants for joint replacement: Part I: Metals. Journal of Biomedical Materials Research Part B: Applied Biomaterials. 2016.

[32] Cooper HJ, Della Valle CJ, Berger RA, Tetreault M, Paprosky WG, Sporer SM, Jacobs JJ. Corrosion at the head-neck taper as a cause for adverse local tissue reactions after total hip arthroplasty. The Journal of Bone and Joint Surgery. 2012; 94(18):1655-1661.

[33] Gilbert JL. Mechanically assisted corrosion of metallic biomaterials. ASM International Handbook. 2006; 13:826-836.

[34] Swaminathan V. Fretting Crevice Corrosion of Metallic Biomaterials: Instrument

Development and Materials Analysis. Ph.D thesis, Syracuse University. 2012.

[35] Cooper HJ, Urban RM, Wixson RL, Meneghini RM, Jacobs JJ. Adverse local tissue reaction arising from corrosion at the femoral neck-body junction in a dual-taper stem with a cobalt-chromium modular neck. Journal of Bone and Joint Surgery, American Volume. 2013; 95(10):865-872.

[36] Molloy DO, Munir S, Jack CM, Cross MB, Walter WL, Walter WK. Fretting and corrosion in modular-neck total hip arthroplasty femoral stems. Journal of Bone and Joint Surgery American Volume. 2014; 96(6):488-493.

[37] Hallab NJ, Jacobs JJ. Orthopedic implant fretting corrosion. Corrosion Reviews. 2003; 21(2-3):183-214.

[38] Skendzel JG, Blaha JD, Urquhart AG. Total hip arthroplasty modular neck failure. The Journal of Arthroplasty. 2011; 26(2):338-e1.

[39] Jacobs, JJ, Cooper, HJ, Urban RM, Wixson RL, Della Valle C. Clinical Aspects of Bio-Tribocorrosion in Orthopedics. Orthopaedic Research Society Annual Meeting. 2014.

[40] Gill HS, Grammatopoulos G, Adshead S, Tsialogiannis E, Tsiridis E. Molecular and immune toxicity of CoCr nanoparticles in MoM hip arthroplasty. Trends in Molecular Medicine. 2012; 18(3):145-155.

[41] Lewis AC, Ladon D, Heard PJ, Peto L, Learmonth I. The role of the surface chemistry of CoCr alloy particles in the phagocytosis and DNA damage of fibroblast cells. Journal of Biomedical Materials Research Part A. 2007; 82(2):363-372.

[42] Howie DW, Rogers SD, McGee MA, Haynes DR. Biologic effects of cobalt chrome in cell and animal models. Clinical Orthopaedics and Related Research. 1996; 329:217-232.

[43] Willert HG, Buchhorn GH, Fayyazi A, Flury R, Windler M, Köster G, Lohmann CH. Metal-on-metal bearings and hypersensitivity in patients with artificial hip joints. Journal of Bone and Joint Surgery, American Volume. 2005; 87(1):28-36.

[44] Prasad MN. Trace elements as contaminants and nutrients: consequences in ecosystems and human health. John Wiley & Sons. 2008.

[45] Jacobs JJ, Skipor AK, Doorn PF, Campbell P, Schmalzried TP, Black J, Amstutz HC. Cobalt and chromium concentrations in patients with metal on metal total hip replacements. Clinical Orthopaedics and Related Research. 1996; 329:256-263.

[46] Merritt K, Brown SA. Release of hexavalent chromium from corrosion of stainless steel and cobalt—chromium alloys. Journal of Biomedical Materials Research. 1995; 29(5):627-633.

[47] Mao X, Wong AA, Crawford RW. Cobalt toxicity—an emerging clinical problem in patients with metal-on-metal hip prostheses. Medical Journal of Australia. 2011; 194(12):649-651.

[48] Tower SS. Arthroprosthetic cobaltism: neurological and cardiac manifestations in two patients with metal-on-metal arthroplasty. Journal of Bone and Joint Surgery, American Volume. 2010; 92(17):2847-2851.

[49] Haeri M, Wöllert T, Langford GM, Gilbert JL. Electrochemical control of cell death by reduction-induced intrinsic apoptosis and oxidation-induced necrosis on CoCrMo alloy in vitro. Biomaterials. 2012; 33(27):6295-6304.

[50] Haeri M, Gilbert JL. Study of cellular dynamics on polarized CoCrMo alloy using time-lapse live-cell imaging. Acta Biomaterialia. 2013; 9(11):9220-9228.

[51] Anderson JM, Rodriguez A, Chang DT. Foreign body reaction to biomaterials. Seminars in Immunology. 2008; 20(2): 86-100.

[52] Anderson JM. Biological responses to materials. Annual Review of Materials Research. 2001; 31(1):81-110.

[53] Laskin DL, Pendino KJ. Macrophages and inflammatory mediators in tissue injury. Annual Review of Pharmacology and Toxicology. 1995; 35(1):655-677.

[54] Rosen GM, Pou S, Ramos CL, Cohen MS, Britigan BE. Free radicals and phagocytic cells. The Federation of American Societies for Experimental Biology Journal. 1995; 9(2):200-209.

[55] Hampton MB, Kettle AJ, Winterbourn CC. Inside the neutrophil phagosome: oxidants, myeloperoxidase, and bacterial killing. Blood. 1998; 92(9):3007-3017.

[56] Silver IA, Murrills RJ, Etherington DJ. Microelectrode studies on the acid microenvironment beneath adherent macrophages and osteoclasts. Experimental Cell Research. 1988; 175(2):266-276.

[57] Cadosch D, Chan E, Gautschi OP, Simmen HP, Filgueira L. Bio-corrosion of stainless steel by osteoclasts—in vitro evidence. Journal of Orthopaedic Research. 2009; 27(7): 841-846.

[58] Cadosch D, Al-Mushaiqri MS, Gautschi OP, Meagher J, Simmen HP, Filgueira L. Biocorrosion and uptake of titanium by human osteoclasts. Journal of Biomedical Materials Research Part A. 2010; 95(4):1004-1010.

[59] Lin HY, Bumgardner JD. Changes in the surface oxide composition of Co–Cr–Mo implant alloy by macrophage cells and their released reactive chemical species. Biomaterials. 2004; 25(7):1233-1238.

[60] Pan J, Thierry D, Leygraf C. Hydrogen peroxide toward enhanced oxide growth on titanium in PBS solution: blue coloration and clinical relevance. Journal of Biomedical Materials Research. 1996; 30(3):393-402.

[61] Bearinger JP, Orme CA, Gilbert JL. Effect of hydrogen peroxide on titanium surfaces: In situ imaging and step-polarization impedance spectroscopy of commercially pure titanium and titanium, 6-aluminum, 4-vanadium. Journal of Biomedical Materials Research Part A. 2003; 67(3):702-712.

[62] Mabilleau G, Bourdon S, Joly-Guillou ML, Filmon R, Baslé MF, Chappard D. Influence of fluoride, hydrogen peroxide and lactic acid on the corrosion resistance of commercially pure titanium. Acta Biomaterialia. 2006; 2(1):121-129.

[63] Royhman D, Radhakrishnan R, Yuan JC, Mathew MT, Mercuri LG, Sukotjo C. An electrochemical investigation of TMJ implant metal alloys in an artificial joint fluid environment: The influence of pH variation. Journal of Cranio-Maxillofacial Surgery. 2014; 42(7):1052-1061

[64] Brooks E, Tobias M, Krautsak K, Ehrensberger M. The influence of cathodic polarization and simulated inflammation on titanium electrochemistry. Journal of Biomedical Materials Research Part B: Applied Biomaterials. 2014; 102(7):1445-1453.

[65] Fonseca-García A, Pérez-Alvarez J, Barrera CC, Medina JC, Almaguer-Flores A, Sánchez RB, Rodil SE. The effect of simulated inflammatory conditions on the surface properties of titanium and stainless steel and their importance as biomaterials. Materials Science and Engineering: C. 2016; 66:119-129.

[66] Gilbert JL, Sivan S, Liu Y, Kocagöz SB, Arnholt CM, Kurtz SM. Direct in vivo inflammatory cell-induced corrosion of CoCrMo alloy orthopedic implant surfaces. Journal of Biomedical Materials Research Part A. 2015; 103:211-223.

[67] Morris CJ, Earl JR, Trenam CW, Blake DR. Reactive oxygen species and iron—a dangerous

partnership in inflammation. The International Journal of Biochemistry & Cell Biology. 1995; 27:109-122.

[68] Prousek J. Fenton chemistry in biology and medicine. Pure and Applied Chemistry. 2007; 79:2325-2338.

[69] Di Laura A, Hothi HS, Meswania JM, Whittaker RK, De Villiers D, Zustin J, Blunn GW, Skinner JA, Hart AJ. Clinical relevance of corrosion patterns attributed to inflammatory cell-induced corrosion: A retrieval study. Journal of Biomedical Materials Research Part B: Applied Biomaterials. 2015.

[70] Munoz AI, Schwiesau J, Jolles BM, Mischler S. In vivo electrochemical corrosion study of a CoCrMo biomedical alloy in human synovial fluids. Acta Biomaterialia. 2015; 21:228-236.

[71] Nathan CF. Secretory products of macrophages. Journal of Clinical Investigation. 1987; 79(2):319.

[72] Winterbourn CC, Hampton MB, Livesey JH, Kettle AJ. Modeling the reactions of superoxide and myeloperoxidase in the neutrophil phagosome implications for microbial killing. Journal of Biological Chemistry. 2006; 281:39860-39869.

[73] Neyens E, Baeyens J. A review of classic Fenton's peroxidation as an advanced oxidation technique. Journal of Hazardous materials. 2003; 98(1):33-50.

[74] Stohs SJ, Bagchi D. Oxidative mechanisms in the toxicity of metal ions. Free Radical Biology and Medicine. 1995; 18(2):321-336.

[75] Milošev I, Strehblow HH. The composition of the surface passive film formed on CoCrMo alloy in simulated physiological solution. Electrochimica Acta. 2003; 48(19):2767-2674.

[76] Chuang TJ, Brundle CR, Rice DW. Interpretation of the x-ray photoemission spectra of

cobalt oxides and cobalt oxide surfaces. Surface Science. 1976; 59(2):413-429.

[77] Gilbert JL, Bai Z, Bearinger J, Megremis S. The dynamics of oxide films on metallic biomaterials. In Proceedings of the ASM Conference on Medical Device Materials, Anaheim, CA. 2004.

[78] Collier JP, Mayor MB, Williams IR, Surprenant VA, Surprenant HP, Currier BH. The tradeoffs associated with modular hip prostheses. Clinical Orthopaedics and Related Research. 1995; (311):91-101.

[79] Gilbert JL, Mehta M, Pinder B. Fretting crevice corrosion of stainless steel stem-CoCr femoral head connections: comparisons of materials, initial moisture, and offset length. Journal of Biomedical Materials Research B: Applied Biomaterials. 2009; 88 (1):162-173.

[80] Brown SA, Flemming CA, Kawalec JS, Placko HE, Vassaux C, Merritt K, Payer JH, Kraay MJ. Fretting corrosion accelerates crevice corrosion of modular hip tapers. Journal of Applied Biomaterials. 1995; 6(1):19-26.

[81] Swaminathan V, Gilbert JL. Potential and frequency effects on fretting corrosion of Ti6Al4V and CoCrMo surfaces. Journal of Biomedical Materials Research Part A. 2013; 101:2602-2612.

[82] Sun D, Wharton JA, Wood RJ. Effects of proteins and pH on tribocorrosion performance of cast CoCrMo–a combined electrochemical and tribological study. Tribology-Materials, Surfaces and Interfaces. 2008; 2(3):150-160.

[83] Ehrensberger MT, Gilbert JL. The effect of static applied potential on the 24 hour impedance behavior of commercially pure titanium in simulated biological conditions. Journal of Biomedical Materials Research Part B: Applied Biomaterials. 2010; 93(1):106-112.

[84] Ehrensberger MT, Gilbert JL. The effect of scanning electrochemical potential on the short-term impedance of commercially pure titanium in simulated biological conditions. Journal of Biomedical Materials Research Part A. 2010; 94(3):781-789.

[85] Goldberg JR, Gilbert JL. Electrochemical response of CoCrMo to high-speed fracture of its metal oxide using an electrochemical scratch test method. Journal of Biomedical Materials Research. 1997; 37:421-431.

[86] Ehrensberger MT, Sivan S, Gilbert JL. Titanium is not "the most biocompatible metal" under cathodic potential: The relationship between voltage and MC3T3 preosteoblast behavior on electrically polarized cpTi surfaces. Journal of Biomedical Materials Research Part A. 2010; 93(4):1500-1509.

[87] Sivan S, Kaul S, Gilbert JL. The effect of cathodic electrochemical potential of Ti-6Al-4V on cell viability: voltage threshold and time dependence. Journal of Biomedical Materials Research Part B: Applied Biomaterials. 2013; 101(8):1489-1497.

[88] Whitehouse MR, Endo M, Masri BA. Adverse local tissue reaction associated with a modular hip hemiarthroplasty. Clinical Orthopaedic and Related Research 2013; 471:4082-4086.

[89] Lindgren JU, Brismar BH, Wikstrom AC. Adverse reaction to metal release from a modular metal-on-polyethylene hip prosthesis. Journal of Bone & Joint Surgery, British Volume 2011; 93:1427-1430.

[90] Gilbert JL, Kubacki GW, "Oxidative Stress, Inflammation and the Corrosion of Metallic Biomaterials: Corrosion Causes Biology and Biology Causes Corrosion", Oxidative Stress and Biomaterials, Ed. TD Dziubla, DA Butterfield, Elsevier Press, in press, 2015, Chapt. 3.

[91] Halliwell B, Clement MV, Ramalingam J, Long LH. Hydrogen peroxide. Ubiquitous in cell culture and in vivo?. Journal of the International Union of Biochemistry and Molecular Biology 2000; 50:251-257.

[92] Pourbaix M. Electrochemical corrosion of metallic biomaterials. Biomaterials 1984; 5:122-134.

[93] Gilbert JL, Sivan S, Liu Y, Kocagöz SB, Arnholt CM, Kurtz SM. Evidence of Direct Cell Induced Corrosion of CoCrMo Implant Systems. Abstract 452. Society for Biomaterials Annual Meeting. 2014.

[94] Kehrer JP. The Haber–Weiss reaction and mechanisms of toxicity. Toxicology. 2000; 149:43-50.

[95] Jones, DA. Principles and Prevention of Corrosion. MacMillan.1992; 85–91.

[96] Sivan S. Electrochemical Aspects of Metalllic Biocompatibility. Ph.D thesis, Syracuse University. 2015.

[97] Schaffer AW, Schaffer A, Pilger A, Engelhardt C, Zweymueller K, Ruediger HW. Increased blood cobalt and chromium after total hip replacement. Journal of Toxicology: Clinical Toxicology. 1999; 37:839-844.

[98] Luetzner J, Krummenauer F, Lengel AM, Ziegler J, Witzleb WC. Serum metal ion exposure after total knee arthroplasty. Clinical Orthopaedics and Related Research. 2007; 461:136-142.

[99] Biemond P, Swaak AJ, Van Eijk HG, Koster JF. Intraarticular ferritin-bound iron in rheumatoid arthritis: A factor that increases oxygen free radical-induced tissue destruction. Arthritis and Rheumatism 1986; 29:1187-1193.

[100] Weber J, Julius HW, Verhoef CW, Werre JM. Absorption and retention of iron in

rheumatoid arthritis. Annals of the Rheumatic Diseases 1973; 32(1):83.

[101] Liao Y, Hoffman E, Wimmer M, Fischer A, Jacobs J, Marks L. CoCrMo metal-on-metal hip replacements. Physical Chemistry Chemical Physics. 2013; 15(3):746-756.

[102] Gilbert JL, Buckley CA, Jacobs JJ. In vivo corrosion of modular hip prosthesis components in mixed and similar metal combinations. The effect of crevice, stress, motion, and alloy coupling. Journal of Biomedical Materials Research. 1993;27(12):1533-1544.

[103] Catelas I, Wimmer MA. New insights into wear and biological effects of metal-on-metal bearings. Journal of Bone and Joint Surgery, American Volume. 2011;93(2):76-83.

[104] Liu Y, Gilbert JL. The effect of simulated inflammatory conditions and Fenton chemistry on the electrochemistry of CoCrMo alloy. Journal of Biomedical Materials Research Part B: Applied Biomaterials. 2017.

[105] Agner K. Biological effects of hypochlorous acid formed by" MPO"-peroxidation in the presence of chloride ions. Structure and Function of Oxidation-Reduction Enzymes. 2014; 18:329-335.

[106] Prokopowicz ZM, Arce F, Biedron R, Chiang CL, Ciszek M, Katz DR, Nowakowska M, Zapotoczny S, Marcinkiewicz J, Chain BM. Hypochlorous acid: a natural adjuvant that facilitates antigen processing, cross-priming, and the induction of adaptive immunity. The Journal of Immunology. 2010; 184(2):824-835.

[107] Mainnemare A, Megarbane B, Soueidan A, Daniel A, Chapple IL. Hypochlorous acid and taurine-N-monochloramine in periodontal diseases. Journal of Dental Research. 2004; 83(11):823-831.

[108] Muijsers RB, van Den Worm E, Folkerts G, Beukelman CJ, Koster AS, Postma DS, Nijkamp

FP. Apocynin inhibits peroxynitrite formation by murine macrophages. British Journal of Pharmacology. 2000; 130(4):932-936.

[109] Zuo QP, Li ZJ, Hu YH, Li B, Huang LH, Wang CJ, Liu SK, Liao HQ. A highly sensitive fluorescent probe for HClO and its application in live cell imaging. Journal of Fluorescence. 2012; 22(5):1201-1207.

[110] Lee G, Hering JG. Oxidative dissolution of chromium (III) hydroxide at pH 9, 3, and 2 with product inhibition at pH 2. Environmental Science & Technology. 2005; 39(13):4921-4928.

[111] Gilbert JL, Jacobs JJ. The mechanical and electrochemical processes associated with taper fretting crevice corrosion: a review. Modularity of Orthopedic Implants, ASTM International. 1997.

[112] Stott FH, Wood GC, Stringer J. The influence of alloying elements on the development and maintenance of protective scales. Oxidation of Metals. 1995; 44(1-2):113-145.

[113] Apel K, Hirt H. Reactive oxygen species: metabolism, oxidative stress, and signal transduction. Annual Review of Plant Physiology. 2004; 55:373-399.

[114] Dedon PC, Tannenbaum SR. Reactive nitrogen species in the chemical biology of inflammation. Archives of Biochemistry and Biophysics. 2004; 423(1):12-22.

[115] Jiang H, Rao L, Zhang Z, Rai D. Characterization and oxidation of chromium (III) by sodium hypochlorite in alkaline solutions. Inorganica Chimica Acta. 2006; 359(10):3237-3242.

[116] Zoski CG, editor. Handbook of electrochemistry. Elsevier; 2006.

[117] Candeias LP, Patel KB, Stratford MR, Wardman P. Free hydroxyl radicals are formed on reaction between the neutrophil-derived species Superoxide anion and hypochlorous acid. Federation of European Biochemical Societies letters. 1993; 333(1-2):151-153.

[118] Augusto O, Miyamoto S. Oxygen radicals and related species. Principles of Free Radical Biomedicine. 2011; 1:19-42.

[119] Beverskog B, Puigdomenech I. Revised Pourbaix diagrams for chromium at 25–300 C. Corrosion Science. 1997; 39(1):43-57.

[120] Costa M, Klein CB. Toxicity and carcinogenicity of chromium compounds in humans. Critical Reviews in Toxicology. 2006; 36(2):155-163.

[121] Wise SS, Holmes AL, Wise Sr JP. Hexavalent chromium-induced DNA damage and repair mechanisms. Reviews on Environmental Health. 2008; 23(1):39-58.

[122] Vidal CV, Muñoz AI, Olsson CO, Mischler ST. Passivation of a CoCrMo PVD alloy with biomedical composition under simulated physiological conditions studied by EQCM and XPS. Journal of the Electrochemical Society. 2012; 159(5):233-243.

[123] Hodgson AW, Kurz S, Virtanen S, Fervel V, Olsson CO, Mischler S. Passive and transpassive behaviour of CoCrMo in simulated biological solutions. Electrochimica Acta. 2004; 49(13):2167-2178.

[124] Disegi JA, Kennedy RL, Pilliar R. Cobalt-base alloys for biomedical applications. West Conshohocken, PA, ASTM. 1999.

[125] Niinomi M. Recent metallic materials for biomedical applications. Metallurgical and Materials Transactions A. 2002; 33(3):477-486.

[126] Milošev I. CoCrMo alloy for biomedical applications. Biomedical Applications, Springer. 2012: 1-72. .

[127] Park J, Lakes RS. Biomaterials: an introduction, Springer Science and Business Media. 2007.

[128] Virtanen S, Milošev I, Gomez-Barrena E, Trebše R, Salo, J, Konttinen, YT. Special modes of corrosion under physiological and simulated physiological conditions. Acta Biomaterialia. 2008; 4(3):468-476.

[129] Cook RB, Bolland BJ, Wharton JA, Tilley S, Latham JM, Wood RJ. Pseudotumour formation due to tribocorrosion at the taper interface of large diameter metal on polymer modular total hip replacements. The Journal of Arthroplasty. 2013; 28(8):1430-1436.

[130] Restrepo C, Ross D, Restrepo S, Heller S, Goyal N, Moore R, Hozack WJ. Adverse clinical outcomes in a primary modular neck/stem system. The Journal of Arthroplasty. 2014; 29(9):173-178.

[131] Watanabe H, Takahashi K, Takenouchi K, Sato A, Kawaji H, Nakamura H, Takai S. Pseudotumor and deep venous thrombosis due to crevice corrosion of the head–neck junction in metal-on-polyethylene total hip arthroplasty. Journal of Orthopaedic Science. 2015; 20(6):1142-1147.

[132] Haeri M, Goldberg S, Gilbert JL. The voltage-dependent electrochemical impedance spectroscopy of CoCrMo medical alloy using time-domain techniques: Generalized Cauchy–Lorentz, and KWW–Randles functions describing non-ideal interfacial behaviour. Corrosion Science. 2011; 53(2):582-588.

[133] Munoz AI, Julián LC. Influence of electrochemical potential on the tribocorrosion behaviour of high carbon CoCrMo biomedical alloy in simulated body fluids by electrochemical impedance spectroscopy. Electrochimica Acta. 2010; 55(19):5428-5439.

[134] Bearinger JP, Orme CA, Gilbert JL. Direct observation of hydration of TiO 2 on Ti using electrochemical AFM: freely corroding versus potentiostatically held. Surface Science. 2001;

491(3):370-387.

[135] Bearinger JP, Orme CA, Gilbert JL. In situ imaging and impedance measurements of titanium surfaces using AFM and SPIS. Biomaterials. 2003; 24(11):1837-1852.

[136] Hu R, Ornberg A, Pan J. Investigation of influence of small particles in MP35N on the corrosion resistance in synthetic biological environment. Journal of the Electrochemical Society. 2009; 156(10):341-344.

[137] Bettini E, Leygraf C, Lin C, Liu P, Pan J. Influence of grain boundaries on dissolution behavior of a biomedical CoCrMo alloy: In-situ electrochemical-optical, AFM and SEM/TEM studies. Journal of the Electrochemical Society. 2012; 159(9): 422-427.

[138] Bettini E, Eriksson T, Boström M, Leygraf C, Pan J. Influence of metal carbides on dissolution behavior of biomedical CoCrMo alloy: SEM, TEM and AFM studies. Electrochimica Acta. 2011; 56(25):9413-9419.

[139] Yu F, Addison O, Davenport AJ. A synergistic effect of albumin and $H_2O_2$ accelerates corrosion of Ti6Al4V. Acta Biomaterialia. 2015; 26:355-365.

[140] Ohnsorge J, Holm R. Surface investigations of oxide layers on cobalt-chromium-alloyed orthopedic implants using ESCA technique. Medical progress through technology. 1978:5:171-177.

[141] Hanawa T, Hiromoto S, Asami K. Characterization of the surface oxide film of a Co–Cr–Mo alloy after being located in quasi-biological environments using XPS. Applied Surface Science. 2001; 183:68-75.

[142] Vidal CV, Muñoz AI. Electrochemical characterization of biomedical alloys for surgical implants in simulated body fluids. Corrosion Science. 2008; 50:1954-1961.

[143] Bosker BH, Ettema HB, Boomsma MF, Kollen BJ, Maas M, Verheyen CC. High incidence of pseudotumour formation after large-diameter metal-on-metal total hip replacement: A prospective cohort study. Journal of Bone and Joint Surgery, British Volume. 2012; 94:755-761.

[144] Meftah M, Haleem AM, Burn MB, Smith KM, Incavo SJ. Early corrosion-related failure of the Rejuvenate modular total hip replacement. Journal of Bone and Joint Surgery, American Volume. 2014; 96:481-487.

[145] Vidal CV, Juan AO, Muñoz AI. Adsorption of bovine serum albumin on CoCrMo surface: effect of temperature and protein concentration. Colloids and Surfaces B: Biointerfaces. 2010; 80:1-11.

[146] Contu F, Elsener B, Böhni H. Electrochemical behavior of CoCrMo alloy in the active state in acidic and alkaline buffered solutions. Journal of the Electrochemical Society. 2003; 150:419-424.

[147] Aladjem A. Anodic oxidation of titanium and its alloys. Journal of Materials Science. 1973; 8:688-704.

[148] Gilbert JL, Mali S, Urban RM, Silverton CD, Jacobs JJ. In vivo oxide-induced stress corrosion cracking of Ti6Al4V in a neck–stem modular taper: Emergent behavior in a new mechanism of in vivo corrosion. Journal of Biomedical Materials Research Part B: Applied Biomaterials. 2012; 100:584-594.

[149] Hedberg YS, Pettersson M, Pradhan S, Odnevall Wallinder I, Rutland MW, Persson C. Can cobalt (II) and chromium (III) ions released from joint prostheses influence the friction coefficient? ACS Biomaterials Science and Engineering. 2015; 1:617-620.

[150] Yan Y, Neville A, Dowson D. Biotribocorrosion of CoCrMo orthopaedic implant materials—assessing the formation and effect of the biofilm. Tribology International. 2007; 40:1492-1499.

[151] Fialho JC, Fernandes PR, Eça L, Folgado J. Computational hip joint simulator for wear and heat generation. Journal of Biomechanics. 2007; 40:2358-2366.

[152] Gilbert JL, Mali SA, Liu Y. Area-dependent impedance-based voltage shifts during tribocorrosion of Ti-6Al-4V biomaterials: theory and experiment. Surface Topography: Metrology and Properties. 2016; 4(3):034002.

[153] Olmedo DG, Tasat DR, Duffó G, Guglielmotti MB, Cabrini RL. The issue of corrosion in dental implants: a review. Acta Odontol Latinoam. 2009; 22(1):3-9.

[154] Aulisa L, Di Benedetto A, Vinciguerra A, Lorini G, Tranquilli-Leali P. Corrosion of the Harrington's instrumentation and biological behaviour of the rod-human spine system. Biomaterials. 1982; 3(4):246–248.

[155] Akazawa T, Minami S, Takahashi K, Kotani T, Hanawa T, Moriya H. Corrosion of spinal implants retrieved from patients with scoliosis. Journal of Orthopaedic Science. 2005; 10(2):200-205.

[156] Halwani DO, Anderson PG, Brott BC, Anayiotos AS, Lemons JE. Clinical device-related article surface characterization of explanted endovascular stents: Evidence of in vivo corrosion. Journal of Biomedical Materials Research Part B: Applied Biomaterials. 2010; 95(1):225-238.

[157] Thomas SR, Shukla D, Latham PD. Corrosion of cemented titanium femoral stems. Bone and Joint Journal. 2004; 86(7):974-978.

[158] Kwon YM, Gill HS, Murray DW, Kamali A. Retrieval Wear Analysis of Metal-on-Metal Hip

Resurfacing Implants Revised Due to Pseudotumours. Tribology in Total Hip Arthroplasty 2011:121-132

[159] Campbell P, Ebramzadeh E, Nelson S, Takamura K, De Smet K, Amstutz HC. Histological features of pseudotumor-like tissues from metal-on-metal hips. Clinical Orthopaedics and Related Research®. 2010; 468(9):2321-2327.

[160] Gilbert JL, Buckley CA, Jacobs JJ, Bertin KC, Zernich MR. Intergranular corrosion-fatigue failure of cobalt-alloy femoral stems. A failure analysis of two implants. Journal of Bone Joint Surgery, American Volume. 1994; 76(1):110-115.

[161] Cook SD, Barrack RL, Clemow AJ. Corrosion and wear at the modular interface of uncemented femoral stems. Bone and Joint Journal. 1994; 76(1):68-72.

[162] Collier JP, Surprenant VA, Jensen RE, Mayor MB, Surprenant HP. Corrosion between the components of modular femoral hip prostheses. Bone and Joint Journal. 1992; 74(4):511-517.

[163] Collire JP, Surprenant VA, Jensen RE, Mayor MB. Corrosion at the interface of cobalt-alloy heads on titanium-alloy stems. Clinical Orthopaedics and Related Research. 1991; 271:305-312

[164] Lieberman JR, Rimnac CM, Garvin KL, Klein RW, Salvati EA. An analysis of the head-neck taper interface in retrieved hip prostheses. Clinical Orthopaedics and Related Research. 1994; 300:162-167.

[165] Rodrigues DC, Urban RM, Jacobs JJ, Gilbert JL. In vivo severe corrosion and hydrogen embrittlement of retrieved modular body titanium alloy hip-implants. Journal of Biomedical Materials Research Part B: Applied Biomaterials. 2009; 88(1):206-219.

[166] Gilbert JL, Mali SA. Medical implant corrosion: electrochemistry at metallic biomaterial

surfaces. Degradation of Implant Materials, Springer. 2012:1-28

[167] Kolman DG, Scully JR. On the Repassivation Behavior of High-Purity Titanium and Selected α, β, and β+ α Titanium Alloys in Aqueous Chloride Solutions. Journal of the Electrochemical Society. 1996; 143(6):1847-1860.

[168] Bastek PD, Newman RC, Kelly RG. Measurement of passive film effects on scratched electrode behavior. Journal of the Electrochemical Society. 1993; 140(7):1884-1889.

[169] Burstein GT, Liu C, Souto RM. The effect of temperature on the nucleation of corrosion pits on titanium in Ringer's physiological solution. Biomaterials. 2005; 26(3):245-256.

[170] Contu F, Elsener B, Böhni H. A study of the potentials achieved during mechanical abrasion and the repassivation rate of titanium and Ti6Al4V in inorganic buffer solutions and bovine serum. Electrochimica Acta. 2004; 50(1):33-41.

[171] Contu F, Elsener B, Böhni H. Characterization of implant materials in fetal bovine serum and sodium sulfate by electrochemical impedance spectroscopy. I. Mechanically polished samples. Journal of Biomedical Materials Research. 2002; 62(3):412-421.

[172] Gilbert JL, Buckley CA. Mechanical-electrochemical interactions during in vitro fretting corrosion tests of modular taper connections. Total Hip Revision Surgery. 1994:41-50.

[173] Papageorgiou N, Mischler S, Electrochemical simulation of current and voltage response in sliding tribocorrosion, Tribology Letters. 2012; 48(3):271–283.

# Vita

**YANGPING LIU**Phone: 315-560-9946    Email: yliusr@syr.edu

**CAREER GOAL:** **Provide engineering expertise in biomaterials research, development and testing**

## EDUCATION

**PhD in Bioengineering (area: biomaterials & orthopedic implant )**, Syracuse University — May 2017

**B.S in Materials Science & Engineering**, Central South University, China — June 2010

## SUMMARY

- Biomedical engineer with 7 years of experience in evaluating the mechanical and corrosion performance of metallic biomaterials (titanium, CoCr alloy & stainless steel), polymers and medical device
- Extensive experience in design and development of testing methods, tools and fixtures
- Significant expertise in wide range of laboratory electrochemical testing methods, instruments, material & surface characterization techniques
- In depth knowledge in performance of mechanical testing and failure analysis of medical devices
- Broad understanding of materials science and solid knowledge of alloy development using materials processing and heat treatment technology

## RESEARCH INTERESTS

- Medical device performance testing/ failure analysis/ retrieval analysis
- Mechanical and corrosion behavior of metallic biomaterials
- Tribology/Tribocorrosion associated with biomaterial interfaces
- Mechanical design, testing and evaluation, ASTM standard tests
- Surface chemistry/surface analysis of materials

## RESEARCH SKILLS

- Triboelectrochemical testing of medical alloys/medical devices (hip, spinal implants)
- Instrumentation design and development for material testing
- Mechanical testing of medical devices (Instron & Materials Testing System)
- Laboratory electrochemical analysis tools and techniques (Potentiostat, Cyclic Voltammetry, EIS etc)
- Material characterization and surface analysis techniques (SEM, EDS, AFM, FTIR, TEM, XPS, DSC, TGA)
- Micromechanical and nanomechanical testing concepts
- High-performance alloy development applying materials processing and heat treatment engineering knowledge

## SOFTWARE SKILLS

- LabView graphical programming tool
- Computer programming languages: C language, Matlab
- Computer design tool: Auto CAD
- Microsoft office tools: Power Point, Word, Excel

201

## WORK EXPERIENCE

**Graduate research assistant**                                                                **Fall 12- Spring 17**

Syracuse Biomaterials Institute, Syracuse University

PhD dissertation    (Research Advisor: Dr. Jeremy L. Gilbert)

Title:The effect of inflammatory cell released chemical species on the corrosion & tribocorrosion of CoCrMo alloy

**Graduate teaching assistant**                                                                      **Fall 10- Fall 12**

Department of Biomedical and Chemical Engineering, Syracuse University

ECS 326-Engineering Materials, Properties and Processing

ECS 104-Engineering Computational Tools (Matlab)

## PROFESSIONAL AFFILIATIONS

- Society for Biomaterials        • Orthopaedic Research Society

## PEER REVIEWED PUBLICATIONS

1. Gilbert JL, Sivan S, *Liu Y,* Kocagöz SB, Arnholt CM, Kurtz SM. Direct in vivo inflammatory cell−induced corrosion of CoCrMo alloy orthopedic implant surfaces. Journal of Biomedical Materials Research Part A, 2015

2. *Liu Y,* Gilbert JL. The effect of simulated inflammatory conditions and Fenton chemistry on the electrochemistry of CoCrMo alloy. Journal of Biomedical Materials Research Part B, 2017

3. Gilbert JL, Mali SA, *Liu Y*. Area-dependent impedance-based voltage shifts during tribocorrosion of Ti-6Al-4V biomaterials: theory and experiment. Surface Topography: Metrology and Properties, 2016

4. Zhou M, Yi D, Jia Y, *Liu Y* . Effect of pre-deformation on precipitation characteristic of 2E12 aluminum alloy." Rare Metal Materials and Engineering, 2010

5. *Liu Y*, Gilbert JL. In-situ Electrochemical AFM study of inflammatory cell released chemical species on corrosion behavior of CoCrMo alloy (To be submitted).

6. *Liu Y*, Gilbert JL. Effect of simulated inflammatory conditions on fretting corrosion behavior of CoCrMo alloy (To be submitted).

7. *Liu Y*, Gilbert JL. Effect of inflammatory species hypochlorous acid and hydrochloric acid on the electrochemical behavior of CoCrMo alloys (To be submitted)

## CONFERENCE PRESENTATIONS

*1. Liu Y,* Mali S, Gilbert, JL "Prediction of voltage shifts during fretting corrosion of titanium alloy: Effect of Area, Impedance and Mechanics". Annual meeting of the Society for Biomaterials, Boston, MA, 2013.

*2. Liu Y,* Gilbert JL "Effect of pH and hydrogen peroxide on corrosion behavior of CoCrMo alloy in phosphate buffered saline". Annual meeting of Society for Biomaterials, Denver, CO, 2014.

3. Gilbert JL, Sivan S, *Liu Y,* Kocagöz SB, Arnholt CM, Kurtz SM. "Evidence of direct cell induced corrosion of CoCrMo implant systems". Annual meeting of Society for Biomaterials, Denver, CO, 2014

*4. Liu Y,* Gilbert, JL "The effect of simulated inflammatory conditions on the corrosion and fretting corrosion of CoCrMo alloy" Annual meeting of Orthopaedic Research Society, Las Vegas, NV, 2015.

5. Kubacki GW, *Liu Y,* Gilbert JL. The effects of the inflammatory species hypochlorous acid on the electrochemical behavior of Co-Cr-Mo alloys, San Diego, CA, 2017